Synthesis and Characterization of Sulfur-Bridged Terpyridine-like Ru(II) Coordination Complexes and Dinuclear Ru(II) Sulfoxide Complexes

by

Trevor Cross

B.S. of Chemistry, Emory University, 2014

A THESIS SUBMITTED IN PARTIAL FULFILLMENT OF

THE REQUIREMENTS FOR THE DEGREE OF

MASTER OF SCIENCE

in

THE FACULTY OF GRADUATE AND POSTDOCTORAL STUDIES

(Chemistry)

THE UNIVERSITY OF BRITISH COLUMBIA

(Vancouver)

August 2019

The following individuals certify that they have read, and recommend to the Faculty of Graduate and Postdoctoral Studies for acceptance, a thesis/dissertation entitled:

Synthesis and Characterization of Sulfur-Bridged Terpyridine-like Ru(II) Coordination Complexes and Dinuclear Ru(II) Sulfoxide Complexes

---

submitted by Trevor Cross in partial fulfillment of the requirements for

the degree of Master of Science

in Chemistry

Examining Committee:

Professor Michael Wolf
Supervisor

Professor Mark Maclachlan
Supervisory Committee Member

Professor Glenn Sammis
Supervisory Committee Member

Professor John Sherman
Additional Examiner

Abstract

A new set of sulfur-bridged oligopyridine proligands was synthesized with each having different functional groups in the 4′ position. Three new homoleptic Ru(II) complexes with these new tridentate ligands were synthesized and were found to have no geometric strain about the Ru(II) metal center due to the expanded ligand cage about the metal. In addition, a heteroleptic Ru(II) complex with one of these new ligands and a terpyridine ligand was made. The heteroleptic complex was found to be emissive at 77 K while the homoleptic compounds were non-emissive. These photophysical and electrochemical properties of these new complexes were also probed, and Lever Electrochemical parameters assigned.

Photoactive mononuclear and dinuclear Ru(II) sulfoxide complexes were synthesized. The mononuclear complexes were found to have photoswitching activity that is consistent with reversible photoisomerization. A dinuclear complex was synthesized to probe if two photoisomerizations on the same complex was feasible. The dinuclear complex was found to undergo an irreversible photoreaction, and no evidence of two photoisomerizations was found.

Lay Summary

Several new inorganic complexes were synthesized to further expand on how ruthenium metal complexes interact with light and electricity. The complexes from Chapter 2 were synthesized to fully understand how geometry and strain affects the absorption and emission properties of different ruthenium metal complexes. It was found that these complexes had almost no strain but did not emit visible light when irradiated with UV light at room temperature. The complexes from Chapter 3 were chosen to determine if modified ruthenium complexes can undergo two separate structural changes when irradiated with light and then return to its original state. It was found that the ruthenium complexes synthesized were unable to undergo two structural changes and underwent one irreversible photoreaction changing its color permanently.

Preface

For all chapters, Dr. Michael Wolf had a supervisory role. Chapter 2 was based on a previous molecule first synthesized by Dr. Chris Brown. X-ray crystallography was performed, and resulting data was solved by Mr. Duane Hean. In chapter 3, I designed, analyzed and carried out all experiments alone.

Table of Contents

List of Tables

List of Figures

List of Charts

List of Schemes

List of Abbreviations and Symbols

^{1}	singlet
^{3}	triplet
Δ	difference or heat
δ	chemical shift
λ	wavelength
λ_{em}	wavelength of emission
λ_{ex}	wavelength of excitation
λ_{max}	wavelength at peak absorption
Σ	sum
τ	lifetime
φ	quantum yield
bpy	2,2’-bipyridine
br	broad (NMR)
CN	cyano group
COSY	correlated spectroscopy
d	doublet (NMR)
DCM	dichloromethane/methylene chloride
dd	doublet of doublets (NMR)
ddd	doublet of doublets of doublets (NMR)
DFT	density Functional Theorem
dmbpy	dimethyl bipyridine

DMF	dimethylformamide
DMSO	dimethyl sulfoxide
EDG	electron donating group
ESI	electrospray Ionization
EtOH	ethanol
EWG	electron withdrawing group
fac	facial
GS	ground state
HMBC	heteronuclear multiple bond correlation
HOMO	highest occupied molecular orbital
HSQC	heteronuclear single quantum correlation
IC	internal conversion
IR	infrared
ISC	intersystem crossing
IUPAC	International Union of Pure and Applied Chemistry
J	indirect dipole-dipole coupling
L	ligand
LC	ligand-centered
LED	light-emitting diode
LF	ligand Field
LMCT	ligand-to-metal charge transfer
LUMO	lowest unoccupied molecular orbital

m	multiplet (NMR)
MALDI	matrix-assisted laser desorption/Ionization
MC	metal-centered
m-CPBA	*meta*-chloroperoxybenzoic acid
Me	methyl
MeCN	acetonitrile
MeOD	deuterated methanol
MeOH	methanol
mer	meridional
MLCT	metal-to-ligand charge transfer
mol	mole
MS	mass spectrometry
NIR	near Infrared
NMR	nuclear magnetic resonance
NOESY	nuclear Overhauser effect spectroscopy
OLED	organic light-emitting diode
ORTEP	Oakridge thermal ellipsoid plot
PDT	photodynamic therapy
ppm	parts per million
py	pyridine
s	singlet (NMR)
S1	first singlet excited state

S2	second singlet excited state
t	triplet (NMR
T1	first triplet excited state
TAIC	thermally accessible internal conversion
TBAF	tetrabutylammonium fluoride
td	triplet of doublet (NMR)
TLC	thin-layer chromatography
TOF	time-of-flight
TPS	terpyridine-like pyridine sulfide
tpy	terpyridine
UV	ultraviolet
Vis	visible
VR	vibrational relaxation

Acknowledgements

I extend my gratitude to the faculty, staff and my cohorts in the chemistry department at UBC. The endless support and cheers have made my time at UBC invaluable. Particularly, I want to thank lab mates, current and old, for being my family away from Georgia.

I have the deepest gratitude for Dr. Susanna Widicus Weaver. You saw potential in me and let me actualize that potential in your lab. Thank you for the many hours spent in your office talking about my hopes and dreams, and what I should move to next.

I thank Dr. Michael O. Wolf for being a supervisor that allowed me to be creative and aspirational. Your fostering of my goals and ideas led me to greater wisdom and intellectual acuity. Thank you for supporting me through the many ups and downs I have had here.

I want to particularly thank Dr. Chris M. Brown for being a motivating force and a shoulder to cry on. Thank you for being the person that pushed me to do better science.

Lastly, I want to thank my family. Broc, thank you for protecting me. Amy, thank you for being my best friend. Mama and Daddy, thank you for letting me chase my dreams, providing every opportunity for me to grow and learn. Thank you to my husband who followed me across the continent to support me when I could not support myself.

To the gay, lesbian, bisexual, trans*, and queer community.

Chapter 1: Introduction

1.1 Overview

Humankind for the last 260,000 years has continually used light with the first anthropogenic source being fire.[1] The use of fire even predates the speciation of *Homo Sapiens* with the first evidence of control of fire by *Homo Erectus* dating to one million years ago.[2] With the advent of fire, the human experience was radically changed with the ability to stay up later, which changed their circadian rhythms. This is supported by the fact that humans have a longer daily waking period than other mammals.[3] As a result of this discovery, humans built communities where people gathered around fire which in turn created language. Humankind even invented their most prolific religions centered around light being a representation of the heavenly, evidenced by the first thing being created on Earth in the Abrahamic faiths being light, as told in Genesis 1:3 (depicted in Figure 1-1). The center of human life revolves around the creation and maintenance of a light source.

As the scientific method was developed and perfected, the nature of light became more evident over time. The mysticism surrounding the creation of light slowly faded as people became more skilled in its manipulation, and with the invention of gas-powered lamps, lightbulbs, and now OLED flat-screen devices reduced light to the ordinary.

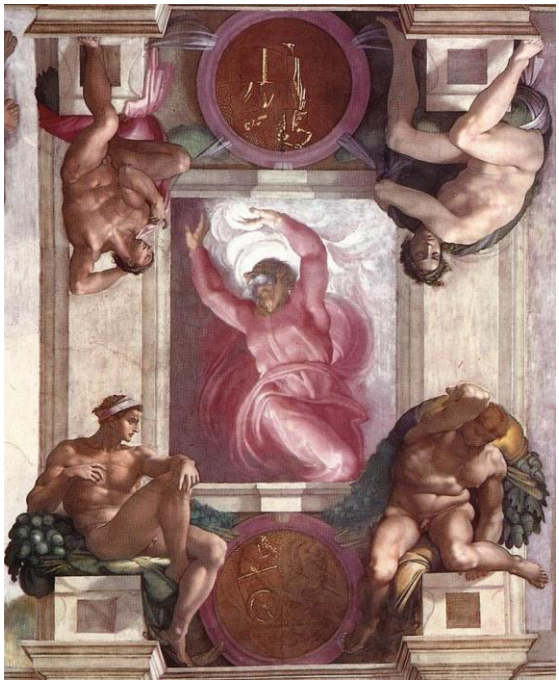

Figure 1-1 Michelangelo's The Separation of Light from Darkness depicts the story of Genesis 1:3-5.

As civilization advanced, the requirements for useful light has constantly changed while the needs have stayed relatively similar. The need to illuminate the world at night to extend the day, to perform tasks, and ward off danger has remained unchanged. However, the requirements for light have altered over time where operability indoors, ease of use, safety and efficiency have become limiting factors on the sources of light used. Open candles for lighting rooms slowly faded into using gas lamps which in turn were phased out by lightbulbs as electricity became widely available. Today with the advances of LED and OLED technology, light sources must be small, have long-term stability, high efficiency and their color must be finely tuned to create dynamic and colorful screens. Currently, most device manufacturers rely on coordination complex emitters to illuminate their OLED screens because they offer efficient, color-precise emission and remain stable over the lifespan of the device.

Another requirement for the advancement of light technology is based on the ability to control and manipulate natural light from the sun. For example, window-blinds are used to easily regulate the amount of light allowed in a room; light can be totally blocked out or completely allowed through depending how open the blinds are. However, blinds are not perfect because they can block the view outside the window, they will eventually wear out, and they are not always aesthetically preferable. Another solution to this problem is window tinting where a certain percentage of light is always blocked out, but this also comes with downsides as it is a static system than cannot be altered. With recent advancements in chemistry, window manufacturers have been looking for solutions where windows can potentially change the amount of light allowed through a window by using electrochromic or photochromic window tinting, which change how much light they block out depending on the environment or stimuli placed on them.[4]

For use in applications that will be used daily for years at a time, finding stable and active molecules is key. For example, the Canadian Standards Association says that a window should last for 25 years, and many windows have been in buildings many times longer. For a window with advanced technological functions, they must be stable enough so that they are not being repeatedly replaced, and they must be cost competitive, either through equal installation and material costs or through potential energy savings. While a window with electrochromic or photochromic function will likely never be equal in material costs to a standard window, the potential money savings from reduced energy usage can make the installation of these windows a compelling choice.

For both OLED emitters and photoactive compounds, the need for long-term stability with exceptional photophysical properties is the main driving force for discovery and research. Coordination complexes offer these properties and have been placed in commercial products already such as iridium emitters in OLED devices. However, the need to improve on these products

remains. Ruthenium(II) coordination complexes have been previously reported as being efficient emitters for potential use for applications in photochemistry including OLED devices,[5] dye-sensitized solar cells,[6] photo- or electro-responsive materials,[5] photo-activated catalysis[7] and photo-dynamic therapy.[8] Within this work, we have reported several new Ru(II) complexes with different synthetic preparations and their interactions with light.

1.2 Introduction to Photochemistry

Photochemistry is the study of the chemical effect of light ranging from ultraviolet (UV) to infrared (IR) light, as defined by IUPAC.[9] Generally, the study of photochemistry focuses on how a molecule absorbs light and then what happens to that energy after absorption. Absorption is the process of exciting an electron from a lower energy to a higher energy electronic state. In coordination complexes such as Ru(II) polypyridyl complexes, there are principally four types of absorptions, as shown in Figure 1-2: ligand-to-metal charge transfer (LMCT), metal centered (MC), metal-to-ligand charge transfer (MLCT), and ligand centered (LC) absorptions. A LMCT absorption is where an electron is excited from a π orbital into a higher energy *d* orbital.[10,11] Conversely, an MLCT absorption has an electron promoted from a *d* orbital into a higher energy π orbital. In LC and MC absorptions, the promoted electron stays localized either on the ligand orbitals or the metal orbitals, respectively.

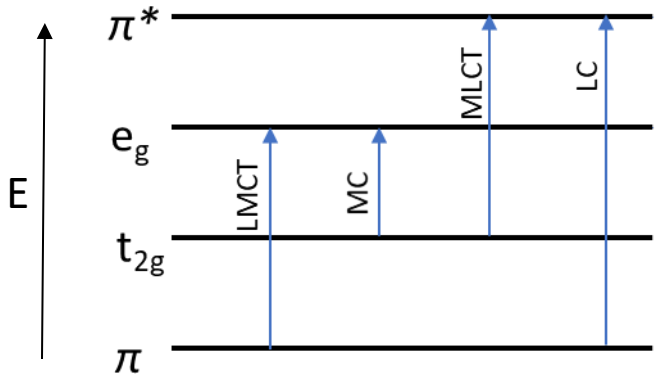

Figure 1-2 A simplified energy diagram showing the four different types of UV-Vis absorptions in a Ru(II) coordination complex.[11]

After absorption, a molecule can undergo three processes. Vibrational relaxation (VR) to the vibrational ground state of the electronic state will occur.[12] Then, the molecule can undergo intersystem crossing (ISC) or internal conversion (IC) in which the electron may transfer to different excited electronic states with other isoenergetic states. Lastly, a molecule will de-excite or relax to the ground state either emitting the energy absorbed through luminescent processes such as fluorescence and phosphorescence or non-radiatively decaying to the ground state, releasing the absorbed energy as heat. Each of these transitions (absorption, ISC/IC, and VR/de-excitation) are more probable if their vibrational wavefunctions and geometries overlap sufficiently, due to the Franck-Condon Principle.[13]

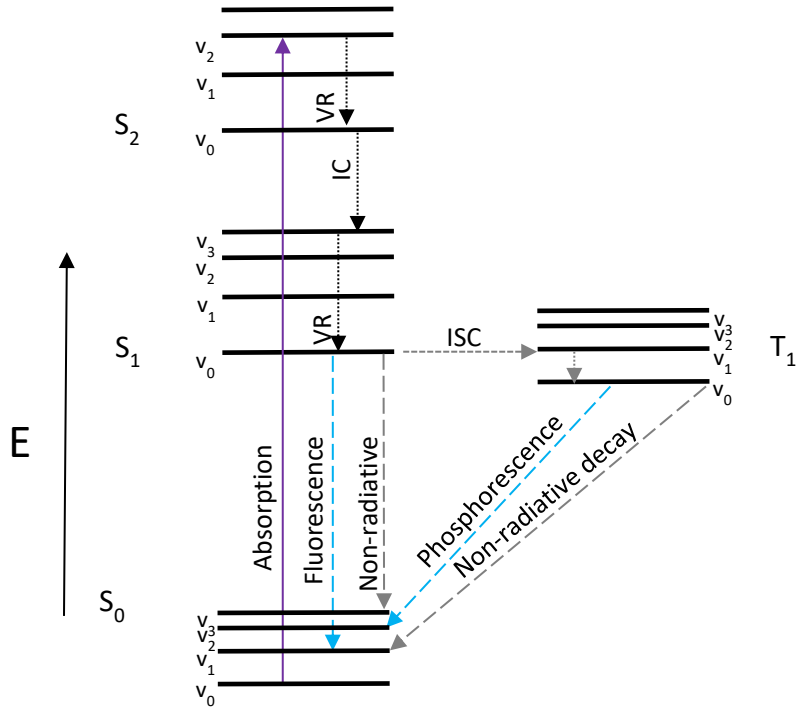

Figure 1-3 A simplified Jablonski diagram depicting the photophysical processes of a photoactive molecule. Different color arrows depict different types of processes (blue = emissive, purple = absorptive, grey = non-radiative). Adapted from reference [12].

The non-radiative processes, ISC and IC, do not involve emission of a photon and involve the overlap of vibrational states of two different electronic excited states. ISC is an energy conserving process where the energy is transferred between different electronic states through overlapping vibrational states of similar energy, as shown by the horizontal grey arrow in Figure 1-3. Intersystem crossing occurs across states with different multiplicities as long as the electronic energy levels between the two states are similar in energy and there is adequate overlap between their vibrational states. Internal conversion is the relaxation of an electron from a higher electronic state to a lower electronic state of the same multiplicity ($S_2 \rightarrow S_1$). $S_1 \rightarrow S_0$ may happen, but the

energy difference between S_1 and the ground state is rarely close enough to allow for vibrational state overlap.

Fluorescence is defined as the emission of light from spin-allowed transitions.[14] In organic molecules, this is generally from an excited singlet state to a singlet ground state ($S_1 \rightarrow S_0$) as shown in Figure 1-3. Conversely, phosphorescence is the emission of light during spin-forbidden transitions typically from a triplet excited state to a singlet ground state ($T_1 \rightarrow S_0$). Despite phosphorescence being spin forbidden, the transition can occur when there is appropriate overlap of the vibrational wavefunctions between the singlet and ground-state which can be aided by spin-orbit coupling distortions induced by the heavy-atom effect.[15] The heavy-atom effect relies on the higher *Z* of an atom with a large electric field that generates a large magnetic field, increasing the spin-orbit coupling of an orbiting electron.[16] The increase in spin-orbit coupling allows the electron to undergo more forbidden transitions because of the increased overlap in the different multiplicity wavefunctions.[17] In inorganic photochemistry, a heavy metal center such as Ru(II) can induce greater spin-orbit coupling leading to increased population of an excited triplet state from the excited singlet state from absorption ($S_1 \rightarrow T_1$). The heavy-atom effect also promotes the radiative decay $T_1 \rightarrow S_0$. Due to the "forbidden" nature of this emission, the lifetimes for phosphorescence emission (μs to s) in inorganic complexes can be significantly longer than fluorescence emission (ns-μs).

1.3 Discovery of the First Emissive Ruthenium(II) Coordination Complex

The emission from Ru(II) chelate species was first reported in 1959 in a time where the only previously reported and believed to be emission from metal complexes were Cu(II) mixtures with aminoanthraquinone and emission from rare earth metals based on electronic f-f transitions.[18] It was noted in this paper that while the emission of $[Ru(bpy)_3]^{2+}$, **1** (Chart 1-1), was similar to f-f

luminescence, there was no concomitant absorption which ruled out an f-f transition as the source of emission.

Chart 1-1

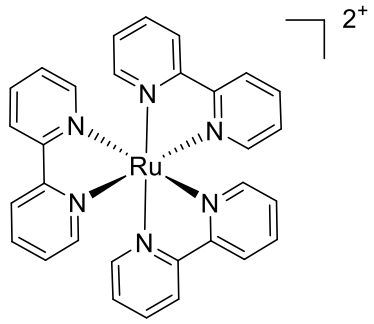

1

To corroborate this assignment, the broad low energy absorption was assigned as a d → π* transition as the absorption would go to the many vibrational states of the antibonding orbitals. This would then relax to the lowest vibrational state as dictated by Kasha's Rule and the fluorescence results. In addition, it was found that either absorption into the π → π * or the d → 2nd antibonding π * orbital would result in the same emission wavelength leading to the conclusion that both absorptions would relax to the same energy state and then emit from that state.

Further research into the luminescence of **1** eventually led to a more sophisticated understanding of the photophysical processes not just for Ru(II) polypyridyl compounds but also of photochemistry in general. In 1965 Klassen *et. al.* thought the emission was solely sourced from singlet states, despite the observed lifetime (5.92 μs) because the lifetime was not as long as in other spin-forbidden luminescent compounds.[19] Of course, this was disproven in 1968 when Demas and Crosby showed that the intersystem crossing S_1→T_1 of **1** is aided by the heavy-atom effect.[20] The heavier Ru(II) atom assists in this spin-forbidden transition as the complete wave-function needs to be considered as Ru(II) center has a large magnetic field.[16] The magnetic field

perturbs the orbital wave function to effectively alter the multiplicity of the transition by mixing several different states so that there is some singlet character. However, it was not until 1974 that there was direct spectroscopic evidence of the existence of the triplet emission level, until then only derived rate constants and theoretical selection rules were used to determine the forbidden nature of the emission state.[21]

In the following decades, more information would be parsed from this system making $[Ru(bpy)_3]^{2+}$ one of the most well-studied and understood ions. The applications of $[Ru(bpy)_3]^{2+}$ were consequently examined as well with extensive work as a photosensitizer and photocatalyst for redox reactions.

1.4 Photophysical Properties of Ruthenium(II) Polypyridyl Complexes

Ruthenium polypyridyl complexes satisfy several conditions that enable them to have advantageous photophysical properties such as long emission lifetimes and photocatalytic activity.[10] One factor that enables this behavior is that Ru(II) polypyridyl complexes have an octahedral geometry with a full set of d^6 electrons in the three degenerate t_{2g} non-bonding orbitals, which comprise the highest-occupied molecular orbital (HOMO), shown in Figure 1-4.[22] Ru(II) polypyridyl coordination complexes are low-spin unlike the d^6 Fe(II) counterparts, so the ground state electrons remain paired. The t_{2g} orbital is completely filled, so when an electron is excited, there is both an energetic electron and a lower-energy hole in the ground state into which the complex could accept an electron. Due to the long excited-state lifetimes, $[Ru(bpy)_3]^{2+}$ is a popular photocatalyst for a multitude of reactions because the long lifetimes allow for the Ru(II) complex to interact with the substrate before the energy is lost.[23–27]

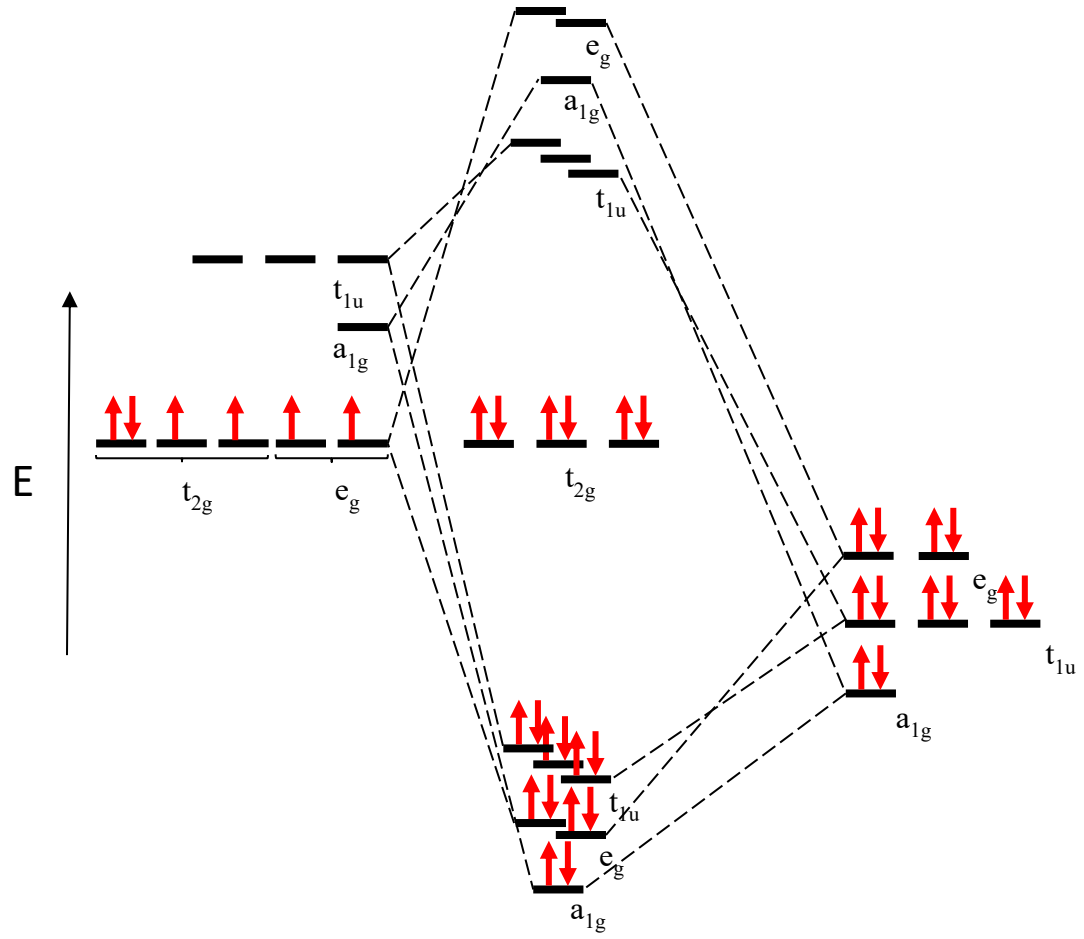

Figure 1-4 Molecular orbital diagram of a generic O_h complex.

The long lifetime of Ru(II) polypyridyl complexes is due to the accessibility of a triplet MLCT energy state where relaxation to the ground-state is spin forbidden due to different multiplicities.[28] Once an electron is excited from the t_2g orbitals to a ^{1}MLCT state, the electron will rapidly undergoes ISC into the ^{3}MLCT state. This ^{3}MLCT state can be long lived because relaxation to the ground state requires a spin flip as well as the release of a photon.[10] In **1** the lifetime for an excited electron can last for (~600 μs).[22] Phosphorescence unlike fluorescence will emit a photon a significant amount of time after excitation due to spin-forbidden nature of the relaxation.

In some cases, the excited state lifetimes of metal complexes can be quenched by accessible metal-centered (MC) states. For Ru(II) polypyridyl species, a populated ^{3}MC state will rapidly non-radiatively decay into the ground state despite having a different spin state. This ^{3}MC state can be thermally accessible at room temperature leading to thermally accessible intersystem crossing (TAIC).[29]

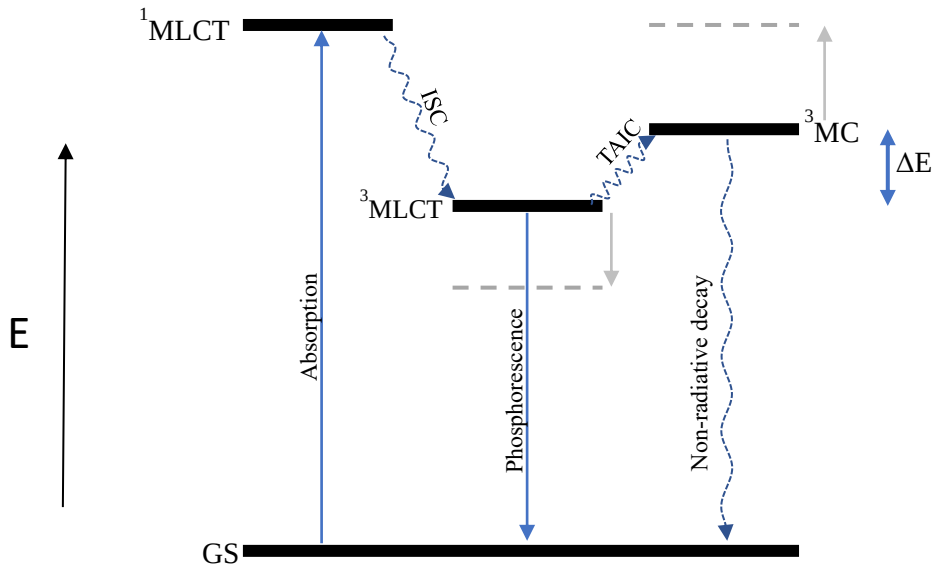

Figure 1-5 A simplified Jablonski diagram showing the energy pathways available once a photon is absorbed in a $[Ru(tpy)_2]^{2+}$ complex. Grey arrows and dashed energy states show the different approaches to changing the ΔE between the ^{3}MLCT and ^{3}MC states.

As depicted in grey in Figure 1-5, there are two main approaches to limiting the effect of TAIC in Ru(II) complexes: stabilizing the ^{3}MLCT state and destabilizing the ^{3}MC state.[30] Both methods increase the ΔE between the ^{3}MLCT and ^{3}MC, as a small energy barrier between these two states allows for significant population of the ^{3}MC state and then leads almost immediately to

non-radiative decay to the ground state. A large ΔE makes populating the ^3MC state nearly impossible from the ^3MLCT state resulting in a longer phosphorescence lifetime.

1.5 Ruthenium(II) Tris(2,2′:6′,2″-terpyridine) Complexes

While **1** exhibits long lifetimes and high quantum yields, $[Ru(tpy)_2]^{2+}$, **2** (Chart 1-2), does not have those qualities. Complex **2** has very low quantum yields ($<10^{-5}$) and short lifetimes (250 ps) at room temperature.[31] However, when cooled to 77 K, **2** exhibits long-lived red-orange emission.[32] Similar observations have been made in other highly strained ligands for Ru(II) complexes, as well as Ir(III) complexes, which also contain a d^6 metal center. Originally, the explanation for this phenomenon was that excitation of the electron would lower the ligand field splitting enough that the complex would go from low-spin to high-spin.[33] A high-spin Ru(II) complex would be paramagnetic, which would induce a large rate of intersystem crossing to nonradiative states due to paramagnetism. This explanation was inferred from the fact that the Fe(II) center is always high-spin and as Ru(II) is in the same group on the periodic table, an excited electron may introduce adequate energy to convert Ru(II) to a high-spin species as well. Further ^1H NMR studies suggested that the pendant pyridyl rings on the ligand were not strongly bound to the Ru(II) due to two different magnetic environments being observed.[34] It was suggested that instead of switching from low to high spin, the pendant pyridines would dissociate while in solution and dissipate energy non-radiatively, but this behavior would not be observed at low temperatures. However, it was determined that the lack of emission from **2** was due to the unfavorable bite angle of the terpyridine (tpy) ligand distorting the octahedral structure of the complex.[35,36] The distortion of the complex caused by terpyridine leads to weaker ligand field splitting than expected.[37] The weak ligand field splitting then allows for higher energy triplet metal-centered (^3MC) states to be thermally accessible from the excited ^3MLCT state. In the case

of **2**, the energy barrier between the ^{3}MC and ^{3}MLCT states is 1500 cm^{-1} while in **1** the energy barrier is 4000 cm^{-1}.[38] These stabilized ^{3}MC states then readily quench the ^{3}MLCT state. Determining the mechanism by which **2** has its emission quenched was incredibly important because effective strategies for increasing its luminescence properties could be developed.

Chart 1-2

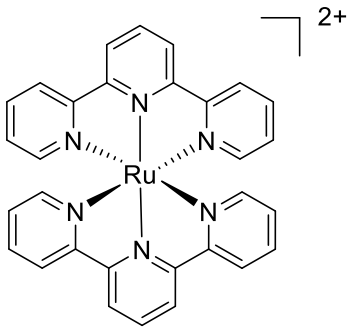

2

1.5.1 Stabilizing Triplet Metal-to-Ligand Charge Transfer States

A significant amount of research has been performed to alter the luminescence qualities, such as lifetime and quantum yield, of **2** through structural changes to the tridentate ligands, so that emission can occur at room temperature.[38] In the previous section, it was discussed that there are predominantly two methods to increase the quantum yields and lifetimes of Ru(II) polypyridyl coordination complexes. The most widely explored method is to stabilize the ^{3}MLCT state, so that the energy barrier between the ^{3}MC and ^{3}MLCT states is large enough that TAIC no longer significantly occurs between the two states.[39] Stabilizing the ^{3}MLCT state has typically involved modifying the terpyridine ligand by either making it more electron donating or withdrawing or by increasing the conjugation of the ligand, usually in the 4′ position. A myriad of terpyridine-based ligands has been synthesized and chelated to Ru(II) in homoleptic and heteroleptic complexes.

Chart 1-3

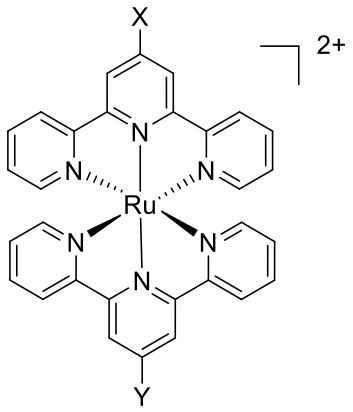

3

Table 1-1 Iterations of complex 3 that highlight that the functionalization of the 4′ position can affect the photophysical properties of $[Ru(tpy)_2]^{2+}$.[39]

-X	**-Y**	λ_{abs}(nm)	λ_{em}(nm)	τ (s)	φ
$MeSO_2$	$MeSO_2$	486	666	25	5×10^{-4}
$MeSO_2$	H	482	679	36	4×10^{-4}
$MeSO_2$	Me_2N	500	~800		
5-cyano-2-pyrimidyl	H	489	713	200	1×10^{-3}
5-cyano-2-pyrimidyl	5-cyano-2-pyrimidyl	506	705	231	1×10^{-3}
CN	CN	490	680	50	2×10^{-3}

As seen in **3** (Chart 1-3) and Table 1-1, the addition of different moieties attached to the pyridyl backbone can have a significant effect on the lifetimes and quantum yields of Ru(II) terpyridyl complexes. The addition of electron-withdrawing groups (EWG) and electron-donating groups (EDG) results in red-shifts in the absorption spectrum for Ru(II) terpyridyl compounds.[40] This is due to the EWG destabilizing the HOMO of the ligand without having much effect on the LUMO. For an EDG, the LUMO of the ligand is stabilized and thus lowers the absorption energy. For example, the addition of a single cyano group in the 4′ position can increase the quantum yield

because the LUMO is stabilized and shifted away from the ^{3}MC state.[41] However adding an EDG does not necessarily increase lifetimes because it does not shift the HOMO of the ligand. Additionally, the juxtaposition of an EWG on one terpyridine and an EDG on the other can have significant effects on the photophysical properties of the complex. The addition of an acceptor group onto the terpyridine will lower the ^{3}MLCT emissive state energy while also destabilizing the ^{3}MC state. On the other hand, a donor group will stabilize the HOMO and the ^{3}MC state of the complex which will also lower the emission energy. In a heteroleptic complex with both donating and accepting ligands the ^{3}MLCT state is stabilized more than the ^{3}MC state; thus, the emission lifetime can be vastly prolonged at room temperature.[40] The increasingly long list of functionalized terpyridine ligands employed has shown that the effect of stabilizing the ^{3}MLCT state is limited with lifetimes reaching only 600 ns.

1.5.2 Destabilizing Triplet Metal-Centered States

As stated in section 1.5, two main strategies to improve the photophysical properties of ruthenium terpyridine complexes is to stabilize the ^{3}MLCT state or destabilize the ^{3}MC state. Both strategies can work because the energy barrier between the ^{3}MLCT and ^{3}MC is increased in both cases. Much work has been done to stabilize the ^{3}MLCT state, and this has been briefly discussed earlier in this chapter. However, ^{3}MLCT stabilization may not always be the most advantageous method depending on the demands of the application. Lowering the ^{3}MLCT energy too much increases the probability that energy will follow non-radiative decay pathways due to the energy-gap law.[42] The energy-gap law states that there is an exponential increase in non-radiative transitions the closer the energy between the two states with small differences between their geometries.[43] In cases where the energy-gap law becomes salient when modifying **2**, destabilizing the ^{3}MC will give better results than stabilizing the ^{3}MLCT.[44]

By altering the sigma-donating ability of the coordinating ligands, the ^{3}MC state on **2** becomes destabilized leading to higher quantum yields and longer lifetimes.[44] The increased sigma-donating ability will predominantly influence only the *d* orbitals of Ru(II) while having only a minimal effect on the anti-bonding π orbitals.[30] This "isolated" effect on the *d* orbitals can be advantageous when considering that there is almost no ^{3}MLCT stabilization effect. However, increased sigma-donating ligands will destabilize the ground state which effectively stabilizes the ^{3}MLCT state.

1.5.2.1 Inserting More Donating Atoms into the Pyridyl Ligand Backbone

One way to increase the sigma-donating capabilities is to insert a nitrogen or more donating atom into the pyridyl backbone.[39] The insertion of a different nitrogen-containing heterocycle can significantly increase the sigma-donating of the chelating ligand while having a minimal effect on the ^{3}MLCT state through destabilization of the ground state due to different resonance structures of the ligand.[45]

Chart 1-4

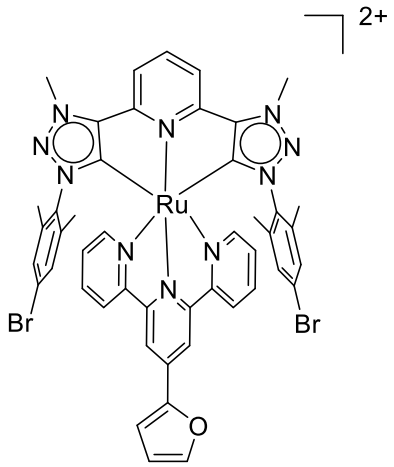

4

The photophysical properties of Ru(II) polypyridyl complexes can be drastically improved by using a N-heterocycle containing three nitrogen atoms and a bonding mode with two carbenes as the ligand.[46] Berlinguette and coworkers were able to achieve this by synthesizing a heteroleptic ruthenium complex with a carbene mesoionic ligand with a terpyridine ligand functionalized in the 4′ position with furan, **4** (Chart 1-4). The use of a strong sigma-donor and pi-acceptor ligand juxtaposed against a terpyridine with additional donating power resulted in the longest lifetime (7.9 μs) known for monometallic ruthenium complexes. However, the species with the longer-lived lifetimes exhibited almost proportional lower quantum yields when compared with other complexes synthesized in the same study.

1.5.2.2 Expanding the Ligand-Cage

One method to significantly adjust the ^{3}MC state that does not significantly affect the ^{3}MLCT state is minimizing the strain about the ruthenium atom.[39,44] The expansion of the ligand cage allows for the Ru(II) center to be more octahedral rather than distorted octahedral. The distorted octahedral structure stabilizes the ^{3}MC state which can lead to a small energy barrier

between the ^{3}MLCT and ^{3}MC states allowing for TAIC. $Ru(tpy)_2^{2+}$ complexes have a N—Ru—N bond angle of ~79˚ between the *cis*-nitrogen atoms, which for the overall complex leads to a significant distortion from octahedral geometry.

Chart 1-5

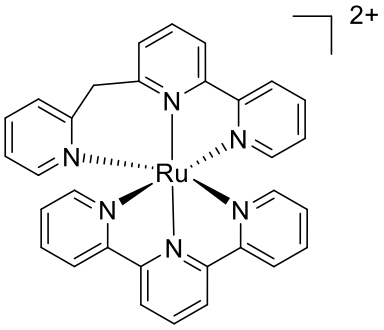

5

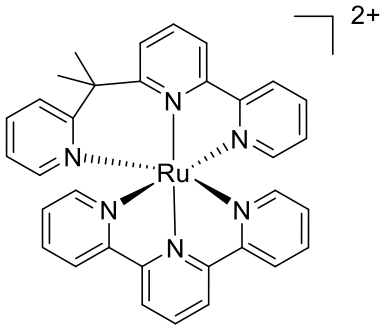

6

One method for expanding the ligand cage is to insert a single atom at the 2′ position of the terpyridine backbone. This approach offers some relief to distortion of the Ru(II) center. Complexes **5** and **6** (Chart 1-5) show where a methylene and isopropylene group have been inserted between a pendant and central pyridine.[44] The expansion of the metallocycle relieves some of the distortion about the Ru(II) center, increasing the *trans*-N-Ru-N angles a significant amount (by ~10˚). However, the lifetimes and quantum yields are still below 1 ns and well below 0.1% for the isopropylene derivative. In this study the authors tried to minimize the difference in electronic effect between **5** and **6**, and it was found that the steric bulk at the linking carbon reduced the ligand field splitting and stabilized the energy of the ^{3}MC state so that it moves lower in energy than the ^{3}MLCT state. This led to almost all energy to be funneled into the ^{3}MC state and subsequent non-radiative decay.

Chart 1-6

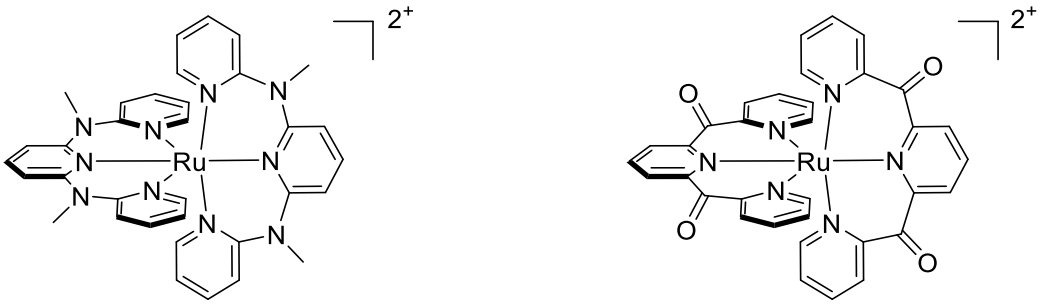

7 **8**

The insertion of a single atom between both pendant pyridines which breaks all conjugation between the three pyridyl groups, has been examined. Complexes **7** and **8** (Chart 1-6) show that this method of destabilizing the ^{3}MC states can increase lifetimes to the microsecond time regime with smart ligand design.[47] In both **7** and **8**, the N—Ru—N angles are almost exactly 90˚ and 180˚ resulting in a quasi-octahedral structure.[47,48] This octahedral structure increases the ligand-field splitting and destabilizes the ^{3}MC state. In these two complexes, the addition of a bridging moiety between both the pendant pyridyl rings in the terpyridine backbone relieves the strain more than just substituting one side which is expected. In the case of **7**, the photophysical properties were described as "disappointing."[44] However, in the case of **8**, the emission at room temperature had drastically longer lifetimes (1.36 μs) and quantum yields of 13% in an aerobic environment. The two strategies used for these complexes were similar, yet they each had different results. While Heinze *et al* do not explain the lack of emission in **7**, it could be related to the effects seen in the complex **6** where the steric bulk of the methyl group assists in the nonradiative decay. In **8,** the oxygen atom is more rigid being an sp^2 carbon linking the pyridines, so non-radiative decay due to steric constraints is not as large of a factor. The long-lived lifetimes and quantum yields at room temperature and in ambient atmosphere are also atypical for a Ru(II) bisterdentate complex. While

the emission was characterized as originating from a ^{3}MLCT state in **8**, it is suggested that there is increased triplet ligand-centered state character in the emission, which could explain the higher quantum yields and longer lifetimes. However, calculations do not suggest this to be the case, and this model of why this complex is less susceptible to oxygen quenching of emission is speculative. While there is improvement in anaerobic environments in lifetimes (3.3 μs) and quantum yields (30%), the increase is not as dramatic as for others in this class of compounds, and these properties at room temperature show that there is potential for homoleptic Ru(II) bisterdentate complexes to have use in further applications.

Chart 1-7

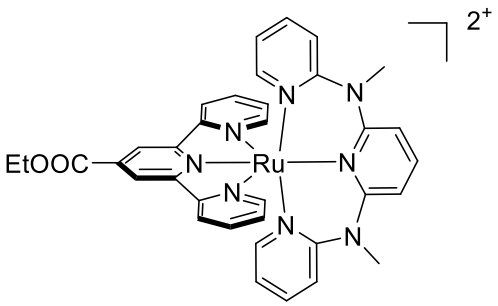

9

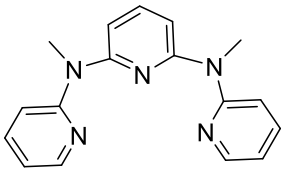

dppd

Despite **dppd** (Chart 1-7) not increasing lifetimes and quantum yields when used in homoleptic Ru(II) complexes such as **7**, it has been found to be a good candidate for formation of heteroleptic Ru(II) complexes when chelated to Ru(II) alongside terpyridine as shown in **9** (Chart 1-7). The electron withdrawing capability of the terpyridine with an ester in the 4′ position was found to increase the quantum yield (0.45%) and the lifetime (720 ns).[49] The increased lifetime was a result of lowering the energy of the ^{3}MLCT state. As would be expected, the terpyridine ligand has strained N—Ru—N bonds of ~79˚, but the dppd ligand has N—Ru—N bond angles

that are close to 90˚. However, these angles are derived from DFT calculations and not X-ray crystallography. The crystal structure was shown here to have the expected geometries where the N—Ru—N bond angles on the terpyridine ligand were 79˚ while in the methylene oligopyridine ligand the bond angles of N—Ru—N were close to 90˚. For these types of complexes, the ligand field splitting from the less strained ligand is still greater than **2** which raises the energy of the ^{3}MC state, and the terpyridine ligand remains conjugated which keeps the ^{3}MLCT state from rising alongside the ^{3}MC state as is in **7** and **8.** Without the conjugation seen in the terpyridine ligand, there are no low-lying π^* orbitals to produce a lower energy ^{3}MLCT state. By using both terpyridine and an expanded non-conjugated ligand, both the increase in energy of the ^{3}MC state and the decrease of energy in the ^{3}MLCT state can be realized and the energy barrier between the two states can be higher.

Another method that has been successfully employed to expand the ligand cage, is to extend the π-conjugation of the pyridyl backbone. In this method, a fused-ring system is typically used to increase the bite angle of the tridentate ligand while still maintaining the conjugation. This method has the benefit of potentially reducing the ^{3}MLCT state energy while also increasing the ^{3}MC states as well.[39]

Chart 1-8

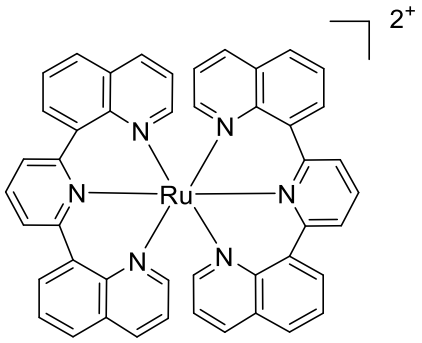

10

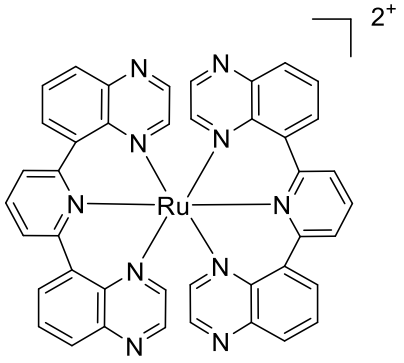

11

Complex **10** (Chart 1-8) contains quinoline groups in the 2 and 6 positions of the central pyridine and has a lower energy emission at 700 nm, which is expected because of the stabilization of the ^{3}MLCT state, and results in a lifetime of 3 μs which is a significantly improvement compared to **2**.[50] The stabilization of the emissive triplet state did not result in deactivation directly from the ^{3}MLCT state. This is, however, observed in complex **11** (Chart 1-8), which instead uses quinoxaline, where the emission wavelength is 715 nm and the lifetime is 255 ns. The increased stabilization lowers the energy of the emission, however in this case the ^{3}MLCT is stabilized too much, allowing for non-radiative decay from the ^{3}MLCT state directly to the ground state due to the small energy-gap.

1.6 Ru(II) Polypyridyl Complexes Photoreactivity Overview

The previous sections detailed the interactions of ruthenium polypyridyl complexes with light, the pathways that lead to light emission, and the factors that can lead to nonradiative decay. However, the light absorbed by these complexes can also be used to drive intramolecular and intermolecular reactions such as ligand dissociation,[51,52] ligand isomerization[53,54] and

photocatalysis.[27,55] For example, $[Ru(bpy)_2L_2]^{2+}$, **12** (Chart 1-9) photoejects a monodentate ligand with irradiation. While the photoreactivity of $[Ru(bpy)_2L_2]^{2+}$ complexes have been known since the early 1960s, early research focused on making photostable complexes and their emissive and absorptive properties as well as their single-electron reactivity for photocatalysis reactions. It was not until 1980, that a study focused on the photodissociation and photoisomerization of the monodentate ligands was conducted.[53] Furthermore, the *cis*-/*trans*- isomerization of $[Ru(bpy)_2(H_2O)]^{2+}$ complexes was only characterized in 1980. Subsequently in 2000, photoinduced linkage isomerization of coordinated dimethyl sulfoxide would be reported and explored.[56]

Chart 1-9

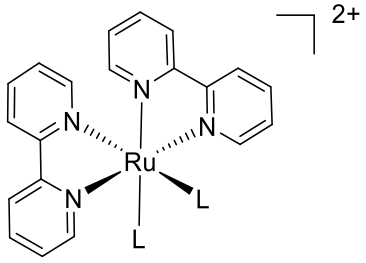

12

1.6.1 Photodissociation Reactivity

Photodissociation of monodentate ligands was observed a few years after the first report of the emission behavior of **1**, when Dwyer *et al*. described a $[Ru(bpy)_2(py)_2]^{2+}$ (py = pyridine) complex that would form $[Ru(bpy)_2(py)(H_2O)]^{2+}$ in 1963. Three years later they reported the photosensitivity of similar compounds in dilute acetone solutions.[52] The photoejection of the ligands, though documented in the literature, was not explored in the following years as the photostability of other Ru(II) bidentate polypyridyl complexes were focused on. In 1980, a full paper detailing the several photodissociation and following ligand association reactions was

published, elucidating the photoreactivity for $[Ru(bpy)_2L_2]^{2+}$ complexes including the photosubstitution and photoejection reactions that take place.[53] Recently, research has looked at exploiting the photodissociation of Ru(II) complexes to deliver a payload (an organic molecule) using light as the stimulus. This strategy has gained increasing interest with the development of photodynamic therapy (PDT), the site-specific delivery of a drug molecule triggered by light.[8,57]

The photophysical mechanism of dissociation (shown in Figure 1-6) is very similar to what is shown in Figure 1-5. In ligand dissociation, the ^{3}MC energy state can lead to the photoejection of a weakly bound monodentate ligand and occasionally bidentate ligands.[58] This is due to the ^{3}MC state allowing access to dissociative MC states. In these systems, the ^{3}MLCT and ^{3}MC states still have a low energy barrier between them, so TAIC can still occur. However, when designing ligands for photodissociation, the population of the ^{3}MC state is important unlike in situations when the goal is to design a ligand to improve the emission properties of Ru(II) complexes. In fact, emission is counterproductive to the labilization of the ligand, as this would prevent population of the dissociative states required for photoejection. Once photoejected from the complex the ligand may remain intact, which makes these complexes of particular use for potential applications such as drug delivery. Additionally, singlet oxygen generation is still possible after the photoejection of the ligand as there are still polypyridyl ligands in place on the Ru(II) center.[59] This adds a second possibility for therapeutic uses of Ru(II) polypyridyl complexes because the complex itself can act as the therapeutic agent while releasing a drug molecule.

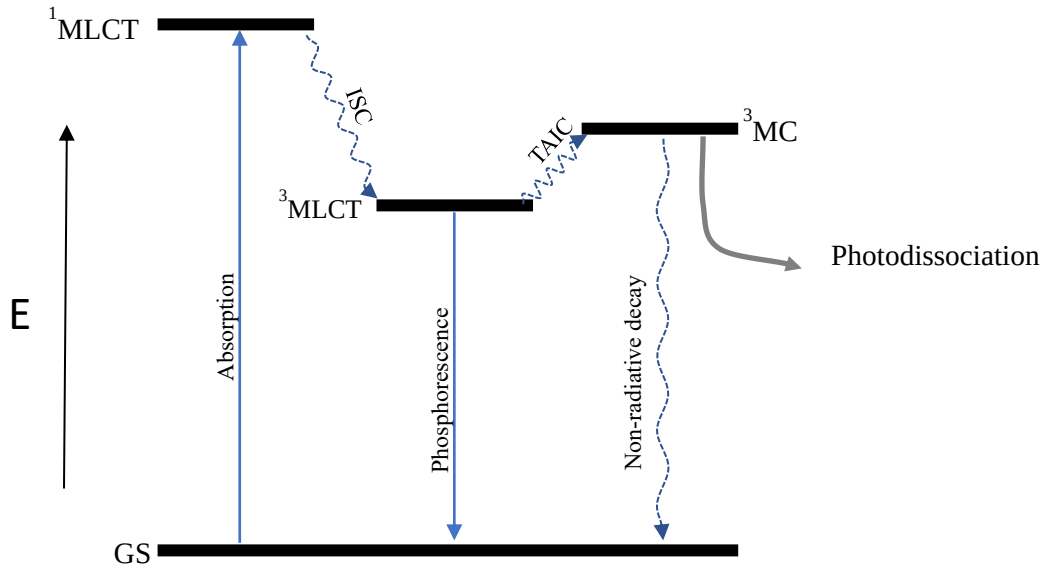

Figure 1-6 A simplified Jablonski diagram showing the general photodissociation pathway for $Ru(bpy)_2L_2]^{2+}$ complexes

1.6.2 Ru(II) Photoisomerization Overview

Photodissociation is not the only intramolecular photoreaction for Ru(II) complexes. In some cases, photoisomerization can occur. Photoisomerization is a structural change that comes about from the absorption of a photon. The first Ru(II) complex observed to undergo this type of reaction, $Ru(bpy)_2(H_2O)]^{2+}$, displays an isomerization from the *cis* isomer, **13,** to the *trans* isomer, **14** upon photoirradiation.[52]

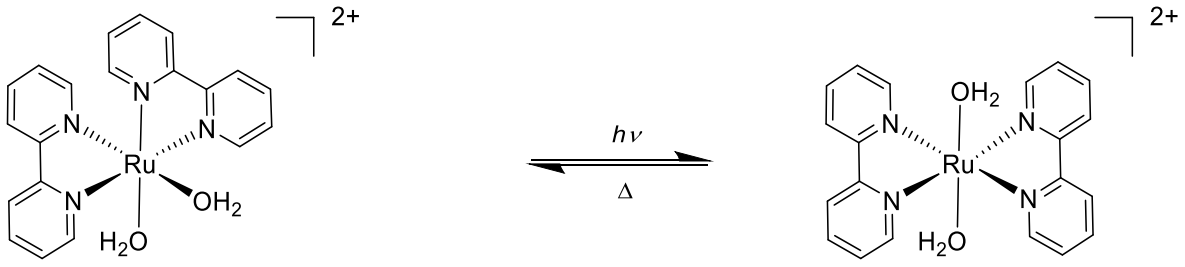

13 **14**

Figure 1-7 The first photoisomerization observed for a Ru(II) complex. [52]

The photoisomerization has quantifiable effects on the physical properties of the complexes with a large red-shift of the MLCT absorption band in the *trans* state.[53] The photoisomerization is also reversible where the absorption spectrum of **14** will slowly revert to that of **13** when stored in the dark at room temperature (shown in Figure 1-7). The emissive properties of complexes **13** and **14** are also different with the *cis* isomer being significantly more emissive than the *trans* isomer. Photoisomerization is not only limited to rearrangement of the ligand about the metal center as in **13** and **14**; other Ru(II) complexes have exhibited photoisomerization through linkage isomerization such as $[Ru(bpy)_2(DMSO)_2]^{2+}$, **15** and **16**.[56]

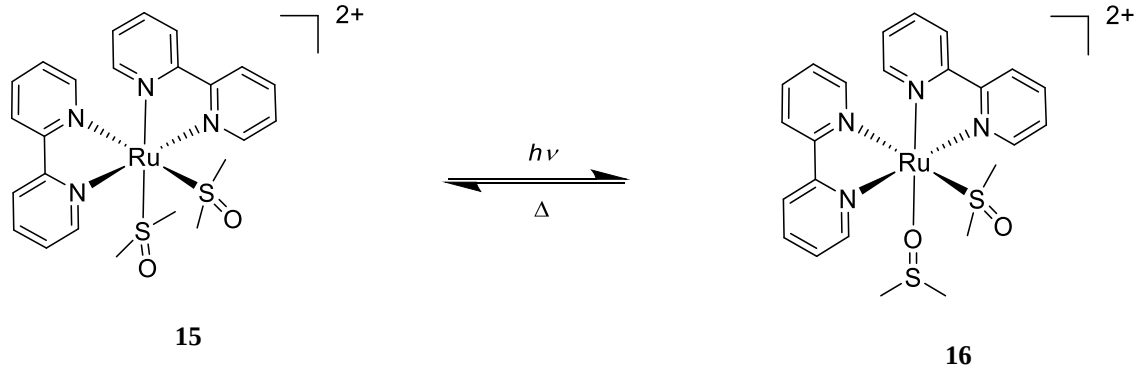

15 **16**

Figure 1-8 The photoisomerization of $Ru(bpy)_2(DMSO)_2$.[56]

The photoisomerization of complexes **15** and **16** (Figure 1-8) takes advantage of the unique ^{3}MLCT state that is responsible for emission as well. The linkage isomerization from S→O and the reverse reaction O→S has a thermal component since the photoisomerization does not occur

at 77 K. The thermal component to the photoisomerization implies an energy barrier between the two different linkage ^{3}MLCT states. The mechanism of the photoisomerization has been studied, and several different complexes containing sulfoxide moieties have been examined showing that this type of photoisomerization is not limited to solvato complexes.[60–62] Monodentate and chelating ligands containing sulfoxide moieties have been shown to undergo this photoisomerization effect.[63]

The mechanism of the Ru(II) photoisomerization for a monodentate species was determined to strictly occur through MLCT states and did not involve any ligand field (LF) or MC states.[54] For the photodissociation of the complex $Ru(bpy)_2(CH_3CN)]^{2+}$, the quantum yield for the reaction is an order of magnitude lower than the photoisomerization of the equivalent DMSO complex. The vastly different quantum yields suggested that the photodissociation and photoisomerization proceed via two completely different mechanisms. To confirm that the isomerization occurs through the excited MLCT states, $[Os(bpy)_2(DMSO)_2]^{2+}$, **17** (Chart 1-10), was synthesized because the ligand field splitting is 30% greater than Ru(II); thus making the MC states inaccessible.[64] The photoisomerization readily occurred with the Os(II) complexes which showed that the ligand field states are not necessary. Transient absorption spectroscopy also showed that the O-bonded species was present in the excited MLCT states, implying that the photoisomerization occurs before relaxation to a ground state.

Chart 1-10

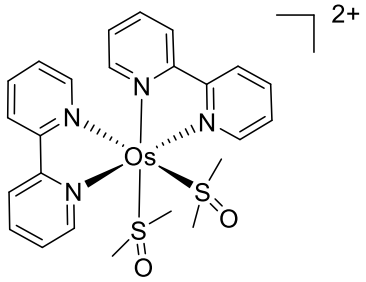

17

Beyond solvato complexes, Ru(II) sulfoxides have been explored with other chelating ligands, so that the sulfoxide moiety stays tethered to the Ru(II) center. These complexes exhibit a different mechanism of photoisomerization than the monodentate sulfoxide complexes, implied by the difference in quantum yields between the different species and confirmed by transient absorption spectroscopy.[63] Transient absorption showed that there was no formation of the O-bonded complex in the ^{3}MLCT state. However, the O-bound complex was found when the complex relaxed to the ground state. The rationale for this phenomenon is that the chelated ligand stabilizes the η^2- coordination of the sulfoxide in the ^{3}MLCT state, which means that the O-bound state is formed when upon relaxation to the ground state.[54] Then in the O-bound ground state, **17** thermally reverts to the S-bound state.

1.7 Goals and Scope

The general goal of this thesis was to synthesize new photoactive Ru(II) polypyridyl complexes and characterize their photophysical properties. In Chapter 2, the work focused on the development of expanded ligand cage Ru(II) bis-tridentate complexes using sulfur-bridged oligopyridines. The expansion of the ligand cage was primarily used to relieve the strain about the Ru(II) core and thus increase the ligand field splitting. Chapter 3 is focused on the synthesis on mononuclear and dinuclear Ru(II) sulfoxide complexes. The goal was to create new Ru(II)

complexes which would undergo multiple photoisomerizations under light, especially in the case of the dinuclear species. The work here looks at the effects of the introduction of sulfur into the ligand system of Ru(II) polypyridyl complexes and how the sulfur affects the photophysical properties of Ru(II) complexes.

Chapter 2: Sulfide-Bridged Expanded Ligand-Cage Ru(II) Complexes

One characteristic of Ru(II) polypyridyl complexes that affects the physical properties is the denticity of the chelating ligands. Due to the nature of the Ru(II) center, homoleptic bidentate pyridyl complexes, such as **1** $[Ru(bpy)_3]^{2+}$, (Chart 1-1), have been the subject of more research and use in applications due to their longer photoluminescence lifetimes (τ_{PL}) and higher photoluminescence quantum yields (Φ_{PL}). The tridentate pyridyl analogue, **2**, $[Ru(tpy)_2]^{2+}$, (Chart 1-2) has extremely low quantum yields ($<10^{-5}$) and short lifetimes (250 ps).[31] Thus, increasing the low quantum yields and low lifetimes by reducing TAIC allows for using **2** for photocatalytic applications as the energy absorbed can be efficiently used. In the case of $[Ru(bpy)_3]^{2+}$, the ΔE between the ^{3}MC state and the ^{3}MLCT state is large enough where non-radiative decay by TAIC to the ^{3}MC state does not allow for non-radiative decay.[38] Tridentate pyridyl complexes such as **2** hav been of interest because they lack of chirality at the central Ru atom which can be beneficial for macromolecular structures and polarized photophysical effects.

A popular approach to changing the aforementioned properties of ruthenium tridentate complexes has relied on stabilizing the ^{3}MLCT state and thereby raising the energy barrier between the ^{3}MLCT and ^{3}MC states, to reduce TAIC.[30] Generally, this involves modifying the terpyridine ligand with activating moieties which generally stabilizes the ^{3}MLCT state when chelated to ruthenium or by introducing further conjugation into the ligand which reduces overlap between vibrational states in the excited and ground state, thereby reducing non-radiative decay due to Franck-Condon principle.

Another strategy involves destabilizing the ^{3}MC state instead of stabilizing ^{3}MLCT states, shown in Figure 1-5. One way of doing this is relieve the distortion about the ruthenium atom, so that it may be more octahedral.[30] In many ruthenium tridentate polypyridyl ligands, the distortion

of the coordination complex stabilizes ^{3}MC states. Ligand field theory suggests that by relieving the strain about the Ru(II) atom and increasing its octahedral character, the ^{3}MC state will become destabilized. The coordination of polypyridyl ligands creates a five-membered metallocycle with strained geometry about the Ru(II) core. In the case of complex **1**, the bidentate ligand results in a strained metallocycle with N—Ru—N angles of 79˚,[65] but the distortion away from octahedral structure does not stabilize the ^{3}MC state to allow for TAIC from the ^{3}MLCT state. In contrast, complexes **2** have increased strain in this metallocycle which does significantly distort the octahedral structure. This distortion in **2** stabilizes the ^{3}MC state leading to TAIC from the ^{3}MLCT state. Thus, research has been done with the purpose of expanding the metallocycle in **2** to improve its photophysical properties. This expansion of the metallocycle has involved inserting an additional atom between the pyridyl backbone. Recently, a more octahedral structure in Ru(II) tridentate polypyridyl complexes has been achieved by expanding the metallocycle ring from a five-membered metallocycle to a six-membered metallocycle.

Chart 2-1

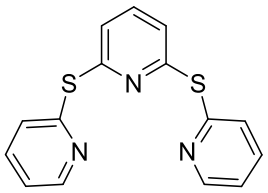

18

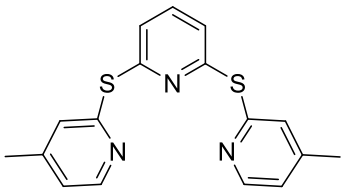

19

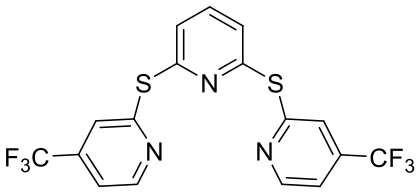

20

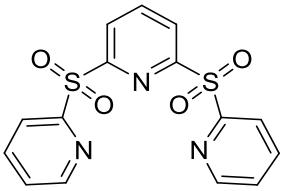

21

Previously, our group has shown that sulfur bridges modify the photophysical properties of similar metal chelates, and those sulfurs can be oxidized to tune emission on Ir(III)$(ppy)_2$(N^N) complexes.[66] Consequently, in these modifications, the bidentate bite angle was expanded and the geometry around the Ir(III) center was more octahedral. To follow up on the Ir(III) bidentate ligand expansion, the following research focuses on the ability to create and tune expanded oligopyridine ligands (shown in Chart 2-1) by inserting a sulfide linker between the pyridyl rings on a terpyridine backbone (**TPS**) to expand the ligand-cage about the ruthenium center as shown in Chart 2-2.

Chart 2-2

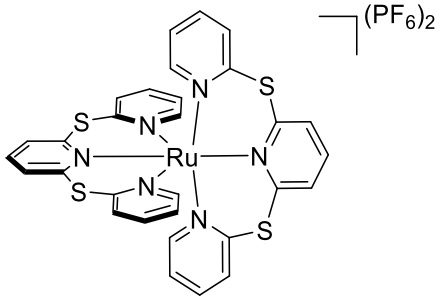

22

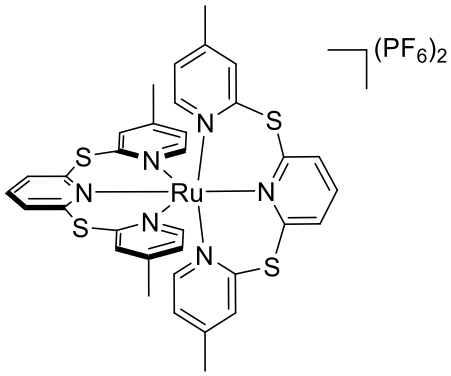

23

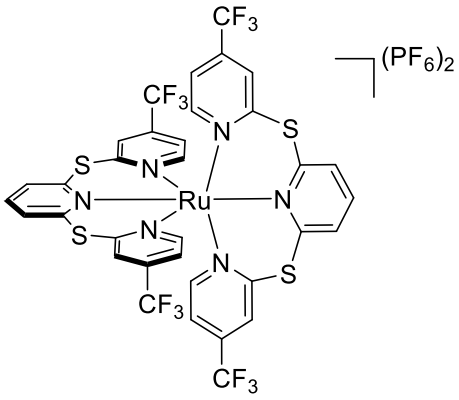

24

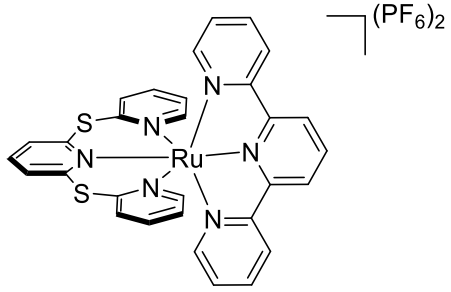

25

2.1 Synthetic Methods

2.1.1 Pro-Ligand Synthesis

Three different **TPS** ligands were synthesized with different functional groups at the 4 and 4″ positions (-H, -CF_3, -CH_3) with different activating ability (**18**-**20**). A sulfone-bridged **TPS** pro-ligand (**21**) was also successfully synthesized.

To synthesize the **TPS** ligands, **18**-**21**, two different pathways were used, with one method. 2-mercaptopyridine and 2,6-dibromopyridine were added together in dimethylformamide to undergo a double substitution reaction to form the proligand **18**. This reaction was not

straightforward with 4-substituted 2-thiolpyridines and had small yields. To obtain compounds **19** and **20** in adequate yields, the thiopyridone was oxidized into the pyridine disulfides **26** (**CF_3-DSF**) and **27** (**Me-DSF**) in almost quantitative yields. The resulting disulfides were then reacted with 2,6-dibromopyridine with NaOH and dimethyl sulfoxide to yield the resulting tridentate proligands, **19** and **20**, as shown in Scheme 2-1.

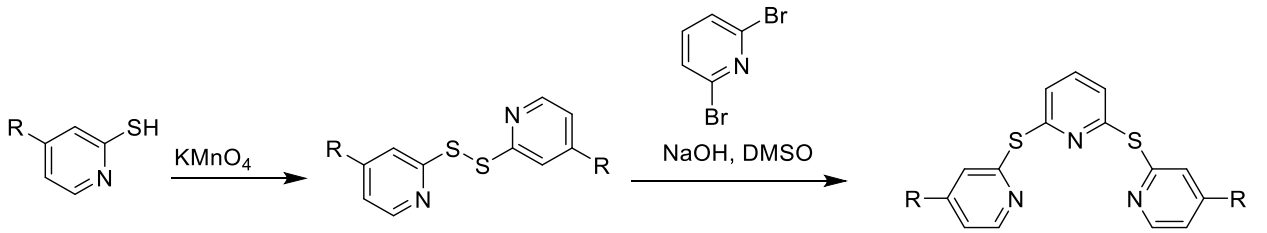

26 R = CF_3 (96%)
27 R = CH_3 (51%)

19 R = CH_3 (61%)
20 R = CF_3 (27%)

Scheme 2-1 Synthetic route used to synthesize proligands 19 and 20.

The fully oxidized pro-ligand **21** was synthesized by oxidizing compound **18** with hydrogen peroxide with Pd/C as the catalyst in EtOH at 60 ˚C. This reaction fully oxidized the bridging sulfurs and was quantitative in yield.

2.1.2 Ru(II) Complex Synthesis and Characterization

These newly synthesized pro-ligands were then chelated to ruthenium, resulting in three different homoleptic compounds (**22-24**) and a heteroleptic compound with **18** and tpy as ligands. However, no evidence was found of **21** coordinating to ruthenium using several different synthetic approaches. These Ru(II) complexes were then characterized using NMR, X-ray crystallography, UV-Vis spectroscopy, and cyclic voltammetry to probe their redox and photophysical properties.

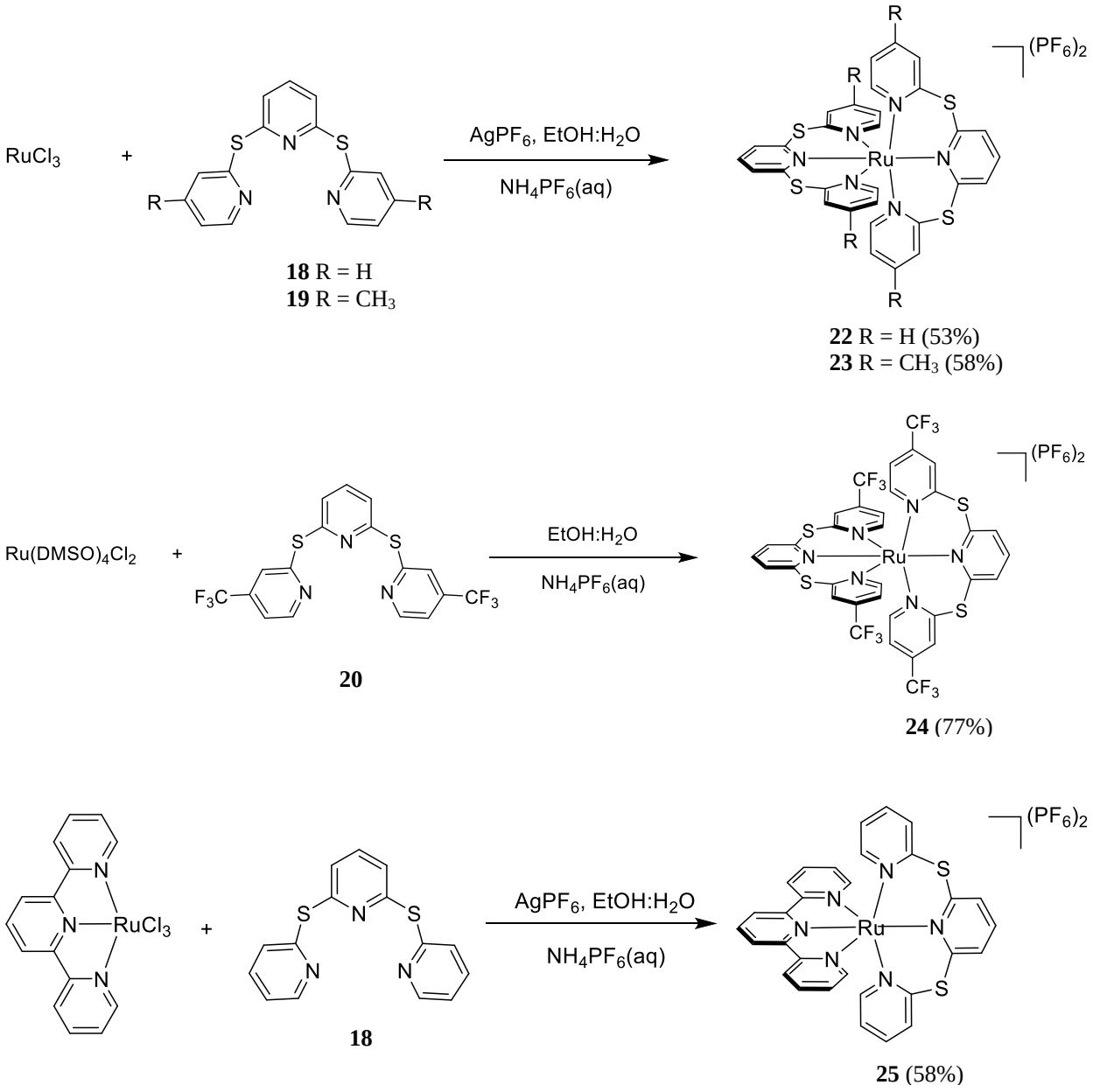

Scheme 2-2 Methods used to synthesize the coordination complexes 22-25.

All Ru(II) ligand coordination reactions followed a general scheme of starting with either $RuCl_3$ or $RuCl_3$(tpy) where $AgPF_6$ was used to remove chloride to drive the reaction forward while under reflux. In cases where the proligand had enough electron-withdrawing activity (such as in the case of **20**), $Ru(DMSO)_4Cl_2$ was used as the Ru(II) source because the previous reactions did

not yield any product. The same work up was generally followed where after heating, the solution was evaporated and reconstituted in acetonitrile. The acetonitrile mixture would then be added slowly to saturated aqueous solution of NH_4PF_6. This would then be recovered with vacuum filtration. Purification was performed by column chromatography if necessary. All new pro-ligands and Ru(II) complexes were characterized by NMR (^1H, ^{13}C, ^1H-^1H COSY, ^1H-^{13C} HMBC, ^1H-^{13}C HSQC).

Attempts were made to synthesize the homoleptic complex using the pro-ligand **21**; however, no evidence of the formation of the desired complex was found. Several reactions using $RuCl_3$ and $Ru(DMSO)_4Cl_2$ as the starting Ru(II) source were carried out as well as using a microwave reactor. It is proposed that the SO_2 bridge was too electron withdrawing and hindered the pyridyl groups from chelating effectively to the Ru(II) center.

2.2 Structural Characterization

Single crystals were prepared for **22**, **23**, and **25** by vapor diffusion of diethyl ether into acetonitrile. The structures of **22**, **23**, and **25** were obtained by X-ray diffraction and show each of the complexes to be a six-coordinate octahedral structure (Figure 2-1) with specific angles being displayed in Table 2-1. Complexes **22** and **25** have crystal structures showing only the *mer* isomer. Given that the ligands on these complexes are flexible, it is important to discern whether it is principally *fac* or *mer*. The ^1H NMR spectra for complexes **22** and **25** also show that there are no other isomers in the solution state. Complex **23** was shown to have both *mer* and *fac* isomers in a 1:1 ratio when crystallized into a single crystal. Furthermore, the *fac* isomer also shows two different isomers within it as well *Λ* and *Δ* isomers. The refined crystal structure showed that these isomers were present in a 1:1 ratio. The two *fac* isomers were found to have equivalent protons from NMR spectroscopy, so they could not be discerned separately from one another; however,

the presence of *fac*-**23** and *mer*-**23** isomer is corroborated by NMR spectroscopy experiments which showed two unique molecules in solution in a 54:46 *mer*/*fac* ratio. In Figure S26, the methyl peaks in the ^{1}H NMR show the most distinct evidence that there are two different isomers in solution. There is one peak for the *mer* isomer which indicates that all the methyl groups are within the same electronic environment. With the split methyl peaks, they are of equal intensity and are slightly downfield of the *mer* isomer peak, indicating that the methyl peaks on the *fac* isomer have two different environments. In addition to ^{1}H NMR, ^{13}C, 2D NMR experiments were performed to confirm that the two isomers were completely independent and did not correlate to one another. In the *mer*-**23** species, the ligand is in an unstrained position where the pendant pyridyl groups are twisted out of plane from one another ranging between 76-84˚ even in the heteroleptic species. The central pyridyl rings from each ligand are only twisted 20˚ out of plane in a helical-like structure; however, the heteroleptic complex shows more torsion when comparing the central pyridyl rings with a torsion angle of 48˚. The Ru—N bond lengths in complex **23** are within .005 Å of one another and *cis* N-Ru-N angles within 85-95˚and *trans* N-Ru-N angles within 178-180˚ which indicates an octahedral structure with no distortion. It also exhibits a higher space group symmetry than complexes **22** and **25**.

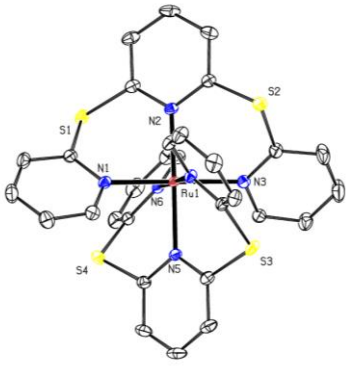

22

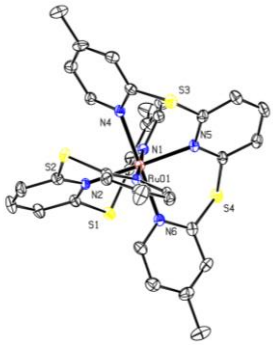

***mer*- 23**

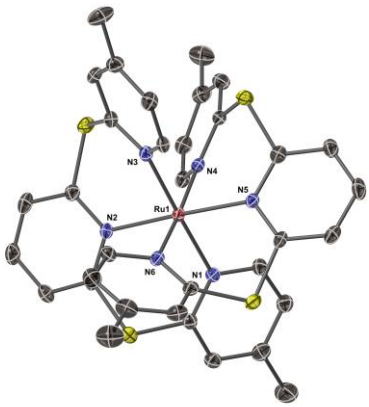

fac- **23**

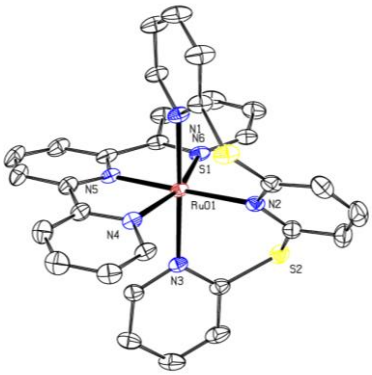

25

Figure 2-1 Crystal structures depicted with thermal ellipsoids at 50% probability, gathered by X-ray crystallography. Hydrogen atoms, solvent molecules (diethyl ether and MeCN) and PF_6 counterions omitted for clarity.

Table 2-1 Selected angles of complexes 22, *mer*-23, and 25 highlighting the near perfect octahedral structure of the complexes.

Complex	**22**	*mer*-**23**	**25**
N2-Ru-N5	178.402	178.640	178.189
N1-Ru-N3	178.973	178.399	178.606
N1-Ru-N2	90.253	90.276	91.109
N2-Ru-N3	90.385	91.300	91.189
N4-Ru-N6	179.434	177.581	158.877

Complex **25** has the most distortion from the synthesized complexes because of the strain from the terpyridine ligand. When comparing to the N-Ru-N angle of $Ru(tpy)_2$ (158.2°), the N-Ru-N angle of the pendant pyridines in complex **25** is not greatly affected. The **TPS** ligand remains relatively unstrained in a twisted conformation, but the terpyridine ligand has strained N-Ru-N bonds of 79˚. The bond lengths are also the most distorted with the central terpyridine ligand being significantly shorter while the TPS ligand Ru-N bond lengths are essentially equal. For the

prototypical $Ru(tpy)_2$ complex, bond lengths are 1.9-2.0 Å. The bond lengths of the **TPS** ligands are longer, but within expected Ru-N bond lengths for larger bite angle ligands.

Complex **24** did not crystallize after several attempts. Discoloration in the acetonitrile and ether slow diffusion set up occurred after several days, indicating that the complex is not stable in solution for long periods, especially in a coordinating solvent. However, the NMR spectra (^1H, ^{13}C, COSY, HMBC and HSQC) were collected. The ^1H NMR spectrum showed splitting patterns and expected integrations similar to the previous homoleptic compounds in the study, as well as the COSY spectrum. In the ^{13}C NMR spectrum, the presence of fluorine was detected by the splitting of the carbon peaks, resulting in a quartet for the trifluoromethyl carbon. The number of peaks in the ^1H spectrum also indicates that the *mer* isomer is the only isomer present in solution because the splitting pattern closely resembles **22**, and there is no evidence of the Γ and Δ isomers that would form if there were *fac* isomers.

2.3 Photophysical Properties

Table 2-2. Absorption data of 22-25

Compound	λ_{max}(nm) [ε (L mol^{-1} cm^{-1})]
22	369 [14515], 445 [5450]
23	362 [9768] , 450 [3677]
24	391 [11604]
25	365 [5279], 448 [3640], 486 [4579], 539 [1225], 560 [~600]

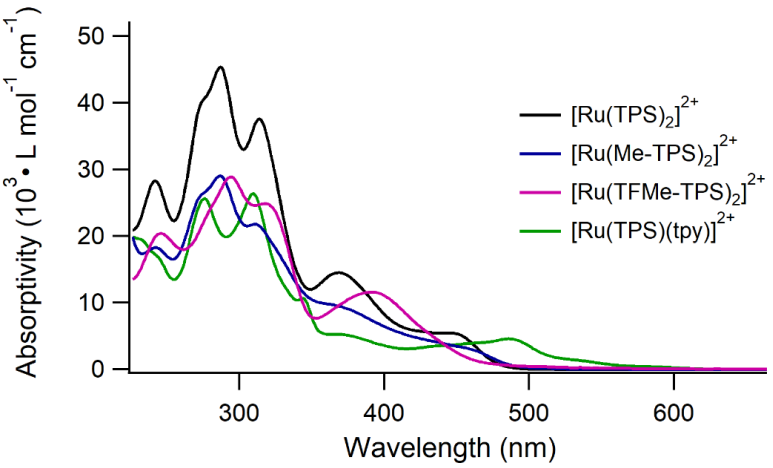

Figure 2-2. UV-Vis spectra of [Ru(TPS)$_2$]$^{2+}$ family of complexes. Performed in degassed CH$_3$CN.

UV-Vis absorption spectroscopy was performed on complexes **22-25** in degassed acetonitrile. The spectra are shown in Figure 2-2 with selected peaks and their extinction coefficients shown in Table 2-2. Complex **22** exhibited two peaks in the visible (near visible) region at 369 and 445 nm. The peak at 445 nm is assigned to the ^{1}MLCT because the ^{1}MLCT state is the lowest energy state with a spin-allowed transition. The 445 nm peak is also considerably blue-shifted from **2** which absorbs at 475 nm. In [Ru(py)$_6$]$^{2+}$ (where py = pyridine) solvento complex, the maximum absorption lies at 345 nm.[67] A similar spectrum is obtained for **23** which has weaker absorption bands at 362 and 450 nm. These absorption bands, however, are more broad and have less structure than **22** possibly due to the *mer* and *fac* isomers that forms. Previous research from the Hanan Group has shown that the *fac* isomer has less absorptivity at this transition.[68] Further experiments that focus on isolating these two isomers would need to verify if a similar phenomenon is happening. However, no new absorption bands form despite the different conformations.

The [Ru(TFM-TPS)$_2$]$^{2+}$ species is different in this series as it only exhibits a blue-shifted spectrum compared to **23** and **22**. One single large absorption is seen at 391 nm with an extended

weak absorption to around 500 nm. It is possible that the two transitions exhibited in **22** above 330 nm coalesce into one feature when the 4 and 4″ positions are strong electron-withdrawing moieties; further experiments and DFT calculation would need to be carried out to confirm.

The heteroleptic complex **25** has a structured feature with two maxima at higher wavelengths than 330 nm at 365 and 489 nm. The feature at 489 nm has a structured absorption feature with several peaks ranging from 365 and 560 nm. A similar structured absorption has been reported for heteroleptic Ru(II) complexes where one tridentate ligand was tpy and the other was a **dppd** ligand which when chelated led to an expanded metallocycle as seen in complex **9**. Compared to the previously reported species, the work reported here shows significant blue-shifts where the TPS ligand has a weaker sigma donation compared to the **dppd** ligand found. Initial studies into possible NIR fluorescence of this compound has shown no evidence of fluorescence at room temperature despite its similar molecular structure and spectroscopic absorption profile to previously reported Ru(II) complexes with emission in the NIR.[69] The lack of emission at room temperature means that the energy barrier preventing TAIC is still overcome by ambient thermal energy. When cooled to 77 K, complex **25** emits a vibrant pinkish-red color by eye which denotes that the emissive ^{3}MLCT state is being populated seen in Figure 2-3. This also indicates that TAIC into the ^{3}MC at room temperature because the lack of emission at warmer temperatures indicates there is enough thermal energy to allow TAIC.

Figure 2-3 Emission of a dilute solution of 25 after being placed in liquid nitrogen (77 K) and irradiated with 365 nm light from a UV hand lamp.

2.4 Electrochemical Properties

Cyclic voltammetry (CV) was performed on complexes **22-25** as shown in Figure 2-4. The data are\ reported in Table 2-3. Each complex exhibited a single oxidation peak, Ru(II/III). However, these complexes were dissimilar for the reduction. Complexes **22** and **24** only have anodic reductions peaks while **23** and **25** have anodic and cathodic peaks. This indicates that the first reduction likely occurs on the tpy for **25** as well as the similar Ru(II/I) reduction potential as **2**; however, this does not explain the anomaly that **23** has both a cathodic and anodic peak.

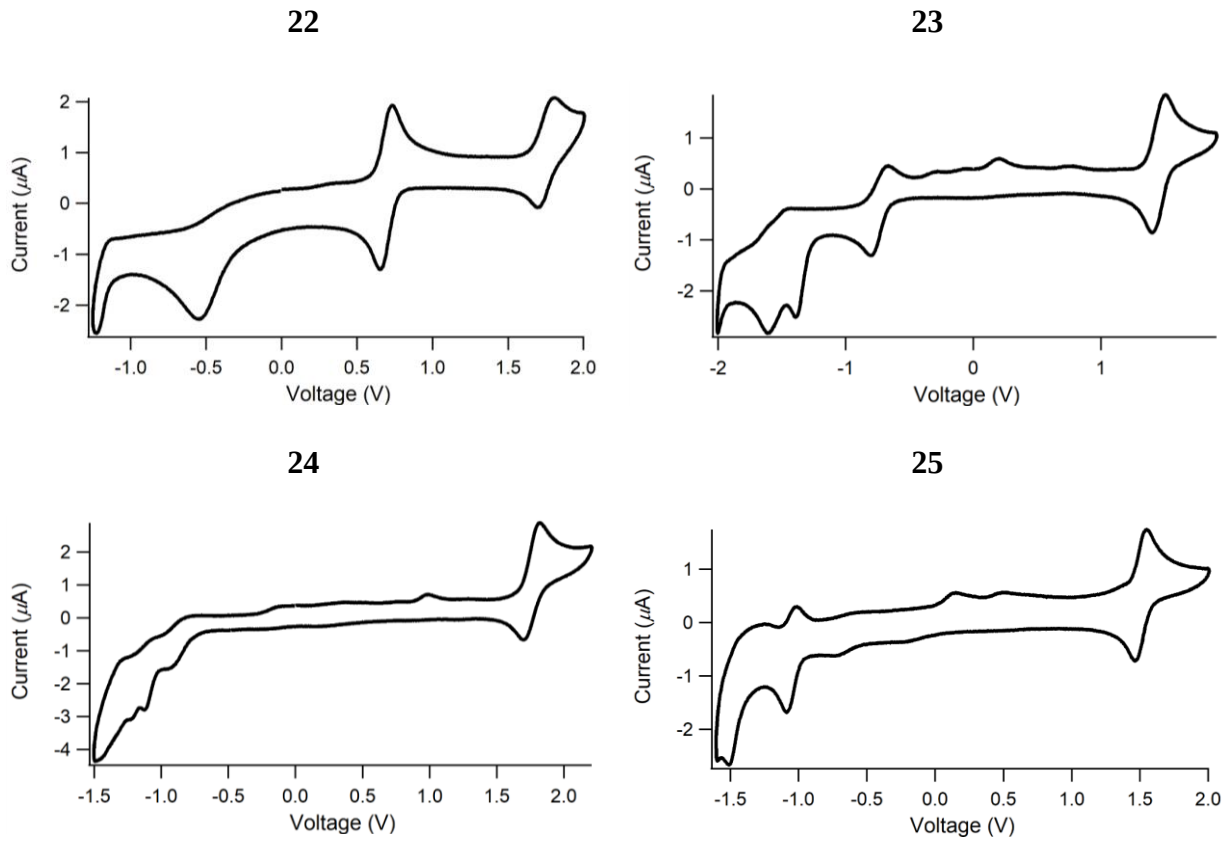

Figure 2-4 Cyclic voltammograms of complexes 22-25 in degassed MeCN. Ferrocene standard peak shown in 22 at 0.65 V. (0.1M TBAF, under N_2 atmosphere with a glassy carbon electrode, silver wire and platinum mesh electrode with a sweep rate of 100 mV/s with solute concentrations of 1 mM.)

Table 2-3. Potentials are in volts vs ferrocene in acetonitrile solutions. 0.1M TBAF, under N_2 atmosphere with a glassy carbon electrode, silver wire and platinum mesh electrode with a sweep rate of 100 mV/s with solute concentrations of 1 mM. The number in parentheses represents the difference between anodic and cathodic peaks (in millivolts).

Compound	E_{ox}	E_{red}	E_g
22	1.06(120)	–1.24	2.30
23	0.92(110)	–1.31, -1.96, -2.17	2.23
24	1.30(110)	–1.33,-1.64, -1.74	2.63
25	0.97	–1.56, -2.08	2.53
2	0.92	–1.67	2.59

When compared to complex **2** redox couple values, complex **22** has a Ru(II/III) couple 140 mV higher in potential, and the Ru(II/I) is less negative by 430 mV. Taken all together, the difference between the two couples for complex **22** is 300 mV smaller than that of complex **2**, $[Ru(tpy)_2]^{2+}$. This corresponds to a decrease in the MLCT state which serves as the HOMO for Ru(II) polypyridyl complexes. Additionally, the LUMO is raised significantly in energy.

By adding a methyl group to the 4 and 4″ positions, complex **23** exhibits a lower Ru(II/III) couple than **22** as well as the tpy reduction being less negative. The first reduction is also 90 mV less negative that $Ru(tpy)_2^{2+}$. For **22** and **23**, the lower first reduction energy demonstrates that **TPS** not only relieves geometric strain around the Ru(II), but that this reduction in strain also significantly reduces the energy gap between the HOMO and LUMO of these complexes. Additionally, the absorption spectra of these two complexes show the expected redshift that the electrochemical results would imply.

For all complexes **22-25**, there were not multiple oxidation peaks which supports the fact that the sulfides on the ligand are not prone to electrochemical oxidation when complexed to the metal. This supports the conclusion that the ligands do not dissociate when electrochemically oxidized on the timescale of the cyclic voltammetry experiment, especially as the anodic and cathodic peaks are similar in intensity. The difference in cathodic and anodic peaks for the oxidation support that the oxidation is quasi-reversible.

In complex **24** the Ru(II/III) redox couple is at 1.30 V which is 380 mV higher than $Ru(tpy)_2^{2+}$ and significantly higher than complex **23** and **22** as shown in Figure 2-4. The difference between the anodic and cathodic waves is 110 mV which indicates quasi-reversibility. The first reduction potential is -1.33 V for complex **24** which is slightly less negative than **22**. With no cathodic peak present, it is assumed that the first reduction is irreversible as there is no positive current indicating the oxidation of Ru(I) back to Ru(II) . The higher oxidation potential is most likely related to the electron-withdrawing strength of the CF_3 moiety in the 4 and 4″ positions. The CF_3 groups pull electron density away from the metal making the oxidation from Ru(II)/Ru(III) couple requiring a higher potential. The relatively unchanged reduction potential is expected as the reduction occurs on the tpy ligand, so the unmodified tpy does not have a significant change electronically.

The heteroleptic compound **25** has an oxidative potential at 0.97 V vs the ferrocene couple which is lower than complex **2** and **3**, and only 50 mV higher than complex **22**. Additionally, the reduction potential of –1.56 V vs. ferrocene is more negative than in $[Ru(tpy)]^{2+}$ and the family of **22** complexes by 160 mV and ~250 mV respectively. The more negative reduction potential for heteroleptic compounds with expanded tridentate ligands and tpy have been observed by other research groups as well.[49]

Complex **23** is unique in this series because its first reduction is reversible while the other homoleptic compounds do not have a reversible first reduction potential. It also has two different *fac* and *mer* isomers. The cathodic current for the first reduction is also not as large as the current in the cathodic oxidation potential of complex **23** which implies that not all of the complex is active for the oxidation from Ru(I) to Ru(II). Despite the two isomers of **23**, the oxidation only shows one peak with a 110 mV difference between anodic and cathodic sweeps which is no different than for the homoleptic complexes **22** and **24**. Complex **23** also has the lowest Ru(II/III) potential out of all these species. The donating ability of the methyl group likely increases the electron density on the metal making the complex easier to oxidize. The opposite happens with **24** where the withdrawing power increases the oxidation potential.

Table 2-4 Lever Electrochemical Parameters (E_L) calculated from the data in

Table 2-3

Compound	E_L (V)	E_L / pyridine (V)
18	0.53	0.18
19	0.46	0.15
20	0.65	0.22

tpy	0.46	N/A

Table 2-4 shows the Lever electrochemical parameters for the ligands.[70] Each ligand has a higher E_L than **2,** which is expected as the conjugation is broken by the sulfur atom between the pyridyl rings. The E_L for ligand **18** was calculated from complex **22**. When using the values from Table 2-4, the Ru(II/III) couple can be predicted for complex **25**. When these two values are added together, the predicted value is 0.99 V for the Ru(II/III) couple for the heteroleptic complex **25**. The experimental value was 0.97 V.

When comparing the ΔE between the Ru(II/III) and Ru(II/I) couples, the energy values obtained correspond with the absorption spectra for these complexes. The first oxidation is usually assigned to removing an electron from the t_{2g} metal-centered orbitals, and the first reduction is assigned to the π^* ligand-based orbital. As seen in Figure 1-4, these orbitals correspond to the HOMO-LUMO gap as well; thus, the lowest energy transition can be assigned to the GS $\rightarrow$ ^{1}MLCT absorption. The most blue-shifted complex, **24**, has the largest difference between redox couples probed which is expected. Complex **23** also was the most red-shifted homoleptic complex while also having the smallest ΔE. In the case of the heteroleptic complex **25**, the absorption spectrum correlates well with the redox couples especially considering that **25** also has structured absorption and the cyclic voltammogram shows several peaks where the Ru(I/II) reduction. This is not unprecedented for these heteroleptic complexes as complex **9** displays similar properties with a significantly red-shifted and structured absorption spectrum with multiple tpy ligand reductions.

2.5 Conclusions

Four different polypyridyl pro-ligands **18-21**with a sulfur-atom bridge between the pyridyl rings were successfully synthesized. Pro-ligands **18-21** were then chelated to Ru(II) to form three new homoleptic complexes, **22-24** and one heteroleptic complex, **25**. In complexes **22-25**, the expansion of the metallocycle to a six-membered ring relieves the distortion away from an octahedral structure that $[Ru(tpy)_2]^{2+}$ has about its Ru(II) center as shown in structures obtained from X-ray crystallography. As shown in complex **22** with only hydrogen in 4 and 4″ position, the redox potential of ruthenium(II/III) is reduced due to the increased ligand-field splitting due to the decreased distortion. However, the sulfide-bridge disturbs the extended conjugation that is seen in tpy ligands; thus, the ^{1}MLCT absorption in the UV-Vis spectrum is significantly blue-shifted. By modifying the 4 and 4″ positions on the pendant pyridyl rings on the ligands as shown in complexes **23** and **24**, the redox potentials can be altered by the activating efficiency of the attached moiety. In conjunction with changing the redox potentials, modification of the 4 and 4″ positions can shift the ^{1}MLCT absorption significantly as seen in complex **24** with the CF_3 group in those positions, leading to a coalescence of the higher energy absorption at 345 nm and the ^{1}MLCT transfer usually seen around 475 nm in $Ru(tpy)_2^{2+}$.

Complex **23** was different from the other homoleptic complexes as it shows almost a 1:1 mixture of *mer* and *fac* isomers that were inseparable by column chromatography and recrystallization techniques. The X-ray crystallography shows that these two isomers co-crystallize with one another in the same asymmetric unit cell. This is also corroborated by NMR spectroscopy to exist in a 1:1 ratio in the solution state as well. The existence of two isomers in solution, however, does not give rise to significant changes in ruthenium (II/III) oxidation potentials or change in the UV-Vis spectrum. The formation of the *fac* isomer was only seen for

23 and no evidence was found in **22** and **24** that the *fac* isomer was synthesized even in trace amounts.

The heteroleptic complex, **25**, is not directly comparable to the homoleptic complexes **22-24**. It has a comparable ruthenium (II/III) redox couple to Complex **2** (Chart 1-2) and has a structured absorption band at what is assigned to be the ^{1}MLCT absorption. Similar structured absorptions have been seen before in other works of expanded metallocycle ruthenium complexes. In work by the Heinze group, the absorption band is more red-shifted however than the heteroleptic complex here.[71] This is because complex **25** has less donating capability, and more donating groups at the 4 and 4″ positions would red-shift this absorption since the HOMO-LUMO energy gap is lowered by the stabilization of the ^{1}MLCT state. Unlike in the work by Heinze, complex **25** does not emit in the red or near-infrared in degassed acetonitrile at room temperature. When cooled to 77 K, the complex in non-deaerated acetonitrile will emit a pink-red color by eye, but this was not examined quantitatively.

2.5.1 Future work

The original intent of this work was to examine how the different oxidation states of the sulfur change the electrochemical and photophysical properties of the ruthenium complex which is why the sulfone-bridged ligand was synthesized. However, it was found that the sulfone-bridged species did not chelate to ruthenium even in trace amounts.

The newly synthesized complexes have the potential to be oxidized at the sulfur atom for post-synthetic modification of the complex. There was no observation of these sulfur sites becoming oxidized despite some samples being left in solution for over a month, and samples did not decompose while stored in the solid state. More effort could be focused on seeing if there is a viable way to oxidize these sulfur groups that would not require intensive synthetic or purification

techniques. For example, introducing a mild oxidizing agent to a solution of complex **22** could stimulate the oxidation of the sulfur bridges. As the results in this work show that the completely oxidized sulfone groups do not chelate to the ruthenium center, the ligands upon oxidation at the sulfur could dissociate from the ruthenium center. This could have potential applications for drug delivery with clever ligand design. In the immediate future, the synthesis of proligands with more donating groups in the 4 and 4″ positions would create a more complete picture of the trends of how activating groups affect the photochemical and electrochemical properties of these compounds. It is encouraging that the heteroleptic complex **25** synthesized in this work has strong emission by eye when cooled, suggesting that an increased ΔE in a similar complex could allow for room temperature emission. By adding a methoxy group or extending the conjugation at the 4 and 4″ positions, it could stabilize the ^{3}MLCT state to lower ΔE between the ^{3}MC and ^{3}MLCT states to allow for phosphorescence at room temperature in a heteroleptic compound similar to **9**. This behavior is seen in the work done by Heinze group, so it is not unprecedented. Further tuning at the 4′ position can be explored as there is literature where the 4′ position is modified especially in terpyridine ligands. Altering the 4 and 4″ positions simultaneously change the electronics of the complex more aggressively as a homoleptic complex with modified 4 and 4″ positions will have a total of four groups rather than two groups if the 4′ position is changed in a homoleptic compound. Modification of the 4 and 4″ position also makes it difficult to create a push/pull system whereas modification of the 4′ position allows for facile synthesis of push/pull type complexes.

2.6 Experimental

2.6.1 General Considerations

Reactions were performed under air unless specified in methods. $RuCl_3$(tpy) and $Ru(DMSO)_4Cl_2$ were synthesized from $RuCl_3$ hydrate using previously reported methods. 2-

mercaptopyridine, ferrocene, tetrabutylammonium hexafluorophosphate and 2,6-dibromopyridine were purchased from Sigma Aldrich and used as is. 2-chloro-4-trifluoromethylpyridine was purchased from Matrix Scientific. 2-hydroxy-4-methylpyridine and Pd/C (10% Pd, type 487, dry) were purchased from Alfa Aesar. $AgPF_6$ and NH_4PF_6 were purchased from Strem and used as is. Ferrocene was purchased from Sigma Aldrich and recrystallized. Tetrabutylammonium potassium hexafluoride (TBAF) was recrystallized three times from ethanol and kept under dry conditions. All other reagents were also purchased from Sigma Aldrich. Solvents used were purchased from Sigma Aldrich except for EtOH which was distilled at UBC. Thiols/thiones were prepared from previously reported methods.[72,73] Disulfides are prepared using previously reported methods.[74] Solvents were from Sigma-Aldrich except for ethanol which is distilled at UBC. NMR Solvents were either from Sigma-Aldrich or from Cambridge Isotopes. UV-Vis spectroscopy was performed on a Varian-Cary 5000 UV-vis-near-infrared spectrophotometer. ^{1}H, ^{13}C and 2D NMR spectroscopic experiments were performed on Bruker NMR spectrometers (300 and 400 MHz) and referenced to the residual solvent peaks. UV-Vis spectrometry was performed on a Varian Cary UV-vis-near-IR spectrophotometer.

Vapor diffusion experiments for single crystal growth was performed in a 20 mL scintillation vial with ~4 mL of diethyl ether. Inside the 20 mL scintillation vial, 1.0-5.0 mg of the sample were placed in a smaller 5 mL scintillation vial with ~1 mL of MeCN. The 20 mL scintillation vial was then capped and sealed with parafilm. The samples were left in a dark cabinet until crystals formed (after 5-14 days).

Electrochemistry was performed under inert conditions in an airtight three-electrode cell in N_2 sparged MeCN. A glassy carbon electrode (working electrode), silver wire (reference electrode) and platinum mesh (counter electrode) was used for cyclic voltammetry with a sweep

rate of 100 mV/s with solute concentrations of 1 mM and counter-ion (TBAF) concentrations of 1 mM. Sweep rates of the cyclic voltammetry experiments were held at 100 mV/s. Potentials are measured vs Ferrocene as an internal standard.

2.6.2 Methods

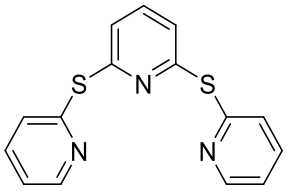

2,6-bis(pyridin-2-ylthio)pyridine (TPS) (18**)** To a 250 mL round bottom flask containing 50 mL of dimethylformamide 2,6-dibromopyridine (1.25 g, 5.29 mmol, 2.4 eq), of 2-mercaptopyridine (1.4 g, 12 mmol, 1 eq) and potassium carbonate (1.7 g, 12 mmol, 1 eq) were added. This heterogenous mixture was heated to reflux which resulted in dissolution of all contents. The solution was stirred at reflux under air for twelve hours. Then, the DMF was removed using a rotary evaporator. The remaining residue was dissolved in DCM and then extracted three times with water and then washed with brine. The final product was a clear golden oil. Isolated yield 1.3 g (82%). ^{1}H NMR (400 MHz, DCM-d_2) δ 8.53 (ddd, J = 4.9, 2.0, 0.9 Hz, 2H), 7.62 (td, J = 7.7, 1.9 Hz, 2H), 7.57 (t, J = 7.8 Hz, 1H), 7.47 (dt, J = 8.0, 1.0 Hz, 2H), 7.29 (d, J = 7.8 Hz, 2H), 7.20 (ddd, J = 7.5, 4.9, 1.1 Hz, 2H).

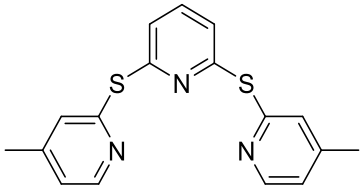

2,6-bis((4-methylpyridine-2-yl)thio)pyridine **(Me-TPS)(**19**)** To a 100 mL Schlenk flask, 2,6-dibromopyridine (0.24 g, 1.0 mmol, 1 eq) , **Me-DSF** (0.30 g, 1.2 mmol, 1.2 eq) 0.12 g of sodium hydroxide and 2 mL of dimethyl sulfoxide were added. After 12 hours, the flask and its contents

were allowed to cool and then the solution was diluted in a large volume of water (more than 50 mL) and then extracted with methylene chloride three times. The final product was then purified using column chromatography with methylene chloride as the eluent. The final product was a clear, orange oil. Despite small amount of impurities shown in ^{1}H NMR, the product was used to chelate to Ru(II). Yield 0.20g (61%). 1H NMR (400 MHz, DCM-*d*2) δ 8.67 (s, 2H), 7.71 (d, J = 8.3 Hz, 3H), 7.49 – 7.31 (m, 4H), 1.57 (t, J = 2.4 Hz, 6H).

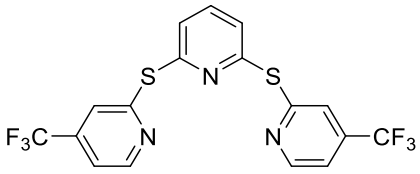

2,6-bis((4-(trifluoromethyl)pyridine-2-yl)thio)pyridine **(TFM-TPS)(**20**)** To a 100 mL Schlenk flask **CF_3-DSF** (0.39 g, 1.1 mmol, 1.2 eq), and 2,6-dibromopyyridine (0.22 g, 0.94 mmol, 1eq) and 2 mL of DMSO was added. The flask was then sealed, and the flask heated to 120 ˚C for 12 hours. The solution turned to a dark brown color as the reaction proceeded. The same procedure as **19** was then followed. The final product solidified into an off-white solid. The product was used without further purification despite impurities present. Yield 0.11 g (27%). ^{1}H NMR (400 MHz, DCM-d_2) δ 8.67 (d, J = 5.1 Hz, 2H), 7.73 – 7.67 (m, 3H), 7.45 (d, J = 7.8 Hz, 2H), 7.39 – 7.34 (m, 2H)

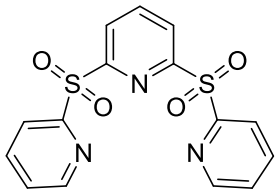

2,6-bis(pyridin-2-ylsulfonyl)pyridine **(SO_2-TPS)(21)** To a 20 mL scintillating vial, **18** (0.250 g, .842 mmol) was added to a solution of 30% H_2O_2, (1.26 mL), EtOH (10 mL), and 10% Pd/C (0.020g). This was stirred for 24 hours at 60 ˚C. The solution as the reaction proceeded turned a cloudy grey color. The reaction mixture was monitored by TLC to determine when all the react and intermediates were completely used up. After 24 hours, the reaction had not progressed fully to completion, so another portion of 30% H_2O_2 and Pd/C were added. After another 24 hours and all the starting materials was consumed as determined by TLC, the solution was then extracted three times using DCM. The organic layer was then filtered through a frit filter and Celite and washed several times with 10 mL of DCM. The solution was then collected and evaporated using a rotary evaporator. A white powdery solid formed. The yield was quantitative, 0.360 g (99%). ^{1}H NMR (400 MHz, MeCN-*d*3) δ 8.48 – 8.43 (m, 5H), 8.06 (dt, J = 7.9, 1.1 Hz, 2H), 7.98 (td, J = 7.7, 1.7 Hz, 2H), 7.57 (ddd, J = 7.6, 4.7, 1.2 Hz, 2H).

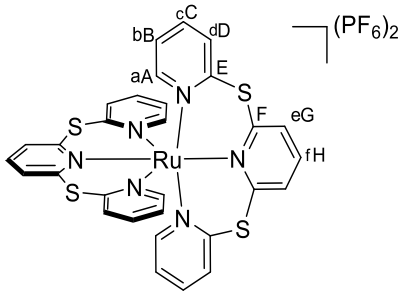

[Ru(TPS)$_2$](PF$_6$)$_2$ (22***)***- To a solution of 10 mL of 1:1 water and ethanol in a 50 mL three-necked round bottom flask, 0.050 g of $RuCl_3$ (.050g, 0.24 mmol, 1 eq), 0.125 g of **TPS** (0.125 g, 0.420 mmol, 1.8 eq), and 0.150 g of $AgPF_6$ (0.150 g, 0.595 mmol, 2.5 eq) were added. The solution was stirred and heated to reflux where it was a brown cloudy solution. It was left at reflux for 12 hours. After 12 hours, the flask was removed from heat and cooled. Once cool, it was filtered over a frit with Celite filter agent. A yellow solution was collected after washing the Celite with acetone. The collected solution was then reduced using rotary evaporation, and then reconstituted in 2-3 mL of acetonitrile. This was added dropwise to a 20 mL solution of saturated NH_4PF_6 where a yellow solid immediately precipitated. The solid was collected using vacuum filtration where it was washed with three portions of water (~5 mL) and one portion of diethyl ether (~10 mL). The collected solid was then columned on silica gel with a 90:10:1 eluant composed of 90 parts acetonitrile, 10 parts water and 1-part saturated aqueous solution of potassium nitrate. (R_f =0.40 on silica TLC plate). The yellow portion was collected and recrystallized in aqueous NH_4PF_6 yielding 0.13 g of $Ru(TPS)_2(PF_6)_2$. The product was a yellow powder. Yield 53%. ^{1}H NMR (400 MHz, DCM-d_2) δ **a** 8.53 ddd(4H),**c** ddd 7.62 (4H), **f** t 7.57 (2H), **e** d 7.49 (4H),**d** d 7.29 (4H), **b** ddd 7.21 (4H). ^{13}C **F** 157.50, **E** 156.28, **A** 150.09, **H** 137.77, **C** 136.98, **G** 126.34, **D** 122.98, **B** 121.96. *hydrogens labeled in lowercase; uppercase denotes carbons.

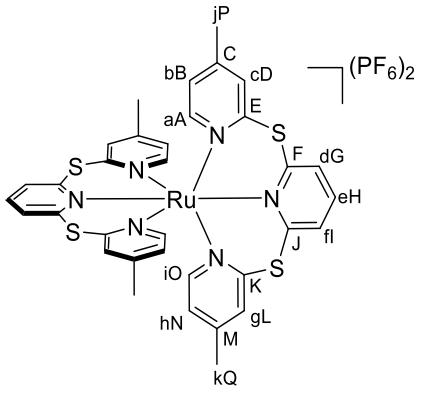

[Ru(Me-TPS)$_2$](PF$_6$)$_2$ **(**23**)** – To a solution of 10 mL of 1:1 water and ethanol in a 50 mL three-necked round bottom flask, $RuCl_3$ (0.022 g, 0.11 mmol, 1 eq), Me-TPS (0.080 g,0.24 mmol, 2.2 eq), and 0.100 g of $AgPF_6$ (0.100 g, 0.397 mmol, 3.6 eq) was added. The solution was stirred and heated to reflux for 12 hours where it was a brown cloudy solution. The flask was then removed from heat and cooled. Once cool, it was filtered over a frit with Celite. A yellow solution was collected after washing the Celite with acetone. The collected solution was then reduced using rotary evaporation, and then reconstituted in 2-3 mL of acetonitrile. This was added dropwise to a 20 mL solution of saturated NH_4PF_6 where a yellow solid immediately precipitated. The solid was collected using vacuum filtration where it was washed with three portions of water (~5 mL) and one portion of diethyl ether (~10 mL). The collected solid was then columned on silica gel with a 90:10:1 eluant composed of 90 parts acetonitrile, 10 parts water and 1-part saturated aqueous solution of potassium nitrate. (R_f =0.40 on silica TLC plate). The yellow portion was collected and recrystallized in aqueous NH_4PF_6 yielding 0.050 g of $Ru(CH_3\text{-stpy})_2(PF_6)_2$. The product was a yellow powder. Yield 58%. ^{1}H NMR (400 MHz, DCM-d_2) δ ***Fac*- a** 8.96(d, J=6.3Hz, 2H), **i** 8.55(d,J=6.2 Hz, 2H), **ce** 7.78-7.71 (m, 4H), **g** 7.62 (s, 2H), **d** 7.59 (d, J=6.3 Hz, 2H), **bf** 7.53-7.48 (m, 4H), **h** 7.24 (d, J=8.5, 2H), **j** 2.49 (s, 6H), **k** 2.42 (s, 6H) ***Mer*- ab** 7.97 (s (or m) 6H), **c** 7.69 (s, 4H), **e** 6.90(d, J=6.1 Hz, 4H), **d** 6.80 (d, J= 4.2 Hz,p 4H), **f** 2.39 (s, 12H). ^{13}C ***Fac*- J** 162.37, **F** 161.97, **A** 156.96, **O** 156.41, **E** 154.64, **K** 153.57, **C** 152.63, **M** 152.31, **H** 138.10, **D** 129.46, **L** 129.21, **B** 126.76, **G** 126.40, **N** 126.02, **I** 125.51, **P** 19.48, **Q** 19.40 ***Mer*- C** 159.36, **D** 155.98, **H** 155.29, **F** 151.66, **A** 138.83, **B** 130.12, **E** 128.10, **G** 126.88, **I** 19.68. *lowercase denotes hydrogens; uppercase denotes carbons. The *fac* isomer has equivalent proton environments for

both ligands while the *mer* isomer has equivalent proton environments for both ligands, and the protons **a-e** are equivalent on each side of the ligand.

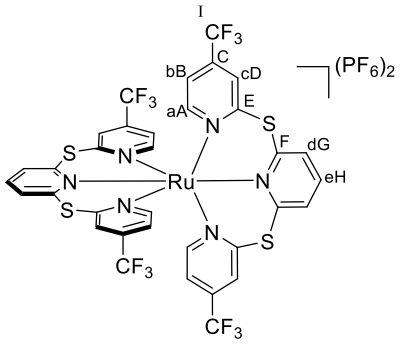

[Ru(TFM-TPS)$_2$](PF$_6$)$_2$ **(**24**)** – To a 10 mL solution of 1:1 water and ethanol, 0.050 g of $Ru(DMSO)_4Cl_2$ (.050 g, 0.10 mmol, 1 eq) and TFM-TPS (0.100 g, 0.231 mmol, 2.3 eq) were added in a 50 mL three-necked round bottom flask. The solution was then heated to reflux for 12 hours. After 12 hours, the flask was removed from heat, allowed to cool, and then the volume was reduced using rotary evaporation. After a majority of solvent was evaporated (1-2 mL left), the residue was then added dropwise to a 20 mL saturated solution of ammonium hexafluorophosphate where a burnt orange precipitate immediately formed. The heterogeneous mixture was then filtered using vacuum filtration. The collected precipitate was then washed in three portions of ~5 mL of water and one portion of ~10 mL of ether. The product was a burnt orange powder. Mass of collected product 0.098 g. Yield 77%. ^{1}H NMR (400 MHz, DCM-d_2) δ **d** s 8.19 (4H), **ef** s 8.09 (6 H), **a** d 7.34 (4H), **b** d 7.24 (4H). ^{13}C **D** 159.22, **C** 157.97 **H** 157.84, **A** 139.88, **F** 139.13 (q, J= 35.5 Hz) **B** 131.27, **E** 124.53 (q, J= 3.7 Hz), **I** 122.02 (q, J= 273.3 Hz), **G** 121.88 (q, J= 3.6 Hz) *lowercase denotes hydrogens; uppercase denotes carbons.

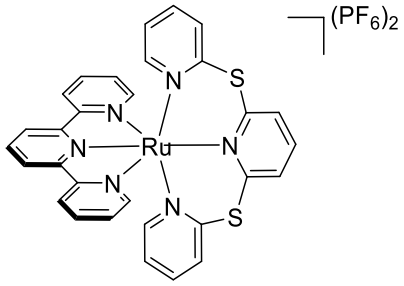

[Ru(TPS)(tpy)](PF$_6$)$_2$ (25***)*** – To a solution of 10 mL of ethanol in a 50 mL three-necked round bottom flask, RuCl$_3$(tpy) (0.100 g, 0.213 mmol, 1 eq), TPS (0.080 g, 0.26 mmol, 1.2 eq) and AgPF$_6$ (0.100 g, 0.397 mmol, 1.8 eq) were added. This brown and cloudy solution was stirred and heated to reflux. It was left at reflux for 12 hours. Over the 12 hours, the solution slowly turned more red. Afterward, the solution was removed from heat and left to cool. It was then vacuum filtered through a frit and Celite and washed with acetone until no red coloration remained in fresh filtrate. The filtrate was then reduced using rotary evaporation. The residue collected was reconstituted in 1-2 mL of acetonitrile. This was then added dropwise to a 20 mL solution of saturated NH$_4$PF$_6$. The precipitate that formed was collected using vacuum filtration, washed with three portions of 5 mL of water, and one portion of 10 mL ether. The red powdery solid was collected and then purified via column chromatography. Silica gel was used for the column and the eluant was 100 parts acetonitrile, 10 parts water and 1-part saturated aqueous KNO$_3$. The R$_f$ was 0.45 on silica TLC plate. The red fraction on the column was collected. 0.039 g was collected. The final product was a red powder. Yield 58%. ^{1}H NMR (400 MHz, MeCN-*d$_3$*) δ 8.58 (d, J = 5.6 Hz, 1H), 8.53 (d, J = 8.1 Hz, 1H), 8.42 (d, J = 8.1 Hz, 1H), 8.27 (dd, J = 8.0, 4.6 Hz, 1H), 8.20 – 8.13 (m, 0H), 8.06 (t, J = 7.8 Hz, 1H), 7.69 (d, J = 7.8 Hz, 1H), 7.62 (t, J = 7.7 Hz, 1H), 7.40 (t, J = 6.7 Hz, 1H), 6.89 (t, J = 6.9 Hz, 1H), 6.74 (d, J = 6.0 Hz, 1H).

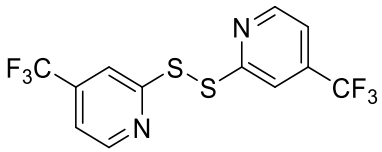

1,2-bis(4-(trifluoromethyl)pyridin-2-yl)disulfide (CF$_3$-DSF) **(**26**)** To 50 mL of methylene chloride in a 100 mL round bottom flask 4-trifluoromethyl-2-mercaptopyridine (0.42 g, 2.3mmol, 1 eq) and potassium permanganate (2.0 g, 12 mmol, 6 eq) was added. This was allowed to stir over three hours. The solution was then filtered through Celite and a frit to remove potassium permanganate and its byproducts. This was then washed thoroughly with additional methylene chloride. The solvent from the filtrate was then removed using rotary evaporation. The final product was collected as a white powder in essentially quantitative yield. Isolated yield 0.40g (96%). The compound was used without further purification.

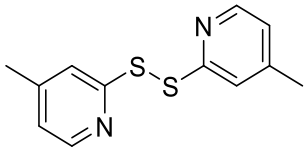

1,2-bis(4-methyl)pyridin-2-yl)disulfide (CF$_3$-DSF) **(**27**)** To 16 mL of methylene chloride in a 50 mL round bottom flask, 4-methyl-2-mercaptopyridine (0.97 g, 7.8 mmol, 1 eq) and potassium permanganate (3.8 g, 24 mmol, 3 eq) were added. This was allowed to stir for one hour. The solution was then filtered through Celite and a frit to remove potassium permanganate and its byproducts. This was then washed thoroughly with additional methylene chloride. The solvent from the filtrate was then removed using rotary evaporation, giving a white powdery solid. The yield was not quantitative, most likely due to the shorter reaction time. Isolated yield 510 mg (51%). The compound was used without further purification.

Chapter 3: Mononuclear and Dinuclear Ruthenium(II) Sulfoxide Complexes

As discussed in Chapter 1, Ru(II) polypyridyl complexes have been shown to be photoactive due to their accessible and reactive charge transfer states. One of the more interesting photoactive processes is linkage photoisomerization. As discussed in Section 1.6, photoisomerization is defined as a change in molecular structure that is induced by the absorption of light. These processes are generally considered reversible as well, meaning that the molecule or complex of interest returns to the original state. Ru(II) complexes have shown a few different photoisomerization processes, with one of the more recent and interesting being the sulfoxide linkage photoisomerization discovered by Rack and Mockus in 2003 as shown in Figure 3-1.[75]

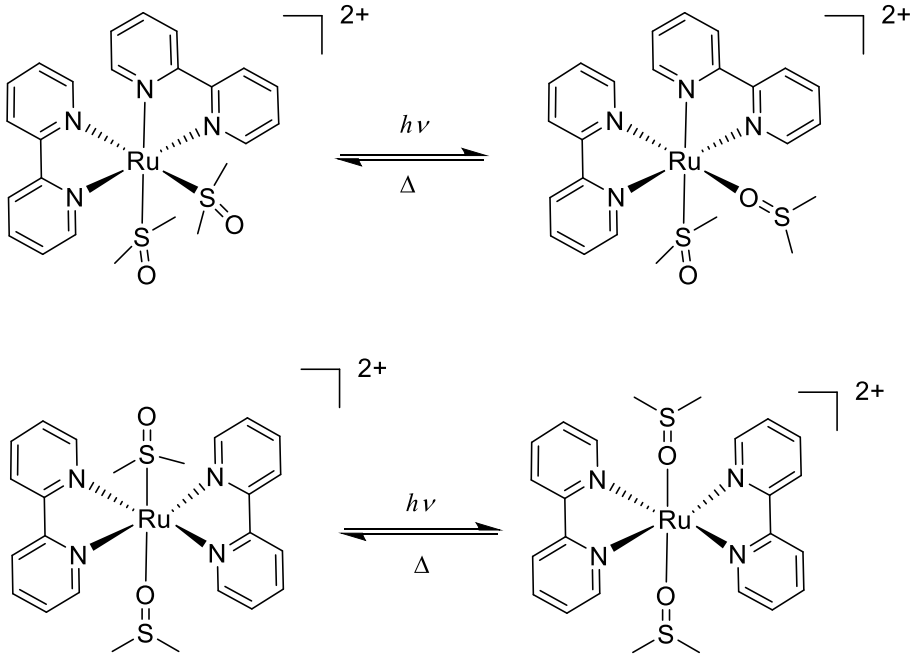

Figure 3-1 Photoisomerization of $Ru(bpy)_2(DMSO)_2$, both isomers shown.

They found that both the *cis*- and *trans*-$Ru(bpy)_2(DMSO)_2]^{2+}$ undergo photoisomerization when irradiated with blue light. This photoisomerization also, unsurprisingly, comes with a change in absorption spectra where the ^{1}MLCT absorption band shifts from 348 nm to 420 nm. However,

the complex, unlike $Ru(bpy)_2(H_2O)_2]^{2+}$ in Section 1.6, does not undergo *cis*/*trans* photoisomerization, and only undergoes isomerization when heated in neat DMSO.

The next decade saw the development of this phenomenon where the photoisomerization could occur with a bidentate ligand which increases the stability of the complex by tethering the sulfoxide to the Ru(II) center, as seen in **28** (Chart 3-1) where photoejection of the sulfoxide ligand would be less likely.[61] Additionally, only one sulfoxide moiety for each Ru(II) was used, and the process simplified in some complexes by eliminating the possibility of *cis*/*trans* isomerization. These tethered sulfoxide complexes offer a more robust platform to modify and tune the photoisomerization for the desired absorption spectra, thermal reversibility or photoisomerization wavelengths.

Chart 3-1

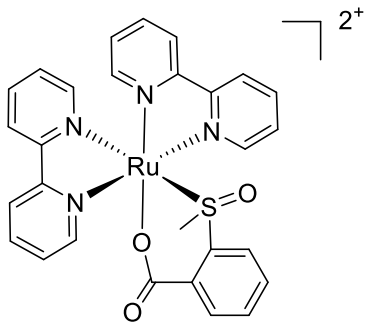

28

Despite Ru(II) sulfoxide complexes being specifically designed to avoid the ejection of the sulfoxide ligand, the photolabilization of a monodentate ligand can have useful applications. For example, the photoejection of a monodentate ligand can be used in targeted photodynamic therapy (PDT).[58] Ru(II) complexes with a drug payload as a monodentate ligand can selectively release the therapeutic agent wherever it is irradiated with light that results in the ejection of the ligand. Work has been done on using Ru(II) complexes for photodynamic therapy where the metal

complex can deliver a drug molecule with a pyridyl ligand.[76] These Ru(II) polypyridyl complexes are generally stable over the lifetime of a drug in the body despite having a photolabile ligand. If this ligand is a drug molecule then it can be selectively released by irradiating the desired area for therapeutic treatment. Specifically, work has been done on using Ru(II) for PDT where the Ru(II) can deliver a drug molecule with a nitrile moiety such as 5-cyanouracil in Ru(II) complex such as **29** (Chart 3-2).[76]

Chart 3-2

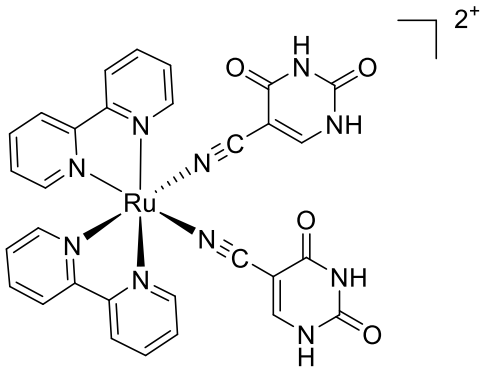

29

Due to the photoreactivity of the Ru(II) polypyridyl complex, singlet oxygen can also be generated upon irradiation with light, essentially acting as both a delivery mechanism for nitrile- or pyridine-containing drugs and an active agent by production of singlet oxygen. However, current research for Ru(II) PDT has not looked into the potential of using dinuclear Ru(II) complexes. These complexes could have potential advantages over their mononuclear analogs as they could deliver two times the payload molecules and generate singlet oxygen.

For PDT, a complex that can undergo sulfoxide linkage photoisomerization is likely a good candidate for ligand photoejection. Indeed, Ru(II) sulfoxide complexes undergo similar photophysical processes as previously discussed in Chapter 1. Based on the previous work by Rack

and Turro, Ru(II) complexes like **29** that undergo photoejection and photoisomerization have promising applications for use pharmaceutically.[77] Thus in this work, the photophysical properties of sulfoxide ligands in dinuclear Ru(II) complexes were probed to further examine the light responsiveness and photoisomerization characteristics.

Two bis-sulfoxide ligands were chosen to examine the difference between conjugated and nonconjugated systems, and how electronics may affect communication between bridged Ru(II) metal centers. They also incorporate the sulfoxide in the bridging ligand itself. Two known bridging ligands were chosen as well to determine if there is "communication" between the two Ru(II) metal centers after one photoisomerization. These respective ligands are shown in Chart 3-3.

Chart 3-3

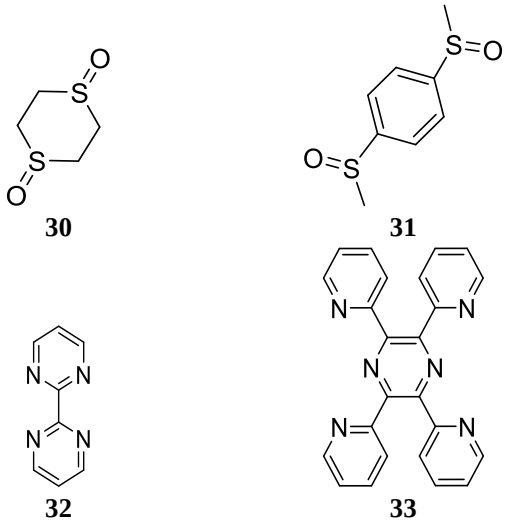

30 **31**

32 **33**

Specifically, five bridged Ru(II) complexes **34-38** (Chart 3-4) were synthesized and analyzed for dual photoisomerization where the bridging ligand was the monodentate **30** and **31**, and the bi- and tridentate **32** and **33.** For the Ru(II) complex with **32** as the bridging ligand,

photoactivity was probed using UV-Vis spectroscopy, however, further work is needed to determine if dinuclear Ru(II) complexes can be useful for applications in photodynamic therapy.

Chart 3-4

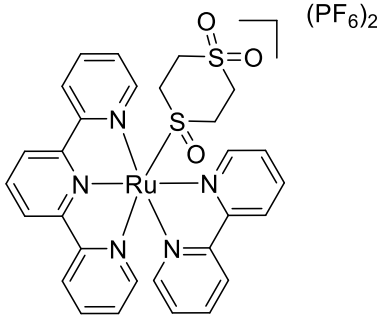

34

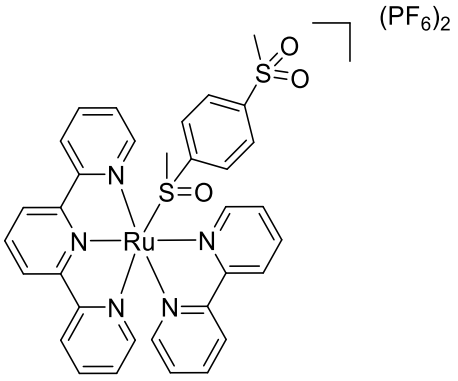

35

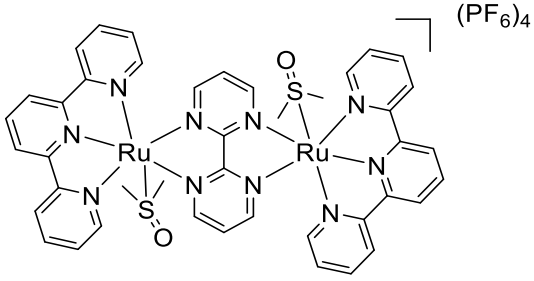

36

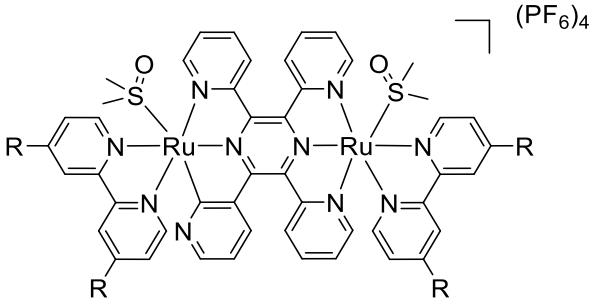

37 R = H
38 R = CH_3

3.1 Synthesis

The synthesis of complexes **34**-**38** is similar to what was discussed in Section 2.1.2. In general, the Ru(tpy)(bpy)Cl (**39**) precursor was synthesized using previously known methods,[78] and the coordination of the chosen sulfide pro-ligand was performed by heating to reflux the sulfide proligand (**30** and **31**) in ethanol with an equimolar amount of $AgPF_6$, as shown in Scheme 3-1. Afterward, the oxidation with *m*-CPBA was performed. Complex **35** was unable to be synthesized as the sulphone ligand did not stay coordinated to the Ru(II). As seen with proligand **21** in Chapter 2, the sulphone is more electron withdrawing than the sulfide hinders coordination.

With two sulphones on the molecule, the coordination of sulfur to the Ru(II) metal center is too weak. The oxidized dithiane ligand was able to be synthesized; however, the fully oxidized complex could not be totally purified and as seen in the ^{1}H NMR spectrum. The sulfurs of the heterocyclic ligand were not all completely oxidized, leading to the extra aliphatic peak from the dithiane heterocycle in the ^{1}H NMR.

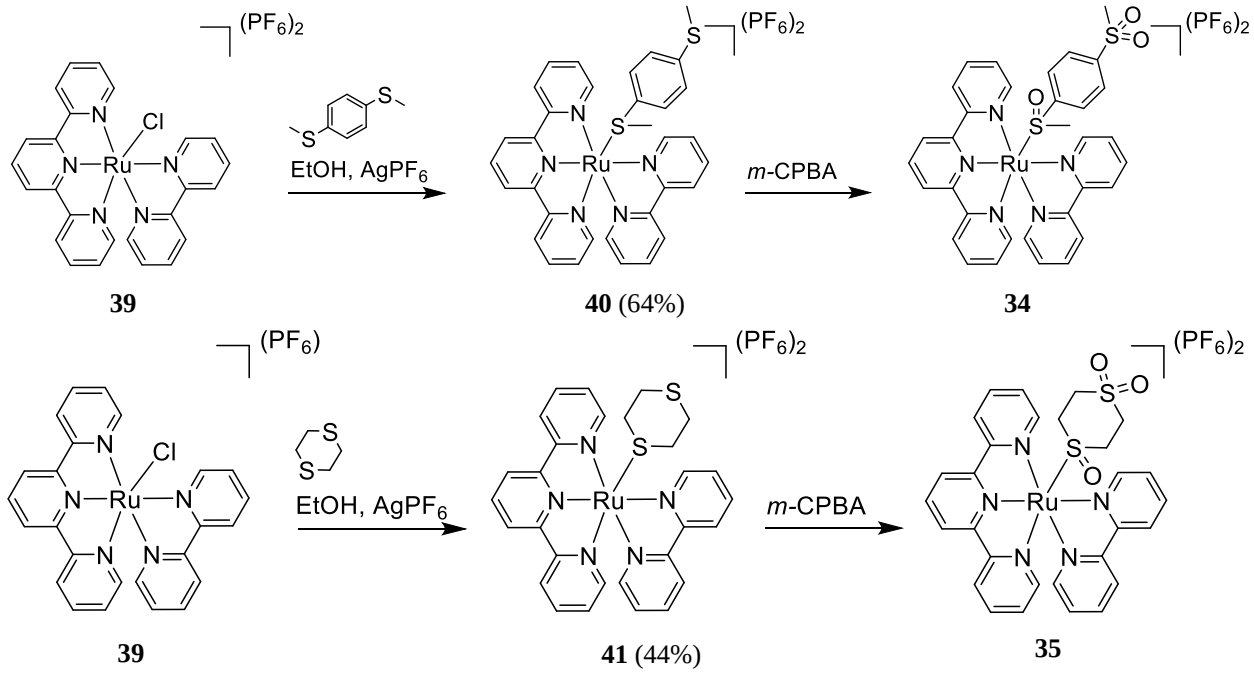

Scheme 3-1 Synthetic pathway for mononuclear Ru(II) sulfoxide complexes

When synthesizing dinuclear Ru(II) species **36**-**38**, the respective Ru(II) chloride with the tridentate ligand was formed to simplify the synthesis process by eliminating the possibility of different side products that can form when starting with the bidentate ligands. In the case of complex **36**, the Ru(tpy)Cl_3 precursor was reacted in a 2:1 ration of 2,2′-bipyrimidine to form complex **42**. The tpy was previously chelated to the Ru(II) metal center to avoid a mixture of Ru(II) bipyrimidine complexes that would form if starting with **30**. After isolating complex **42**, DMSO

was then substituted in the remaining coordination sites occupied by chlorine, yielding complex **36** as shown in Scheme 3-2.

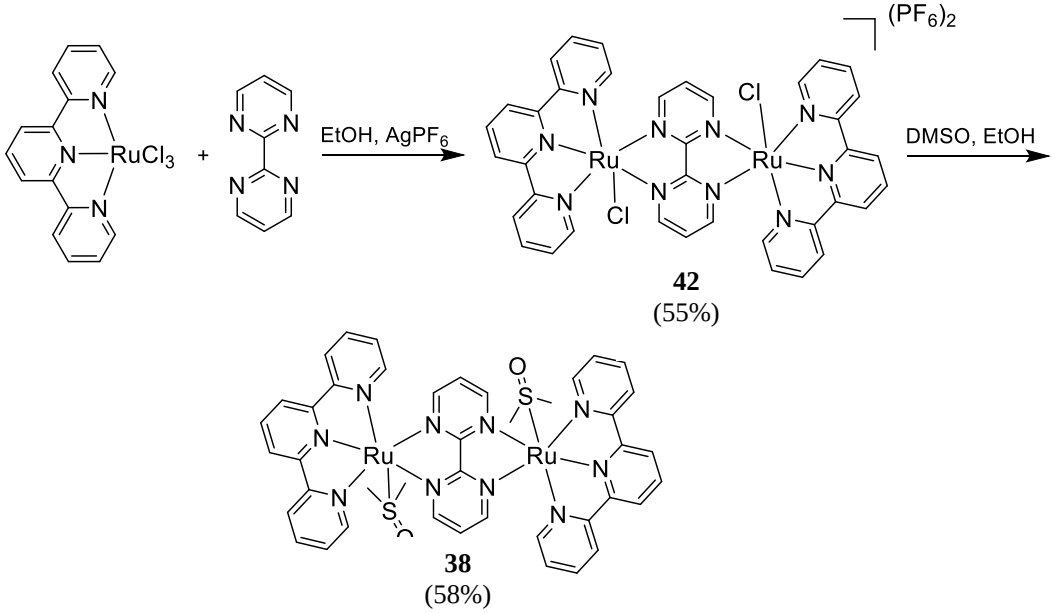

Scheme 3-2 Synthetic pathway for complex 36.

The synthesis of complexes **37** and **38** started with a similar design as for **36** where the tridentate ligand was coordinated to the Ru(II) center first. However in this case, coordinating the tridentate ligand **33** to both Ru(II) metals first to form the dinuclear system was performed. Then bpy (or dmbpy) was chelated to the resulting chloride complex **43** and **44**. This was done in this order to avoid the various Ru(II) metal complexes that could form when bpy is chelated to $RuCl_3$ first. Finally, the DMSO would be coordinated to form complexes **37** and **38** shown in Scheme 3-3.

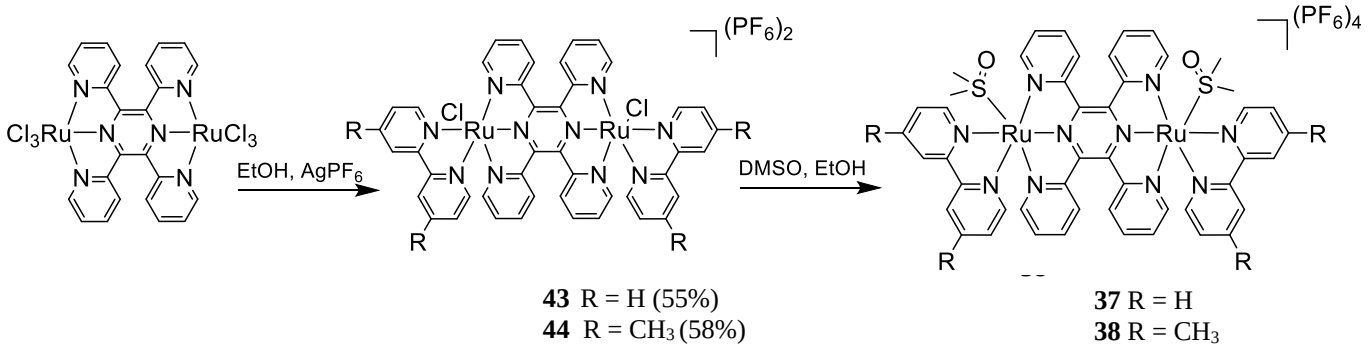

43 R = H (55%)
44 R = CH_3 (58%)

37 R = H
38 R = CH_3

Scheme 3-3 Synthetic pathway to form complexes 37 and 38.

For all these final dinuclear and dinuclear precursor complexes, the product was a mixture of *cis* and *trans* isomers due to the orientation DMSO and Cl ligands on either Ru(II) center being parallel or antiparallel to one another. For **38**, the two isomers were separated using column chromatography but only in trace amounts. Several attempts were made to separate the isomers of the remaining complexes with varying column lengths, sizes, and drip rates; however, there was no success in doing so for complexes **36** and **37**.

3.1.1 Structural Characterization

^{1}H NMR spectroscopy was performed on the synthesized Ru(II) complexes. The key diagnostic signal was the proton peak at ~10 ppm, which is the proton above the coordination site in the 6 position on the bipyridine shown in Figure 3-2. This proton shift can be indicative of photoswitching as well. When the ligand photoisomerization occurs, the oxygen will occupy the coordination space which will affect the shift on the hydrogen near the coordination bond. This isomerization between the S-bound ligand and the O-bound ligand affects the electron shielding environment around the proton of interest. When the photoisomerization occurs, the signal in ^{1}H NMR will either shift upfield or downfield depending if the electron environment about the proton of interest is more or less shielded. In the case of complex **34** with a sulfoxide coordinated to the Ru(II), the photoisomerization can be monitored by observing the ^{1}H NMR spectrum with the

signal at 9.6 ppm. The downfield shift is expected due to the change in electronic environment of the hydrogen proton that hangs over the coordination bond, just as the coordination of the sulfide to replace the chloride in the previous synthetic step. This hydrogen is highlighted in Figure 3-2.

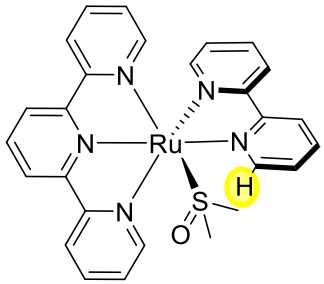

Figure 3-2 Example Ru(II) sulfoxide complex with the hydrogen in the 6 position shown to show the proximity and sensitivity to the coordination of the sulfoxide ligand

3.2 Mononuclear Ru(II) Complexes

Chart 3-5

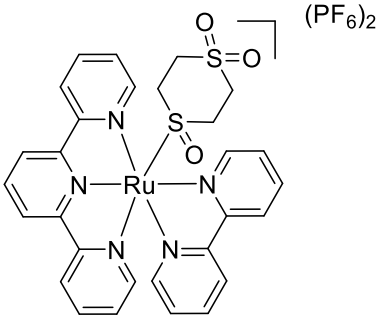

34

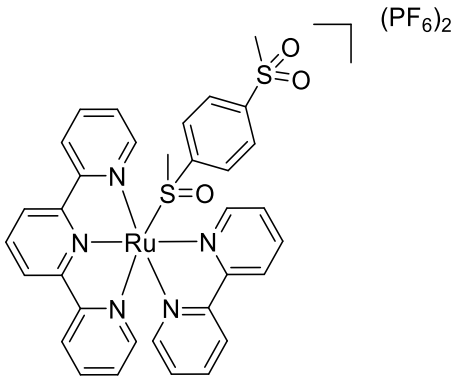

35

UV-Vis spectroscopy was performed on complex **34** (Chart 3-5) to observe the change in the absorption spectra upon irradiation with UV light. Three spectra were obtained with complexes **34**, UV-irradiated (365nm) **34** and **41** (Scheme 3-1). Each complex showed a large peak between 400-500 nm with an extended absorption reaching toward the infrared (720 nm). For previously reported Ru(II) sulfoxide complexes, this is seen as well with the O-bound coordination mode displaying the largest red-shift.[54] The shift from 400 nm to 550 nm for isomerization is expected

as in previously reported work, the $[Ru(II)(tpy)(bpy)(OH_2)]^{2+}$ ion has an absorption peak at 550 nm, so this change is assigned to the O-bound isomer.[53,54] The red-shift is due to the oxygen-coordinated mode having a significant destabilization effect on the LF splitting on the Ru(II) metal, as it is previously reported for Ru(II) sulfoxide complexes that undergo photoisomerization have 0.6 eV difference between the ground state energies of S-bound and O-bound complexes.[54,62]

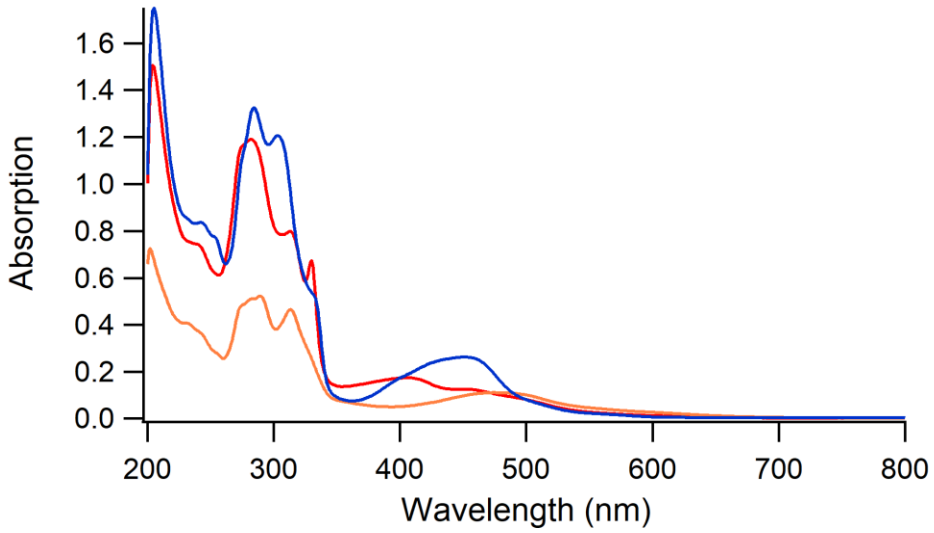

Figure 3-3 UV-Vis Absorption spectra of complexes 34 (red trace), 41 (blue trace) and UV irradiated 34 (orange trace). Performed in MeOH.

The ^{1}MLCT absorption band of **34** has a 100 nm redshift when irradiated with 365 nm light. However, the overall absorption of the complex is lower by ~50% especially in the ligand-centered (LC) and ligand-to-metal charge transfer (LMCT) region at 300 nm. This indicates that some sort of degradation of the product has occurred, which caused the Ru(II) complex to precipitate out of solution. Given that the complex is a bulky heterocycle and is coordinated as a monodentate ligand, the photolabilization is not surprising. However, the precipitation is unexpected as Ru(II) complexes tend to solvate and remain in solution when photoejection occurs as they remain charged complexes. Despite complex **34** degrading under UV light in solution and

having significantly less absorptivity overall in the ligand-dominated region of the UV-Vis spectrum, the red-shifted ^{1}MLCT absorption peak is still comparable to the unirradiated complex. Figure 3-4 shows the ^{1}H NMR of **34** before and after irradiation with 365 nm light. There is still a slight peak at 10.2 ppm which shows that not all of the starting complex underwent a photoreaction. Additionally, the solution after irradiation was left in the dark for 24 hours and showed no evidence of a return to the original state as determined by ^{1}H NMR.

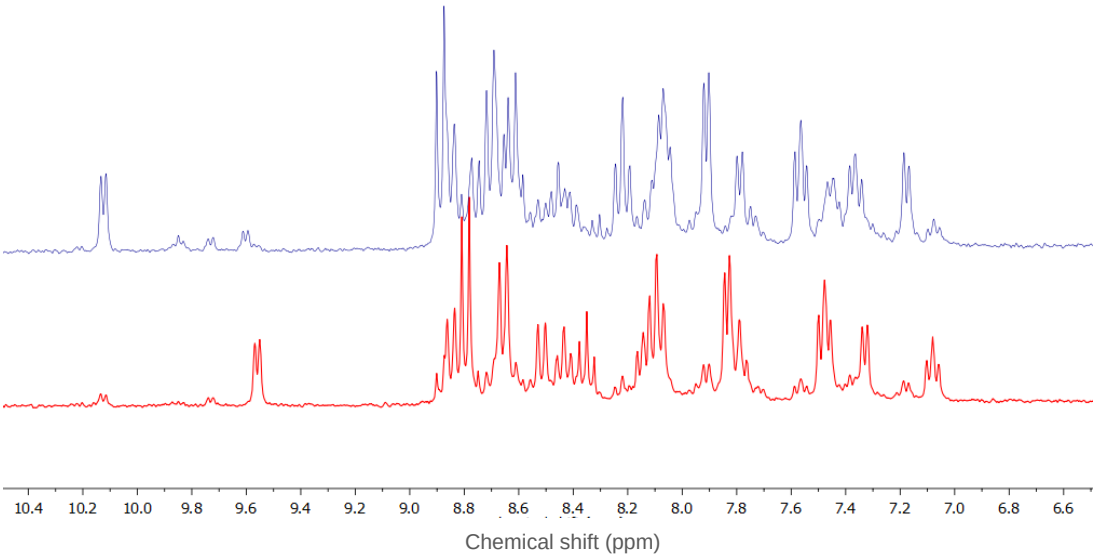

Figure 3-4 ^{1}H NMR spectra of complex 34 (blue trace) and UV-irradiated 34 (red trace). Performed in d_4-MeOD. (λ_{ex} = 365 nm)

Complex **35** (Chart 3-5) could not be synthesized due to the increased electron withdrawing nature of the conjugation of the phenyl sulfone. As with ligand **21** (Chart 2-1) in Chapter 2, the sulfone ligand contains too much electron withdrawing character which renders the ligand unable to stay coordinated to the Ru(II) metal center.

3.3 Dinuclear Ru(II) Complexes

Two dinuclear Ru(II) sulfoxide frameworks were examined to determine if one sulfoxide isomerization would influence the other Ru(II) sulfoxide isomerization. The previous monodentate

ligands were used because **30** and **31** (Chart 3-3) offered a conjugated and unconjugated system to analyze. These ligands were used to probe how bridging with the sulfoxide incorporated into the backbone linking the two Ru(II) metal centers to probe the "communication" across the ligand.

The second framework used was bidentate and tridentate bridging ligands that were previously known **32** and **33** (Chart 3-3). These ligands were chosen because of previously known dinuclear Ru(II) complexes. They also offered full conjugation between the Ru(II) centers to potentially further enhance the potential communicative effect. These ligands also offer a more stable complex that would be less prone to falling apart under irradiation of the complex because they are bound together by several N-donor bonds.

3.3.1 Ru(II) Monodentate Bridging Sulfoxides

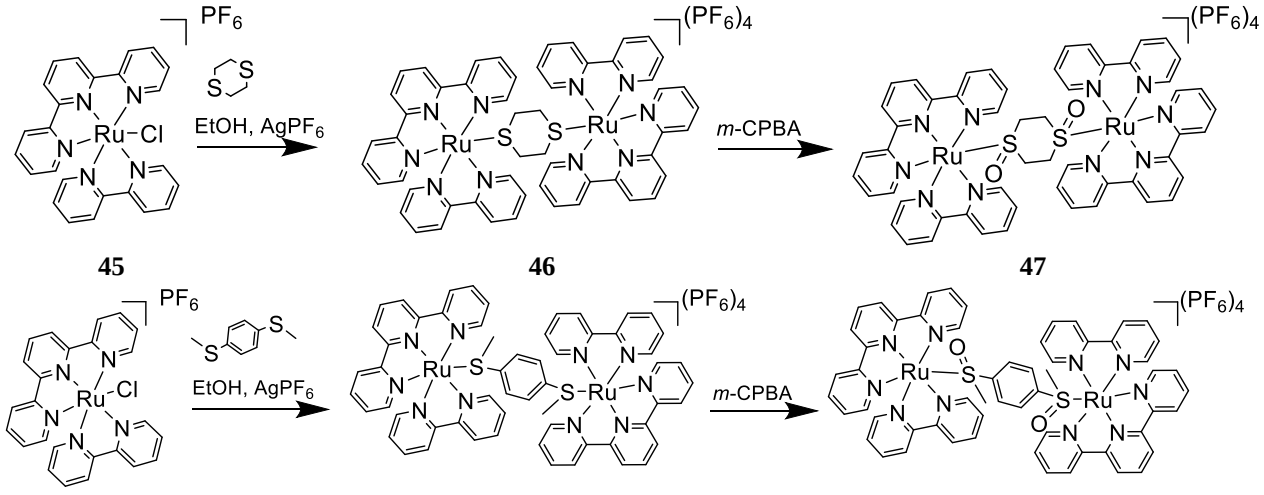

Scheme 3-4 Attempted synthetic route for monodentate-bridged dinuclear Ru(II) sulfoxide complexes using ligands 30 and 31.

Efforts were made to synthesize dinuclear Ru(II) complexes using the monodentate ligands used in Section 3.2 using the synthetic scheme shown in Scheme 3-4. The synthesis of these complexes was done in a similar manner to the mononuclear Ru(II) complexes, but Ru(II) source was used in a 2:1 ratio with the bridging ligand. However, there was no evidence that this synthetic

method yielded the desired product. ^{1}H NMR spectroscopy was performed, no aryl peaks were resolvable, and ESI-MS showed no evidence of coordination.

A second synthetic method was attempted which involved adding $AgPF_6$ to Ru(II) source before adding the bridging ligand, as an attempt to remove the chloride atom and having a solvent molecule coordinate to the Ru(II). The solvated Ru(II) complex was then treated with the bridging ligand. This did not yield the desired final product either. There are three proposed possible reasons for the inability of the bridging ligand to coordinate to both metal centers.

The first is that the coordination to the first metal prevents the coordination of the second Ru(II) center through electronic means. This would imply that for the synthetic route for complex **50** that the coordination of the first metal has enough electron withdrawing influence to prevent the coordination of the second sulfur to the second Ru(II).

The second reason is that there is a lot of steric bulk preventing the coordination of the second Ru(II) metal. Both ligands **30** and **31** are not rigid especially the 1,4-dithane backbone ligand. Given the flexibility of both of these ligands, the second Ru(II) open sulfur site may not be able to align itself with the second Ru(II) center.

A third reason is that the final bridged complexes **47** and **50** may be unstable with accessible ^{3}MC states which can lead to photosubstitution which causes the dinuclear complex to

fall apart before being isolated. Efforts were made to perform the experiments in the dark, but no product was found. The complexes, if formed, appear to be thermally unstable.

3.3.2 Ru(II) Bi/Tri-dentate Bridging Ligands

Chart 3-6

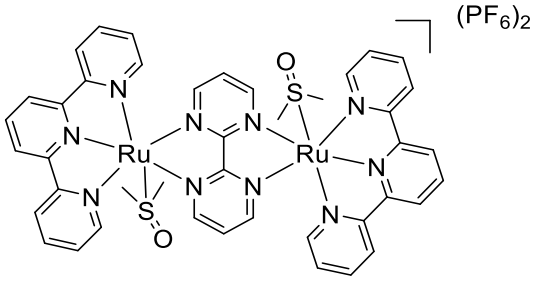

36

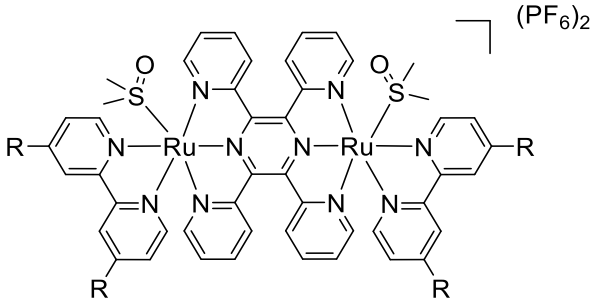

37 R = H
38 R = CH_3

With the synthetic problems of the monodentate bridging ligands in mind, a different framework to discern the communicative effects of the sulfoxide ligand isomerization was used. Two previously known bridging ligands **32** and **33** **(**Chart 3-3) were used to synthesize the precursors **42**, **43** and **44 (**Scheme 3-2, Scheme 3-3). Complex **42** was then used for the coordination of DMSO to give complex **36** (Chart 3-6). Complex **36** showed photoisomerization by eye with a color change from orange to red, so further UV-Vis experiments were performed.

Figure 3-5 shows the change in the absorption spectrum of complex **36** after irradiation with 365 nm light from a UV hand lamp over time. The change in the spectrum shows two different absorption peaks that grow in at 425 and 600 nm. These are significantly redshifted from the unirradiated sample which has absorption wavelengths at 395 and 515 nm. In addition, one isosbestic point was seen for this sample in the ^{1}MLCT regime. These results confirm previous reports of this complex.[76] However, **36** did not show any reversion after being left in the dark for three hours. The single isosbestic point indicates that there was only a change from one species in solution to one other. If there were two photoisomerizations occurring, there would be no

isosbestic point as there would be three separate isomers in solution, the S/S-bound, S/O-bound, and O/O-bound isomers.

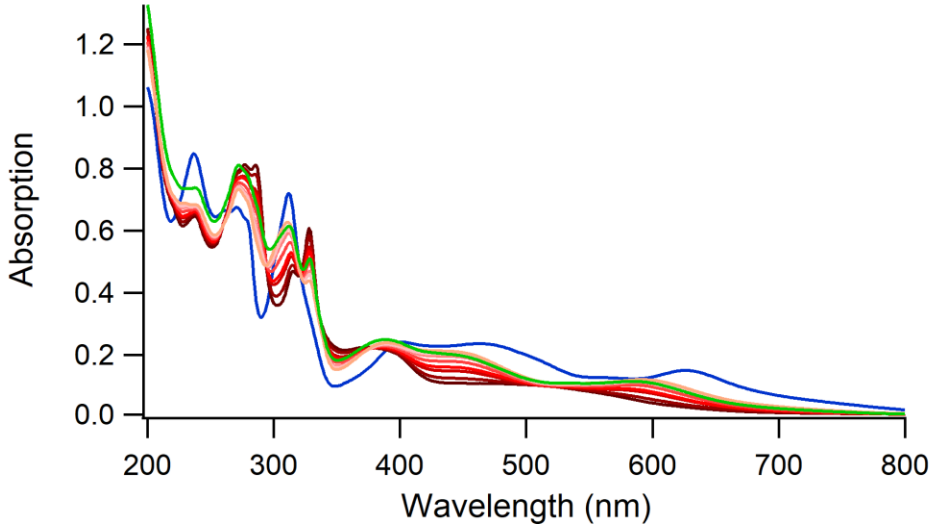

Figure 3-5 UV-Vis spectra of Complex 36 after UV irradiation. Each progressively lighter red trace represents 15 seconds of irradiation (λ = 365 nm). Blue trace is complex 42. Green trace is Complex 36 left in the dark for 3 hours after irradiation. Performed in MeOD.

During the synthesis of **37** (Chart 3-6) it was found that **43** (Scheme 3-3) was aquamarine in color. The aquamarine color by eye implies that the ^{1}MLCT transition is more redshifted. This complex also had discernible isomers in the ^{1}H NMR spectrum which are the different *cis* and *trans* isomer of the Cl ligands on the two Ru(II) metal centers. To assist with the separation of these isomers, a similar complex, **44** (Scheme 3-3), was synthesized with methyl groups in the 4 and 4' positions on the bipyridine. Using this complex, the *cis* and *trans* isomers were isolated in small amounts which was enough to obtain ^{1}H NMR spectra of both compounds, shown in Figure 3-6. However, the separation yielded very small amounts of the individual isomers, and pure isomeric compounds were not isolated in large enough amounts to proceed with coordination of DMSO. Given that the two separate isomers could only be isolated in minute amounts and the

similar conjugated nature as seen in complex **37** (Chart 3-6), the final coordination of the DMSO ligand was not pursued because similar results were expected.

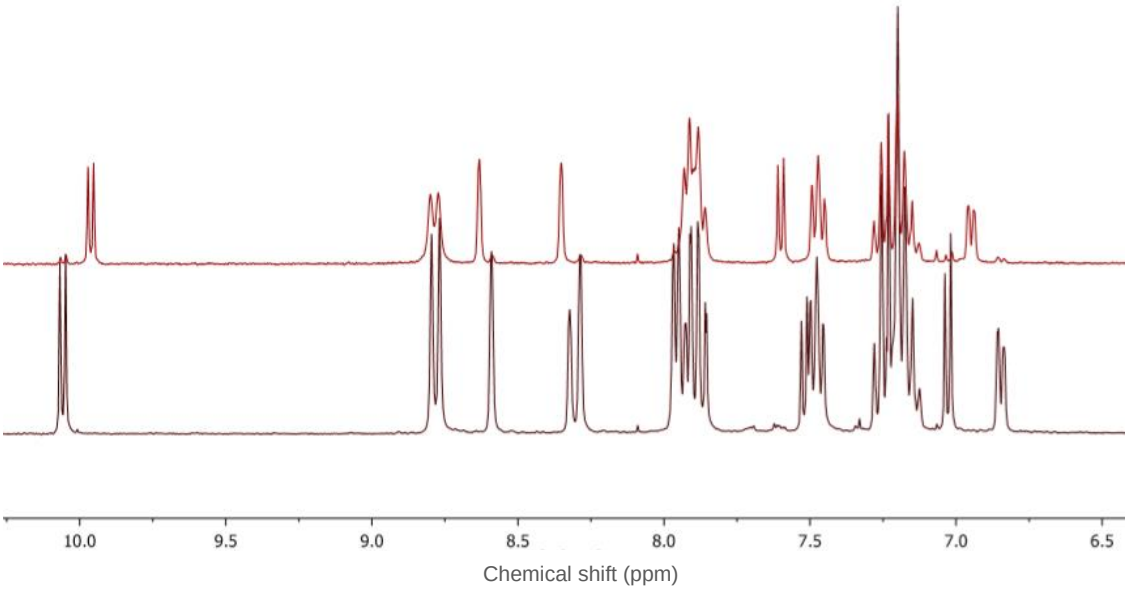

Figure 3-6 The separation of the two isomers of complex 44.

With dinuclear Ru(II) complexes, the Ru(II) centers do not have completely separate, localized molecular orbitals which would allow for energy to be siphoned to a Ru(II) metal center which has already undergone photoisomerization. Thus, after the first isomerization, the S-bound Ru(II) cannot undergo photoisomerization because the O-bound Ru(II) has a lower energy MLCT state which will funnel energy away from the S-bound Ru(II) ^{3}MLCT states that facilitate photoisomerization. Due to the nature of the isomerization and the binding mode of the sulfoxide, the O-bound complex will have a lower MLCT state than the S-bound complex. Thus, the second photoisomerization is not possible if the MLCT orbitals from the two different metal centers have too much overlap. To induce the second photoisomerization, it would be necessary to prevent the transfer of energy from the S-bound Ru(II) side of the complex to the O-bound side. A synthetic approach to potentially allow for two separate photoisomerizations on one dinuclear complex

would need to be aliphatic and nonconjugated in order to keep distance between the two metal centers to prevent energy transfer through bond and through space.

3.4 Conclusion

For the mononuclear complex **34** (Chart 3-5), the photoswitching evidence is consistent with what is observed in the literature.[79] The shift in ^{1}H NMR signals shows that there is a change in the coordination bond where the sulfoxide lies. The downfield shift is consistent with an oxygen atom being coordinated to the Ru(II). Additionally, the UV-Vis spectra show that the ^{1}MLCT absorption is consistent with other sulfur-coordinated sulfoxides that exhibit a red-shift when irradiated with UV light.[54] However, X-ray spectroscopy would need to be performed to confirm that the sulfoxide is not undergoing photosubstitution with a solvent molecule.

The dinuclear Ru(II) complex **36** (Chart 3-6) exhibited an irreversible change in UV-Vis spectrum, but it did not display evidence of two separate photoisomerizations. Previously, it has been shown that the second sulfoxide fully dissociates from the complex. The work here shows that upon irradiation with UV light **36** will undergo an irreversible change resulting in a red-shift in the spectrum.

With the previous work considered, an interesting follow-up would focus on potential therapeutic agents that activate with visible light. Work by Claudia Turro has shown that Ru(II) polypyridyl complexes can be used for targeted delivery of pyridine-based drug molecules that treat cancer due to Ru(II) affinity to collect in tumors and cancerous growths.[76] In addition to drug delivery, the Ru(II) complex can act as a therapeutic agent as well due to its ability to generate singlet oxygen efficiently when irradiated with light. Thus, Ru(II) complexes have great potential for photodynamic therapy which relies on light to activate anti-cancer drugs.

Dinuclear Ru(II) polypyridyl complexes have yet to be thoroughly examined for potential use in PDT. Dinuclear complexes such as **36** and **37** could be used as a potential therapeutic agent with the ability to deliver two drug molecules to the target site. Photolabilization of the target pyridine-based drug can occur with lower energy light than is currently being used. Preliminary experiments would need to be performed to determine if a dinuclear Ru(II) complex could photoeject two pyridines. To do such experiments, ^{1}H NMR spectroscopy studies could be performed to determine the rate of photolabilization, and the subsequent appearance of free pyridine in the solution. After successful ejection of the two pyridines, a complex with two drug molecules could be synthesized and subsequent experiments to determine rate of photolabilization and stability of the complex in solution.

A dinuclear complex that can photoeject two pyridine-containing molecules would be a candidate for therapeutic drug delivery via PDT. Of course, after experiments confirming the synthesis and the ability to photoeject pyridine-containing molecules in solution, studies would need to be performed to determine if the dinuclear Ru(II) complexes have a similar affinity to collect in cancer growths, behave similarly *in vivo* and if their rates of singlet oxygen production is similar to mononuclear Ru(II) complexes used in preliminary PDT studies.

3.5 Experimental

1,4-Bismethylthiobenzene,[80] Ru(III)(tpy)Cl_3,[81] and [Ru(II)(tpy)(bpy)Cl]PF_6[82] were prepared according to literature procedure. Ru(III) chloride hydrate, terpyridine was used as is from Strem chemicals. 1,4-dithiane, 1,4-diiodobenzene, *m*-CPBA, 4,4'-dimethyl-2,2'-bipyridine and tetra-2-pyridinylpyrazine were used as is from Sigma-Aldrich. $AgPF_6$ 2,2-bipyridine, 2,2-bipyridimine and NH_4PF_6 were obtained from Alfa Aesar and used as is. Solvents were from Sigma-Aldrich except for ethanol which was distilled at UBC. NMR solvents were either from

Sigma-Aldrich or from Cambridge Isotopes. UV-Vis spectroscopy was performed on a Varian-Cary UV-vis-near-IR spectrophotometer.. ^{1}H NMR spectroscopy was performed on Bruker NMR spectrometers (300 and 400 MHz) and referenced to the residual solvent peaks. Synthesis for all mononuclear and dinuclear species sulfide and mononuclear and dinuclear sulfoxide adapted from references McClure and Rack.[83,79,62]

3.5.1 Methods

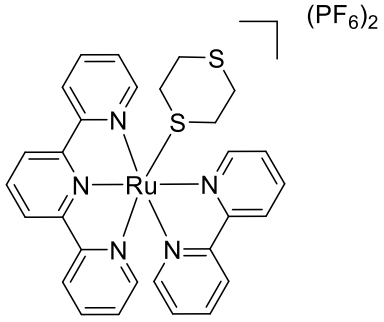

[Ru(II)(tpy)(bpy)(1,4-dithiane)](PF$_6$)$_2$ *and general reaction conditions and work up for monometallic complexes (***41***)*[83,62]

Compound **39** (0.102 g, 0.152 mmol, 1 eq) was dissolved with 1,4-dithiane (0.126 g, 1.05 mmol, 7 eq) and $AgPF_6$ (0.050 g, 0.20 mmol, 1.3 eq) in 10 mL of EtOH. The solution was stirred. It was then heated to reflux for 3 hours after which 76 mg of $AgPF_6$ (0.30 mmol) was added. Then, the reaction was left at reflux for 14 hours. The solution turned from reddish brown to an orange color after 14 hours. It was placed in a freezer (~ -5˚) for 3 hours before undergoing vacuum filtration. The solution was gathered and then dried under rotary evaporation. The dry crude product was red orange in color. The product was then dissolved in a small amount (~5 mL) of methanol. It was then added dropwise to 20 mL of water saturated with NH_4PF_6. An orange precipitate formed and was collected using vacuum filtration. The solid was gathered and dissolved in 5 mL of acetonitrile. The product was then reprecipitated by adding ~ 200 mL of

diethyl ether. Vacuum filtration was performed, and the solid was then washed by ~ 50 mL diethyl ether. The final product was obtained as a fine orange powder. Yield 0.050 g (44%). ^{1}H NMR (400 MHz, MeOD-d_4); 9.85 ppm (d, J=5.5 Hz, 1H), 8.84 ppm (d, J=8.2 Hz, 3H), 8.67 ppm (d, J=8.2 Hz, 2 H), 8.61 (d, J=8.2 Hz, 1 H), 8.45 ppm (m, 2 H), 8.11 ppm (m, 3 H), 7.95(m, 1 H), 7.79 ppm (d, J=5.5, Hz 2 H), 7.46 ppm (ddd, J=7.5 Hz, 5.8 Hz, 1.4 Hz, 2 H), 7.28 ppm (m, 2 H), 2.78 ppm (br. S, 4 H), 1.94 ppm (m, 4 H).

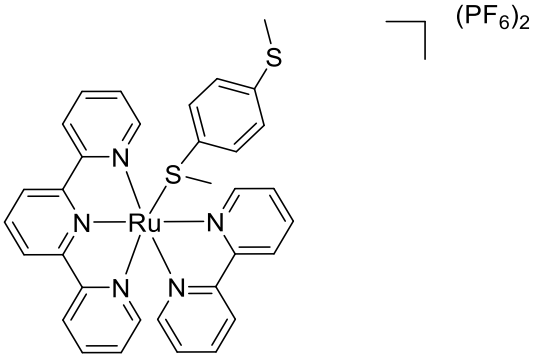

[Ru(II)(tpy)(bpy)(1,4-bismethylthiobenzene)] (PF_6)$_2$ (40)

Compound **39** (0.050 g, 0.074 mmol, 1 eq), 1,4-bismethylthiobenzene (0.060 g, 3.5 mmol, excess) and $AgPF_6$ (0.033 g, 0.13 mmol, 1.8 eq) were dissolved in 5 mL of ethanol. The reaction was stirred and brought to reflux for 3 hours, and additional $AgPF_6$ (0.031 g, 0.12 mmol, 1.8 eq) was added. The reaction was left at reflux and went from a brown-red color to orange after 16 hours. It was then placed in the freezer (~ -5˚ C) for 3 hours before undergoing vacuum filtration. The filtrate was gathered and then dried under rotary evaporation, yielding a crude product that was red orange in color. The crude product was then dissolved in a small amount (~5 mL) of MeOH. It was then added dropwise to 20 mL of water saturated with NH_4PF_6(aq). An orange precipitate formed and was filtered through vacuum filtration. The solid was gathered and dissolved in 5 mL of acetonitrile. The product was then reprecipitated by adding about 200 mL of

diethyl ether. Vacuum filtration was performed, and the solid was then washed by about 50 mL of diethyl ether. The final product was a fine orange-red powder. Yield 0.040 g (64%). ^{1}H NMR (400 MHz, MeOD-*d*$_4$); 9.59 ppm (d, J= 5.3 Hz, 1 H), 8.62 ppm (d, J=8.3 Hz, 1 H), 8.55 ppm (d, J=8.2 Hz, 2 H), 8.49-8.29 ppm (m, 6H), 8.12-7.91 ppm (m, 4 H), 7.81 ppm (td, J=7.9 Hz, 1.5 Hz, 1 H), 7.70 ppm (s, 2 H), 7.44-7.19 ppm (m, 5 H), 7.14-7.07 ppm (m, 1 H), 2.45 ppm (s, 3 H), 2.08 ppm (s, 3H)

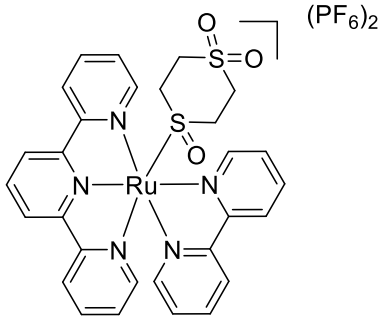

***Ru(bpy)(tpy)(1,4-dithiane, 1-dioxide,4-sulfone) (PF$_6$)$_2$* (34)**

Compound **41** (0.030 g, 0.036 mmol, 1 eq) was dissolved in 4 mL of acetonitrile in a 20 mL scintillating vial. Then, *m*-CPBA (0.040 g, 0.23 mmol, 4 eq) was added to the solution. The vial was wrapped in aluminum foil and left in the refrigerator in the dark for 3 days. Taking care to minimize exposure to light, the solid was worked up by reprecipitation by adding about 50 mL of diethyl ether. The product was then placed under vacuum filtration and washed with diethyl ether. A fine pale-yellow powder was collected after filtration. Yield could not be accurately determined due to impurities. ^{1}H NMR (MeOD-*d*$_4$); however due to impurities assignments cannot be accurately made.

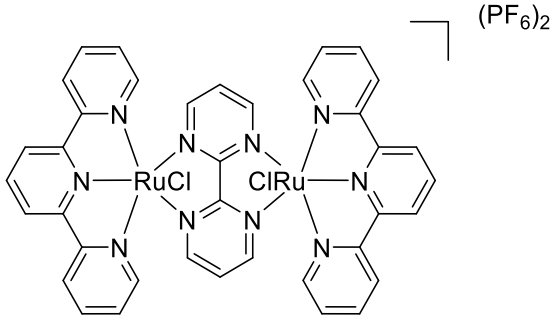

[Ru(II)(tpy)Cl(bipym)(tpy)Ru(II)Cl](PF$_6$)$_4$ (42)[84]

Ru(III)(tpy)Cl$_3$ (0.100 g, 0.213 mmol, 2.2 eq) was suspended in a solution of 2,2′-bipyrimidine (0.015 g, 0.10 mmol, 1 eq) in 40 mL, 1:1 by volume solution water and EtOH. The solution was stirred and was brought to reflux. It was left at reflux for 16 hours. The solution changed from a dark reddish colr to a dark green color over the 16 hours. After removing from the heat, the solution was placed in the freezer (~ -5˚ C) for 3 hours. The solution was filtered by vacuum filtration and then was dried using rotary evaporation. The dry crude product was dissolved in a small amount (~5 mL) of MeOH and added dropwise to saturated NH_4PF_6 in 20 mL of water. The precipitate was filtered by vacuum filtration and then dissolved in a small amount of acetonitrile. The product was reprecipitated by adding about 200 mL diethyl ether. The solid black powder was then filtered by vacuum filtration, and then washed in about 25 mL methylene chloride to wash away any monometallic species. Afterwards, the product was washed with about 50 mL of diethyl ether. The final product was a fine green-black powder. The product yielded two isomers trans and cis in a 55%:45% ratio. Yield 0.080 g (55%). ^{1}H NMR (400 MHz, MeCN-*d*$_3$); 10.44 ppm (d, J=5.7 Hz, 1 H), 9.87 ppm (d, J=5.7 Hz, 1 H), 8.60 ppm (d, J=8.2 Hz, 3 H), 8.52-8.44 ppm (m, 5 H), 8.36 ppm (d, J=8.2 Hz, 2 H), 8.29 ppm (t, J=7.4x(2) Hz, 1 H), 8.17 ppm (t, J=8.1 Hz, 1 H), 8.07-7.95 ppm (m, 7 H), 7.70 ppm (d, J=5.7 Hz, 2 H), 7.54 ppm (t, J=5.6x(2) Hz, 1 H), 7.42 ppm (m, 2 H), 7.35 ppm (d, J=5.7 Hz, 1 H), 7.29 ppm (m, 3 H).

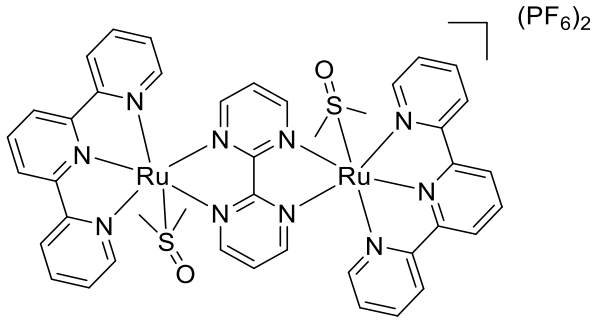

[Ru(II)(tpy)(dmso)(bpym)(dmso)(tpy)Ru(II)](PF$_6$)$_2$ **(**36**)**

Compound **38** (0.049 g, 0.039 mmol, 1 eq) and $AgPF_6$ (0.063 g, 0.25 mmol, 4 eq) was added to a solution of 5 mL of EtOH. DMSO (2.8 mL) was added to the stirring solution. The solution was brought to and left at reflux for 14 hours. The solution had changed after 14 hours at reflux from a dark green to a dark red color. The solution was then removed from the heat and placed in the freezer (~ -5˚ C) for 3 hours. The solution was then filtered by vacuum filtration. The crude solid was collected and dissolved in a small amount (5mL) of MeOH and added dropwise to 20 mL of deionized water saturated with NH_4PF_6. The precipitate was collected by vacuum filtration and dissolved in a small amount of acetonitrile (10 mL). This was then reprecipitated by adding about 200 mL of diethyl ether. The crude product was then washed with about 25 mL of methylene chloride to wash away any monometallic species. Then it was washed with about 50 mL of diethyl ether. The final product was a dark red powder. Yield 34 mg (58%). ^{1}H NMR (400 MHz, MeCN-*d*$_3$); 10.63 ppm (d, J=5.8 Hz, 1 H), 10.25 ppm (d, J=6.0 Hz, 1 H), 2.3 ppm (s, 6 H), 2.4 ppm (s, 6 H). *Aryl region for this species contains a high amount of overlap due to difficulty of isolating the isomers for this compound.

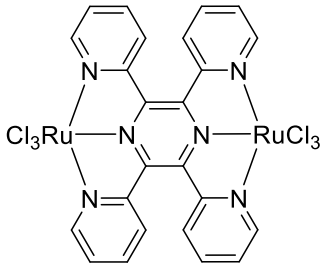

$RuCl_3$(tppz)$RuCl_3$ (*Error! Reference source not found.****)***

$RuCl_3$ (0.508 g, 1.04 mmol, 2 eq) and tetra-2-pyrdinylpyrazine (0.176 g, 0.454 mmol, 1 eq) were added to 175 mL of EtOH. The solution was stirred at heated to reflux and left at reflux for 18 hours. Over the 18 hours, the solution turned a dark blue color. It was allowed to cool to room temperature. It was then filtered by vacuum filtration and washed with excess (30-50 mL) of ethanol and then excess (30-50 mL) diethyl ether. It was then dried under vacuum. The final product was a blue-green powder. Yield 0.350 g (95%).

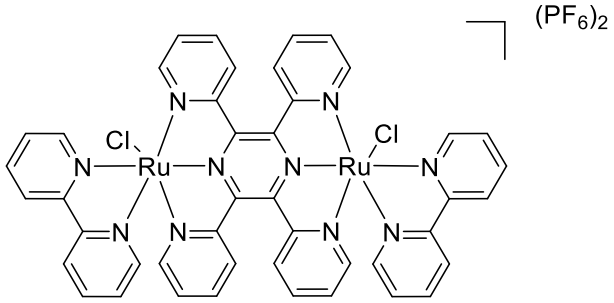

***[(bpy)ClRu(tppz)RuCl(bpy)]$(PF_6)_2$* (43)**[84]

Complex Error! Reference source not found. (0.151 g, 0.188 mmol, 1 eq) and 2,2′-bipyridine (0.090 g, 0.58 mmol, 2.8 eq) was added to a 40 mL 3:1 solution by volume of EtOH and deionized water with 0.3 mL of trimethylamine and 0.095 g of LiCl. This solution was stirred and heated to reflux for 18 hours. The solution turned from a dark blue color to a dark purple color. The solution was then allowed to cool to room temperature, after which time the solution was vacuum filtered. The purple solution was collected and then was dried using rotary evaporation. Once dried, a small

amount of methanol (~5 mL) was added. The methanol solution was then added dropwise to 50 mL of an aqueous solution of saturated NH_4PF_6 which immediately formed a precipitate. The mixture filtered by vacuum filtration again. The purple solution went through, but a dark blue solid was collected. The crude product was collected and was dried under vacuum overnight. The solid was then placed onto a silica column and eluted with a 90:10:1 solution by volume of acetonitrile to deionized water to a full saturated aqueous KNO_3 solution. The blue fraction was collected and was dried under vacuum. The final product was a mixture of *trans* and *cis* isomers in a 3:2 ratio. Yield 0.14 g (55%). MALDI-TOF: 1119.0- [M+PF6] and 974.1 [M]. ^{1}H NMR (400 MHz, MeCN-d_3); 10.27 ppm (d, J=5.2 Hz, 1H), 10.18 ppm (d, J=5.2 Hz, 1H), 8.78 ppm (m, 6H), 8.49 ppm (d, J=7.5 Hz, 1H), 8.42 ppm (m, 3H), 8.08 ppm (m, 2H), 7.92 ppm (m, 9H), 7.81 ppm (m, 2H), 7.47 ppm (t, J=6.4x(2) Hz, 4H), 7.26 ppm (d, J=5.1 Hz, 1H), 7.13 ppm (t, J=6.4x(2) Hz, 1H), 7.02 ppm (t, J=6.7x(2) Hz, 1H)

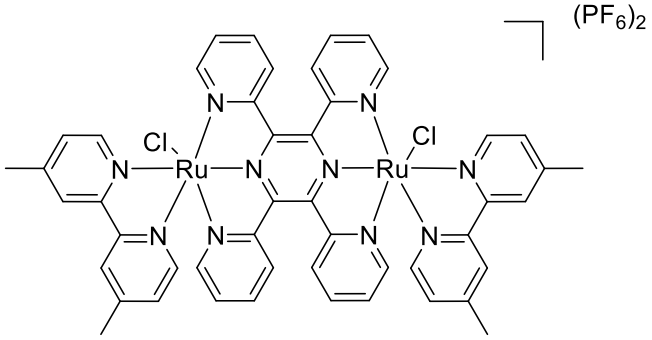

[(dmbpy)ClRu(tppz)RuCl(dmbpy)](PF$_6$)$_2$ (44)[84]

Compound **44** was prepared in the same way as **43.** Complex **43** (0.316 g, 0.394 mmol, 1eq).and 4,4′-Dimethyl-2,2′-bipyridine (0.220 g, 1.18 mmol, 3 eq) was added to a 80 mL 3:1 solution of EtOH and deionized water with 0.6 mL of triethylamine and 0.185 g of LiCl. The final product was a blue-green powder. The ^{1}H NMR indicated that there was a mixture of isomers in solution. An additional alumina column was performed to separate the isomers. A small amount (~50 mg)

of crude product was loaded onto a neutral alumina column and eluted with a 1:1 solution by volume of acetonitrile and toluene.[85] The blue-green fraction slowly split but ran together. However, the first and last fractions of the blue-green band were of pure trans and cis isomers, respectively. Less than 5 mg of each was collected. Yield of the mixed isomers final product was 0.300 g (58%) in a ratio of 3:2. MALDI-TOF- 1175.1-[M+PF_6] and 1030.1 [M]. ^{1}H NMR (400 MHz, MeCN-d_3) ; ***isomer 1***- 10.16 ppm (d, J=5.7 Hz, 2H), 8.78 ppm (d, J=8.2 Hz, 4H), 8.59 ppm (s, 1H), 8.28 ppm (s, 2H), 7.98-7.70 ppm (m, 10H), 7.48 ppm (m, 5H), 7.03 ppm (d, J=5.9 Hz, 2H), 6.84 ppm (d, J=5.8 Hz, 2H), 2.82 ppm (s, 6H), 2.36 ppm (s, 6H) ***isomer 2***- 9.99 ppm (d, J=5.8 Hz, 2H), 8.81 ppm (d, J=7.8 Hz, 4H), 8.66 ppm (s, 2H), 8.38 ppm (s, 2H), 8.00-7.85 ppm (m, 10H), 7.62 ppm (d, J=6.2 Hz, 2H), 7.50 ppm (t, J=6.5x(2) Hz, 4H), 6.97 ppm (d, J=6.1 Hz, 2H), 2.84 ppm (s, 6H), 2.44 ppm (s, 6H). *Could not determine which spectrum corresponding to *cis* or *trans*.

Chapter 4: Conclusion and Future Work

The continual draw of the manipulation of light has shaped the techniques and material development of chemistry. Scientists have unlocked many of the mysteries of chemical interactions of light, and the resulting theories have led to extraordinary materials that would be unfathomable less than a century ago. Still there are new frontiers and boundaries to be pushed as the current energy crisis demands energy be used more efficiently. Thus, research now needs to focus on efficient light emitters, electro- and photo-switchable materials and better light absorbers with the goal of each generated unit of electricity, emitted photon or absorbed photon is not wasted.

Incremental steps that elucidate the relationship between the structure of a molecule or metal complex and the photophysical properties have given a framework of molecular orbitals and charge transfer states that can be used to further tune new molecules with different or advanced photophysical properties. Determining where these trends and patterns finally break also gives way to breakthroughs and more refined understanding.

The insertion of a sulfur atom between the pyridine rings in a terpyridine about a Ru(II) metal was examined in Chapter 2. This led to the expansion of the ligand cage around the Ru(II) which led to less strain about the Ru(II) when compared to $[Ru(tpy)_2]^{2+}$. These new ligands show that a more octahedral Ru(II) structure can have measurable effects on electrochemical and photochemical properties, and they expand the repertoire for expanded bite-angle ligands that can be used for coordination chemistry. The three different ligands show that while the electrochemical and photophysical properties may be modified for the overall complex that the geometry and unstrained octahedral structure for Ru(II) metal center remains intact as well. Further examination is needed as heteroleptic Ru(II) complexes with these sulfur-incorporated oligopyridines have shown low temperature emission, and variable temperature emission studies would elucidate and

provide guidance to further improvements and modifications to the ligand to enhance and modify the photophysical properties.

In Chapter 3, various Ru(II) sulfoxide complexes were examined ranging from mononuclear Ru(II) to dinuclear Ru(II) complexes. These experiments have shown that ligand design is highly important to the development of Ru(II) sulfoxides. The main goal of the project was to synthesize a dinuclear Ru(II) sulfoxide complex which would undergo to photoisomerizations. This goal was not achieved, but a few guiding principles to actualize that goal were found. First, the photoswitch needs to be bridged with a bidentate or tridentate ligand to promote stability. Second, the sulfoxide would potentially work better when not incorporated into the bridge as it helps to isolate the sulfoxide and increases stability. Third, the bridge itself needs to limit the electronic interactions between the two metal centers, so that one isomerization does not impede the second.

Overall, the body of work presented in this thesis shows that Ru(II) complexes still have immense amounts of photochemical and electrochemical properties to harness and understand. The structural characteristics of Ru(II) highly influence their photophysical properties, and the additional ligand backbones adds to the catalog of ligands that can be used to finely generate desired photophysical properties whether it be emission, redshifted absorption or even photoswitchable properties. This work provides further guidance and knowledge into potential structural modifications and its implication on Ru(II) physical properties.

References

(1) Schlebusch, C. M.; Malmström, H.; Günther, T.; Sjödin, P.; Coutinho, A.; Edlund, H.; Munters, A. R.; Steyn, M.; Soodyall, H.; Lombard, M.; et al. Ancient Genomes from Southern Africa Pushes Modern Human Divergence beyond 260,000 Years Ago. *Science.* **2017**, *358* (November), 652–655.

(2) Berna, F.; Goldberg, P.; Horwitz, L. K.; Brink, J.; Holt, S.; Bamford, M.; Chazan, M. Microstratigraphic Evidence of in Situ Fire in the Acheulean Strata of Wonderwerk Cave, Northern Cape Province, South Africa. *Proc. Natl. Acad. Sci. U. S. A.* **2012**, *109* (20), E1215-20.

(3) Wiessner, P. W. Embers of Society: Firelight Talk among the Ju/'hoansi Bushmen. *Proc. Natl. Acad. Sci. U. S. A.* **2014**, *111* (39), 14027–14035.

(4) Wang, Y.; Runnerstrom, E. L.; Milliron, D. J. Switchable Materials for Smart Windows. *Annu. Rev. Chem. Biomol. Eng.* **2016**, *7* (1), 283–304.

(5) Vos, J. G.; Kelly, J. M. Ruthenium Polypyridyl Chemistry; from Basic Research to Applications and Back Again. *J. Chem. Soc. Dalt. Trans.* **2006**, 4869–4883.

(6) Grätzel, M. Solar Energy Conversion by Dye-Sensitized Photovoltaic Cells. *Inorg. Chem.* **2005**, *44* (20), 6841–6851.

(7) Teegardin, K.; Day, J. I.; Chan, J.; Weaver, J. Advances in Photocatalysis: A Microreview of Visible Light Mediated Ruthenium and Iridium Catalyzed Organic Transformations. *Org. Process Res. Dev.* **2016**, *20* (7), 1156–1163.

(8) Heinemann, F.; Karges, J.; Gasser, G. Critical Overview of the Use of Ru(II) Polypyridyl Complexes as Photosensitizers in One-Photon and Two-Photon Photodynamic Therapy. *Acc. Chem. Res.* **2017**, *50* (11), 2727–2736.

(9) Photochemistry. In *IUPAC Compendium of Chemical Terminology*; IUPAC: Research Triagle Park, NC.

(10) Juris, A.; Balzani, V.; Barigelletti, F.; Campagna, S.; Belser, P.; von Zelewsky, A. Ru(II) Polypyridine Complexes: Photophysics, Photochemistry, Eletrochemistry, and Chemiluminescence. *Coord. Chem. Rev.* **1988**, *84* (C), 85–277.

(11) Dixon, I. M.; Lebon, E.; Sutra, P.; Igau, A. Luminescent Ruthenium-Polypyridine Complexes & Phosphorus Ligands: Anything but a Simple Story. *Chem. Soc. Rev.* **2009**, *38* (6), 1621–1634.

(12) Jablonski Diagram - Java Tutorial | Olympus Life Science https://www.olympus-lifescience.com/en/microscope-resource/primer/java/jablonski/lightandcolor/ (accessed Apr 24, 2019).

(13) Condon, E. U. Nuclear Motions Associated with Electron Transitions in Diatomic Molecules. *Phys. Rev.* **1928**, *32* (6), 858–872.

(14) Valeur, B.; Berberan-Santos, M. N. Characteristics of Fluorescence Emission. In *Molecular Fluorescence*; Wiley-VCH Verlag GmbH & Co. KGaA: Weinheim, Germany, 2012; pp 53–74.

(15) Demas, J. N.; Crosby, G. A. On the Multiplicity of the Emitting State of Ruthenium(II) Complexes. *J. Mol. Spectrosc.* **1968**, *26* (1), 72–77.

(16) Yuster, P.; Weissman, S. I. Effects of Perturbations on Phosphorescence: Luminescence of Metal Organic Complexes. *J. Chem. Phys.* **1949**, *17* (12), 1182–1188.

(17) Daniel, C. Photochemistry and Photophysics of Transition Metal Complexes: Quantum Chemistry. *Coord. Chem. Rev.* **2015**, *282–283*, 19–32.

(18) Paris, J. P.; Brandt, W. W. Charge Transfer Luminescence of A Ruthenium(II) Chelate. *J.*

Am. Chem. Soc. **1959**, *81* (18), 5001–5002.

(19) Crosby, G. A.; Perkins, W. G.; Klassen, D. M. Luminescence from Transition-Metal Complexes: Tris(2,2'-bipyridine)and Tris (1,10-phenanthroline) Ruthenium (N). *J. Chem. Phys.* **1965**, *43* (5), 1498–1503.

(20) Demas, J. N.; Crosby, G. A. On the Multiplicity of the Emitting State of Ruthenium(II) Complexes. *J. Mol. Spectrosc.* **1968**, *26* (1), 72–77.

(21) Baker, D. C.; Crosby, G. A. Spectroscopic and Magnetic Evidence for Multiple-State Emission from Tris(2,2′-bipyridine) Ruthenium (II) Sulfate. *Chem. Phys.* **1974**, *4* (3), 428–433.

(22) Roundhill, D. M.; Roundhill, D. M. Photochemistry, Photophysics, and Photoredox Reactions of $Ru(bpy)_3^{2+}$ and Related Complexes. In *Photochemistry and Photophysics of Metal Complexes*; Springer US: Boston, MA, 1994; 165–215.

(23) Hong, D.; Yamada, Y.; Nagatomi, T.; Takai, Y.; Fukuzumi, S. Catalysis of Nickel Ferrite for Photocatalytic Water Oxidation Using $[Ru(bpy)_3]^{2+}$ and $S_2O_8^{2-}$. *J. Am. Chem. Soc.* **2012**, *134* (48), 19572–19575.

(24) Limburg, B.; Bouwman, E.; Bonnet, S. Rate and Stability of Photocatalytic Water Oxidation Using $[Ru(bpy)_3]^{2+}$ as Photosensitizer. *ACS Catal.* **2016**, *6* (8), 5273–5284.

(25) Alpers, D.; Gallhof, M.; Stark, C. B. W.; Brasholz, M. Photoassisted Oxidation of Ruthenium(II)-Photocatalysts $Ru(bpy)_3^{2+}$ and $Ru(bpz)_3^{2+}$ to RuO_4: Orthogonal Tandem Photoredox and Oxidation Catalysis. *Chem. Commun.* **2016**, *52* (5), 1025–1028.

(26) Gueret, R.; Poulard, L.; Oshinowo, M.; Chauvin, J.; Dahmane, M.; Dupeyre, G.; Lainé, P. P.; Fortage, J.; Collomb, M. N. Challenging the $[Ru(bpy)_3]^{2+}$ Photosensitizer with a Triazatriangulenium Robust Organic Dye for Visible-Light-Driven Hydrogen Production

in Water. *ACS Catal.* **2018**, *8* (5), 3792–3802.

(27) Teegardin, K.; Day, J. I.; Chan, J.; Weaver, J. Advances in Photocatalysis: A Microreview of Visible Light Mediated Ruthenium and Iridium Catalyzed Organic Transformations. *Organic Process Research and Development*. American Chemical Society July 15, 2016, 1156–1163.

(28) Lewis, G. N.; Lipkin, D. Reversible Photochemical Processes in Rigid Media. a Study of the Phosphorescent State. *J. Am. Chem. Soc.* **1941**, *63* (11), 3005–3018.

(29) Mukuta, T.; Tanaka, S.; Inagaki, A.; Koshihara, S. Y.; Onda, K. Direct Observation of the Triplet Metal-Centered State in $[Ru(bpy)_3]^{2+}$ Using Time-Resolved Infrared Spectroscopy. *ChemistrySelect* **2016**, *1* (11), 2802–2807.

(30) Medlycott, E. A.; Hanan, G. S. Designing Tridentate Ligands for Ruthenium(II) Complexes with Prolonged Room Temperature Luminescence Lifetimes. *Chem. Soc. Rev.* **2005**, *34* (2), 133–142.

(31) Winkler, J. R.; Netzel, T. L.; Creutz, C.; Sutin, N. Direct Observation of Metal-to-Ligand Charge-Transfer (MLCT) Excited States of Pentaammineruthenium(II) Complexes. *J. Am. Chem. Soc.* **1987**, *109* (8), 2381–2392.

(32) Stone, M. L.; Crosby, G. A. Charge-Transfer Luminescence from Ruthenium(II) Complexes Containing Tridentate Ligands. *Chem. Phys. Lett.* **1981**, *79* (1), 169–173.

(33) Fink, D. W.; Ohnesorge, W. E. Temperature Effects on Charge-Transfer Luminescence Intensity of Some Transition Metal Ion Chelates. *J. Am. Chem. Soc.* **1969**, *91* (18), 4995–4998.

(34) Elytle, F.; Petrosky, L. M.; Carlson, L. R. Proton Magnetic Resonance Studies of Some Group VIII-Polypyridine Complexes. *Anal. Chim. Acta* **1971**, *57* (2), 239–247.

(35) Hecker, C. R.; Fanwick, P. E.; McMillin, D. R. Evidence for Dissociative Photosubstitution Reactions of $[Ru(trpy)(bpy)(NCCH3)]^{2+}$. Crystal and Molecular Structure of $[Ru(trpy)(bpy)(py)](PF_6)^{2+}\bullet(CH3)_2CO$. *Inorg. Chem.* **1991**, *30* (4), 659–666.

(36) Bessel, C. A.; See, R. F.; Jameson, D. L.; Churchill, M. R.; Takeuchi, K. J. Structural Considerations of Terdentate Ligands: Crystal Structures of 2,2′: 6′,2′-Terpyridine and 2,6-bis(pyrazol-1-yl)Pyridine. *J. Chem. Soc. Dalt. Trans.* **1992**, 3223–3228.

(37) Calvert, J. M.; Caspar, J. V.; Binstead, R. A.; Westmoreland, T. D.; Meyer, T. J. Metallopolymer Photochemistry. Photophysical, Photochemical, and Photoelectrochemical Properties of $(bpy)_2$RuII Sites Bound to Poly(4-vinylpyridine). *J. Am. Chem. Soc.* **1982**, *104* (24), 6620–6627.

(38) Sauvage, J. P.; Collin, J. P.; Chambron, J. C.; Guillerez, S.; Coudret, C.; Balzani, V.; Barigelletti, F.; De Cola, L.; Flamigni, L. Ruthenium(II) and Osmium(II) Bis(Terpyridine) Complexes in Covalently-Linked Multicomponent Systems: Synthesis, Electrochemical Behavior, Absorption Spectra, and Photochemical and Photophysical Properties. *Chem. Rev.* **1994**, *94* (4), 993–1019.

(39) Pal, A. K.; Hanan, G. S. Design, Synthesis and Excited-State Properties of Mononuclear Ru(II) Complexes of Tridentate Heterocyclic Ligands. *Chem. Soc. Rev.* **2014**, *43* (17), 6184–6197.

(40) Maestri, M.; Armaroli, N.; Balzani, V.; Constable, E. C.; Thompson, A. M. W. C. Complexes of the Ruthenium(II)-2,2′:6′,2″ -Terpyridine Family. Effect of Electron-Accepting and -Donating Substituents on the Photophysical and Electrochemical Properties. *Inorg. Chem.* **1995**, *34* (10), 2759–2767.

(41) Wang, J.; Fang, Y. Q.; Hanan, G. S.; Loiseau, F.; Campagna, S. Synthesis and Properties

of the Elusive Ruthenium(II) Complexes of 4′-Cyano-2,2′:6′,2″-Terpyridine. *Inorg. Chem.* **2005**, *44* (1), 5–7.

(42) Freed, K. F.; Jortner, J. Multiphonon Processes in the Nonradiative Decay of Large Molecules. *J. Chem. Phys.* **1970**, *52* (12), 6272–6291.

(43) Bixon, M.; Jortner, J.; Cortes, J.; Heitele, H.; Michel-Beyerle, M. E. Energy Gap Law for Nonradiative and Radiative Charge Transfer in Isolated and in Solvated Supermolecules. *J. Phys. Chem.* **1994**, *98* (30), 7289–7299.

(44) Abrahamsson, M.; Lundqvist, M. J.; Wolpher, H.; Johansson, O.; Eriksson, L.; Bergquist, J.; Rasmussen, T.; Becker, H. C.; Hammarström, L.; Norrby, P. O.; et al. Steric Influence on the Excited-State Lifetimes of Ruthenium Complexes with Bipyridyl-Alkanylene-Pyridyl Ligands. *Inorg. Chem.* **2008**, *47* (9), 3540–3548.

(45) Schulze, B.; Escudero, D.; Friebe, C.; Siebert, R.; Görls, H.; Sinn, S.; Thomas, M.; Mai, S.; Popp, J.; Dietzek, B.; et al. Ruthenium(II) Photosensitizers of Tridentate Click-Derived Cyclometalating Ligands: A Joint Experimental and Computational Study. *Chem. - A Eur. J.* **2012**, *18* (13), 4010–4025.

(46) Brown, D. G.; Sanguantrakun, N.; Schulze, B.; Schubert, U. S.; Berlinguette, C. P. Bis(tridentate) Ruthenium-Terpyridine Complexes Featuring Microsecond Excited-State Lifetimes. *J. Am. Chem. Soc.* **2012**, *134* (30), 12354–12357.

(47) Schramm, F.; Meded, V.; Fliegl, H.; Fink, K.; Fuhr, O.; Qu, Z.; Klopper, W.; Finn, S.; Keyes, T. E.; Ruben, M. Expanding the Coordination Cage: A Ruthenium(II) - Polypyridine Complex Exhibiting High Quantum Yields under Ambient Conditions. *Inorg. Chem.* **2009**, *48* (13), 5677–5684.

(48) Breivogel, A.; Förster, C.; Heinze, K. A Heteroleptic Bis(tridentate)Ruthenium(II)

Polypyridine Complex with Improved Photophysical Properties and Integrated Functionalizability. *Inorg. Chem.* **2010**, *49* (15), 7052–7056.

(49) Breivogel, A.; Meister, M.; Förster, C.; Laquai, F.; Heinze, K. Excited State Tuning of Bis(tridentate) Ruthenium(II) Polypyridine Chromophores by Push-Pull Effects and Bite Angle Optimization: A Comprehensive Experimental and Theoretical Study. *Chem. - A Eur. J.* **2013**, *19* (41), 13745–13760.

(50) Parada, G. A.; Fredin, L. A.; Santoni, M. P.; Jäger, M.; Lomoth, R.; Hammarström, L.; Johansson, O.; Persson, P.; Ott, S. Tuning the Electronics of Bis(tridentate)Ruthenium(II) Complexes with Long-Lived Excited States: Modifications to the Ligand Skeleton beyond Classical Electron Donor or Electron Withdrawing Group Decorations. *Inorg. Chem.* **2013**, *52* (9), 5128–5137.

(51) Pinnick, D. V.; Durham, B. Photosubstitution Reactions of $Ru(bpy)_2XY^{n+}$ Complexes. *Inorg. Chem.* **1984**, *23* (10), 1440–1445.

(52) Dwyer, F.; Goodwin, H.; Gyarfas, E. Mono- and Bis-(2,2'-bipyridine) and -(1,10-phenanthroline) Chelates of Ruthenium and Osmium. II. Bischelates of Bivalent and Tervalent Ruthenium. *Aust. J. Chem.* **1963**, *16* (4), 544.

(53) Durham, B.; Wilson, S. R.; Hodgson, D. J.; Meyer, T. J. Cis-Trans Photoisomerization in $Ru(bpy)_2(OH_2)_2^{2+}$. Crystal Structure of Trans-$[Ru(bpy)_2(OH_2)(OH)](ClO4)_2$. *J. Am. Chem. Soc.* **1980**, *102* (2), 600–607.

(54) McClure, B. A.; Rack, J. J. Isomerization in Photochromic Ruthenium Sulfoxide Complexes. *Eur. J. Inorg. Chem.* **2010**, *2010* (25), 3895–3904.

(55) Constable, E. C.; Cargill Thompson, A. M. W.; Armaroli, N.; Balzani, V.; Maestri, M. Ligand Substitution Patterns Control Photophysical Properties of Ruthenium(II)-2,2′:6′,2″-

Terpyridine Complexes-Room Temperature Emission from $[Ru(tpy)_2]^{2+}$ Analogues. *Polyhedron* **1992**, *11* (20), 2707–2709.

(56) Smith, M. K.; Gibson, J. A.; Young, C. G.; Broomhead, J. A.; Junk, P. C.; Keene, F. R. Photoinduced Ligand Isomerization in Dimethyl Sulfoxide Complexes of Ruthenium (II). *Eur. J. Inorg. Chem.* **2000**, *2000* (6), 1365–1370.

(57) Knoll, J. D.; Albani, B. A.; Turro, C. New Ru(II) Complexes for Dual Photoreactivity: Ligand Exchange and $^1O_2$ Generation. *Acc. Chem. Res.* **2015**, *48* (8), 2280–2287.

(58) Knoll, J. D.; Turro, C. Control and Utilization of Ruthenium and Rhodium Metal Complex Excited States for Photoactivated Cancer Therapy. *Coord. Chem. Rev.* **2015**, *282–283*, 110–126.

(59) Gutiérrez, M. I.; Martínez, C. G.; García-Fresnadillo, D.; Castro, A. M.; Orellana, G.; Braun, A. M.; Oliveros, E. Singlet Oxygen ($^1\Delta_g$) Production by Ruthenium(II) Complexes in Microheterogeneous Systems. *J. Phys. Chem. A* **2003**, *107* (18), 3397–3403.

(60) King, A. W.; Wang, L.; Rack, J. J. Excited State Dynamics and Isomerization in Ruthenium Sulfoxide Complexes. *Acc. Chem. Res.* **2015**, *48* (4), 1115–1122.

(61) Butcher, D. P.; Rachford, A. A.; Petersen, J. L.; Rack, J. J. Phototriggered S → O Isomerization of a Ruthenium-Bound Chelating Sulfoxide. *Inorg. Chem.* **2006**, *45* (23), 9178–9180.

(62) McClure, B. A.; Mockua, N. V.; Butcher, D. P.; Lutterman, D. A.; Turro, C.; Petersen, J. L.; Rack, J. J. Photochromic Ruthenium Sulfoxide Complexes: Evidence for Isomerization through a Conical Intersection. *Inorg. Chem.* **2009**, *48* (17), 8084–8091.

(63) Grusenmeyer, T. A.; McClure, B. A.; Ziegler, C. J.; Rack, J. J. Solvent Effects on Isomerization in a Ruthenium Sulfoxide Complex. *Inorg. Chem.* **2010**, *49* (10), 4466–

4470.

(64) Mockus, N. V.; Petersen, J. L.; Rack, J. J. Subnanosecond Isomerization in an Osmium-Dimethyl Sulfoxide Complex. *Inorg. Chem.* **2006**, *45* (1), 8–10.

(65) Biner, M.; Bürgi, H. B.; Ludi, A.; Röhr, C. Crystal and Molecular Structures of $[Ru(bpy)_3](PF_6)_3$ and $[Ru(bpy)_3](PF_6)_2$ at 105 K. *J. Am. Chem. Soc.* **1992**, *114* (13), 5197–5203.

(66) Brown, C. M.; Kitt, M. J.; Xu, Z.; Hean, D.; Ezhova, M. B.; Wolf, M. O. Tunable Emission of Iridium(III) Complexes Bearing Sulfur-Bridged Dipyridyl Ligands. *Inorg. Chem.* **2017**, *56* (24), 15110–15118.

(67) Bernhard, P.; Lehmann, H.; Ludi, A. Synthesis and Properties of Substituted Ruthenium Aqua Complexes. *J. Chem. Soc. Chem. Commun.* **1981**, 1216–1217.

(68) Laramée-Milette, B.; Hanan, G. S. Ruthenium Bistridentate Complexes with Non-Symmetrical Hexahydro-Pyrimidopyrimidine Ligands: A Structural and Theoretical Investigation of Their Optical and Electrochemical Properties. *Dalt. Trans.* **2016**, *45*, 12507–12517.

(69) Bideh, B. N.; Roldán-Carmona, C.; Shahroosvand, H.; Nazeeruddin, M. K. Ruthenium Phenanthroimidazole Complexes for near Infrared Light-Emitting Electrochemical Cells. *J. Mater. Chem. C* **2016**, *4* (41), 9674–9679.

(70) Lever, A. B. P. Electrochemical Parametrization of Metal Complex Redox Potentials, Using the Ruthenium(III)/Ruthenium(II) Couple To Generate a Ligand Electrochemical Series. *Inorg. Chem.* **1990**, *29* (6), 1271–1285.

(71) Breivogel, A.; Meister, M.; Förster, C.; Laquai, F.; Heinze, K. Excited State Tuning of Bis(tridentate) Ruthenium(II) Polypyridine Chromophores by Push-Pull Effects and Bite

Angle Optimization: A Comprehensive Experimental and Theoretical Study. *Chem. - A Eur. J.* **2013**, *19* (41), 13745–13760.

(72) Dunn, A. D.; Norrie, R.; L'Hostis, J.; Marjot, S. The Synthesis and Some Reactions of Novel Pyridine-2(1H)-thiones. *J. für Prakt. Chemie/Chemiker-Zeitung* **1992**, *334* (2), 119–125.

(73) Dunn, A. D. Nucleophilic Displacement in 2-Chloro(trifluoromethyl)pyridines with Amines and Ammonia. *J. Fluor. Chem.* **1999**, *93* (2), 153–157.

(74) Shaabani, A.; Tavasoli-Rad, F.; Lee, D. G. Potassium Permanganate Oxidation of Organic Compounds. *Synth. Commun.* **2005**, *35* (4), 571–580.

(75) Rack, J. J.; Mockus, N. V. Room-Temperature Photochromism in Cis- and Trans-$[Ru(bpy)_2(dmso)_2]^{2+}$. *Inorg. Chem.* **2003**, *42* (19), 5792–5794.

(76) Sgambellone, M. A.; David, A.; Garner, R. N.; Dunbar, K. R.; Turro, C. Cellular Toxicity Induced by the Photorelease of a Caged Bioactive Molecule: Design of a Potential Dual-Action Ru(II) Complex. *J. Am. Chem. Soc.* **2013**, *135* (30), 11274–11282.

(77) Zhao, J.; Liu, N.; Sun, S.; Gou, S.; Wang, X.; Wang, Z.; Li, X.; Zhang, W. Light-Activated Ruthenium (II)-Bicalutamide Prodrugs for Prostate Cancer. *J. Inorg. Biochem.* **2019**, *196*, 110684.

(78) Kaveevivitchai, N.; Zong, R.; Tseng, H. W.; Chitta, R.; Thummel, R. P. Further Observations on Water Oxidation Catalyzed by Mononuclear Ru(II) Complexes. *Inorg. Chem.* **2012**, *51* (5), 2930–2939.

(79) McClure, B. A.; Rack, J. J. Ultrafast Spectroscopy of a Photochromic Ruthenium Sulfoxide Complex. *Inorg. Chem.* **2011**, *50* (16), 7586–7590.

(80) Luo, F.; Pan, C.; Li, L.; Chen, F.; Cheng, J. Copper-Mediated Methylthiolation of Aryl

Halides with DMSO. *Chem. Commun.* **2011**, *47* (18), 5304–5306.

(81) Winter, A.; Hummel, J.; Risch, N. Oligo(U-terpyridines) and Their Ruthenium(II) Complexes: Synthesis and Structural Properties. *J. Org. Chem.* **2006**, *71* (13), 4862–4871.

(82) Rasmussen, S. C.; Ronco, S. E.; Mlsna, D. A.; Billadeau, M. A.; Pennington, W. T.; Kolis, J. W.; Petersen, J. D. Ground- and Excited-State Properties of Ruthenium(II) Complexes Containing Tridentate Azine Ligands, Ru(tpy)(bpy)L^{2+}, Where L Is a Polymerizable Acetylene. *Inorg. Chem.* **1995**, *34* (4), 821–829.

(83) Rack, J. J.; Mockus, N. V. Room-Temperature Photochromism in Cis- and Trans-$[Ru(bpy)_2(DMSO)_2]^{2+}$. *Inorg. Chem.* **2003**, *42* (19), 5792–5794.

(84) Albani, B. A.; Peña, B.; Saha, S.; White, J. K.; Schaeffer, A. M.; Dunbar, K. R.; Turro, C. A Dinuclear Ru(II) Complex Capable of Photoinduced Ligand Exchange at Both Metal Centers. *Chem. Commun.* **2015**, *51* (92), 16522–16525.

(85) Hartshorn, C. M.; Daire, N.; Tondreau, V.; Loeb, B.; Meyer, T. J.; White, P.S. Synthesis and Characterization of Dinuclear Ruthenium Complexes with Tetra-2-pyridylpyrazine as a Bridge. *Inorg. Chem.* **1999**, *38* (13), 3200–3206.

Appendices

Appendix A NMR Data

A.1 NMR data for Chapter 2

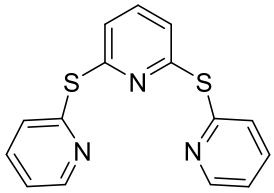

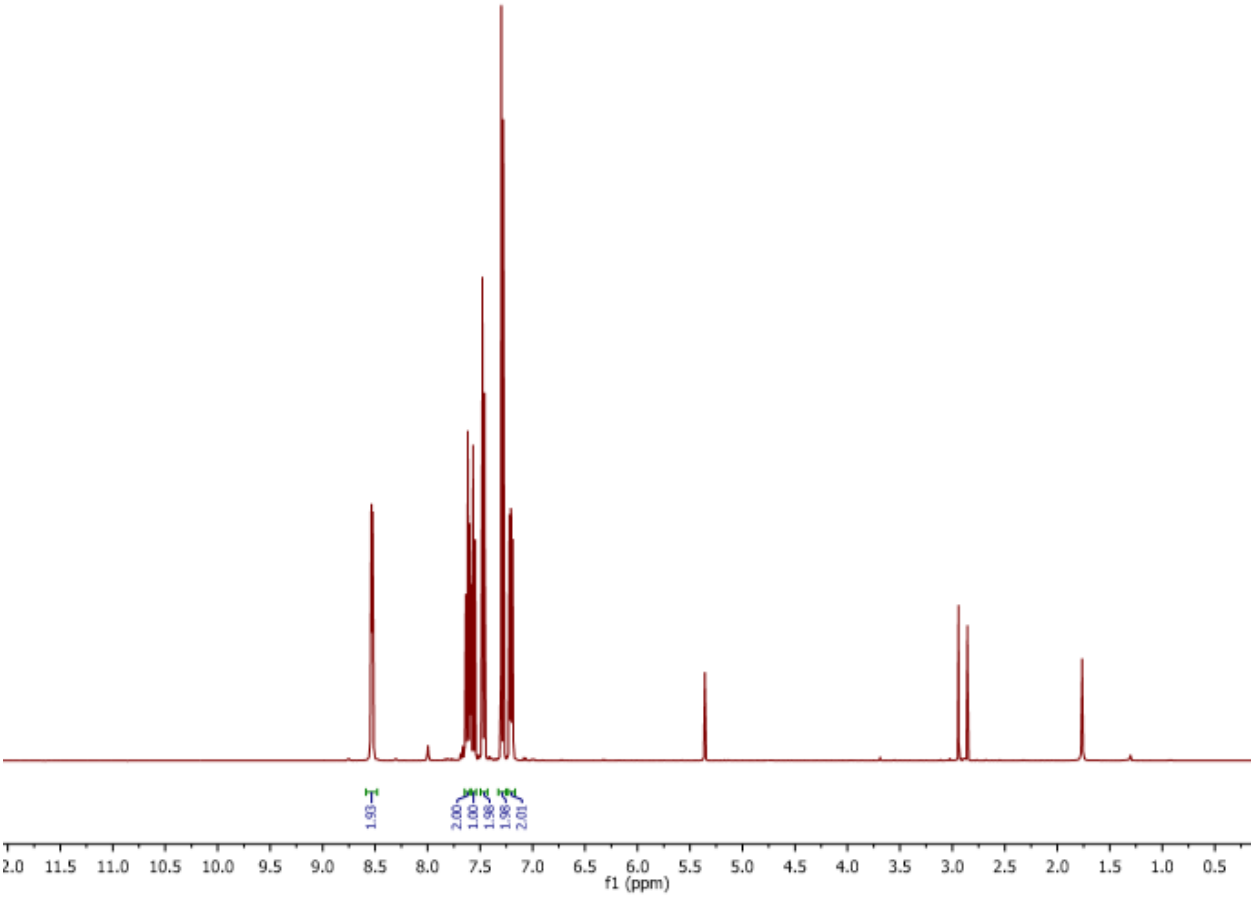

Figure S1. ^{1}H NMR spectrum of TPS (400 MHz, DCM-d_2) (18**)**

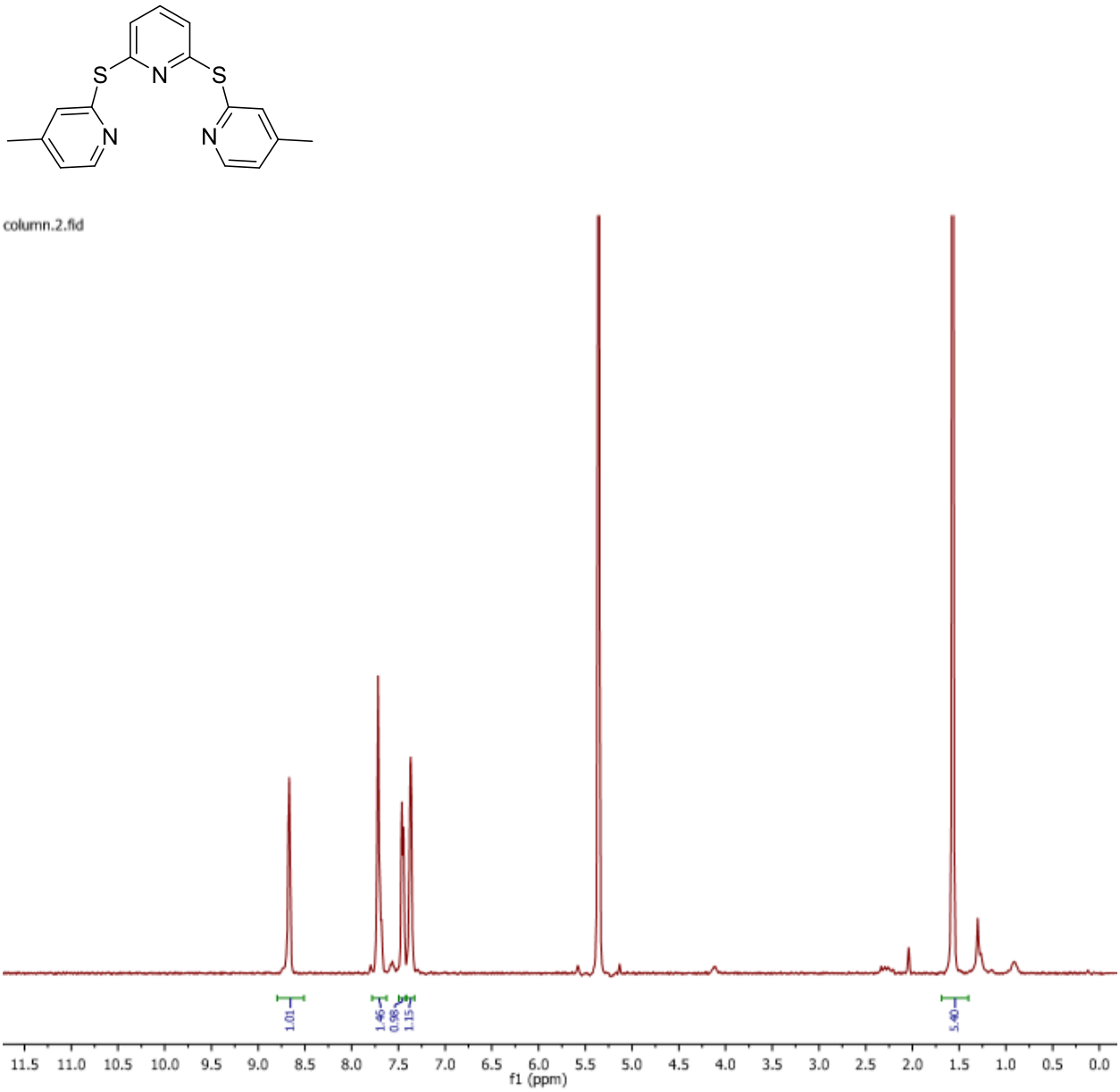

Figure S2. ^{1}H NMR spectrum of MeTPS (400 MHz, DCM-d_2) (19)

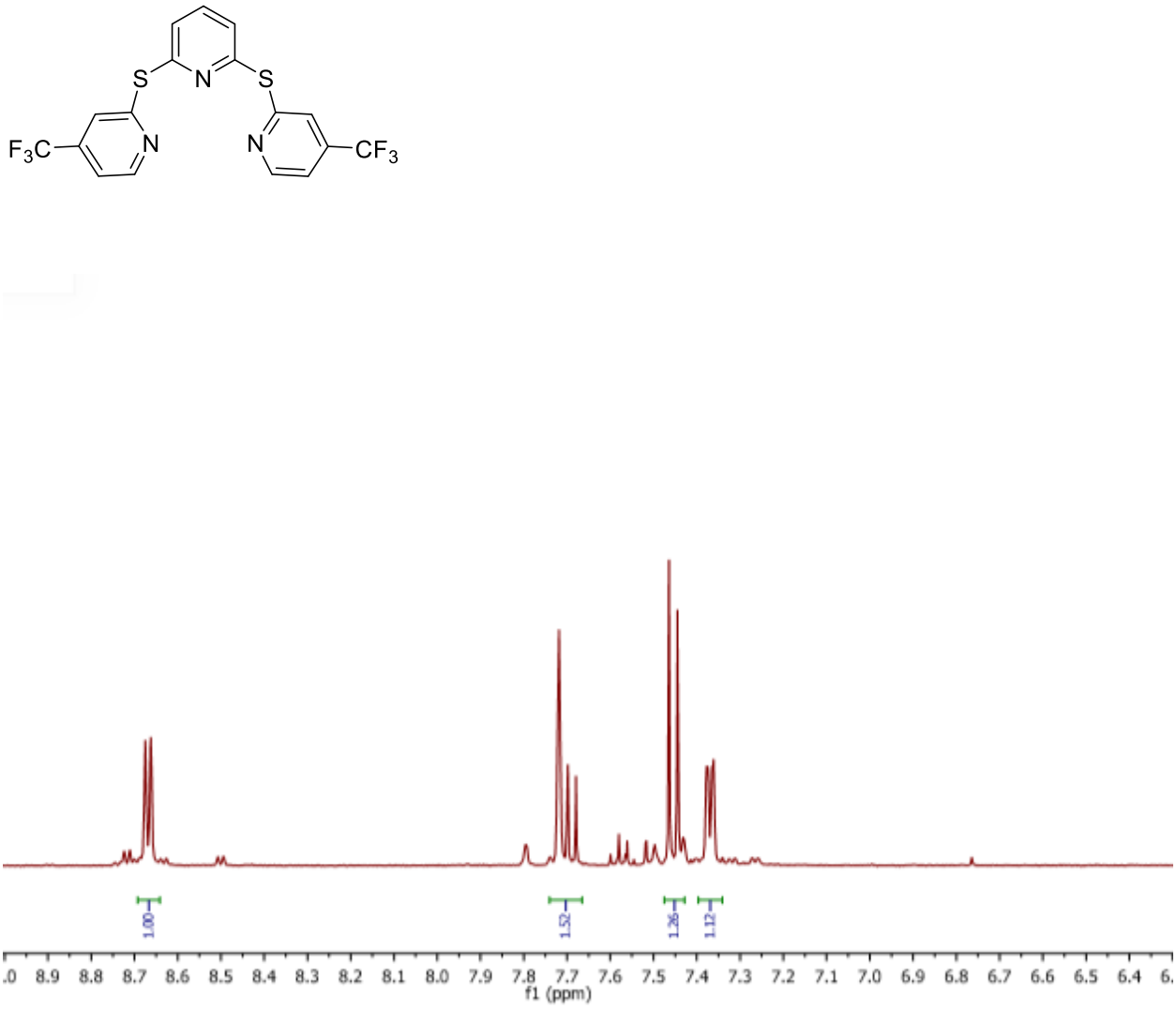

Figure S3. ^{1}H NMR spectrum of TFM-TPS (400 MHz, DCM-d_2) (20)

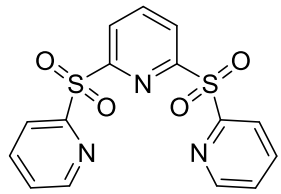

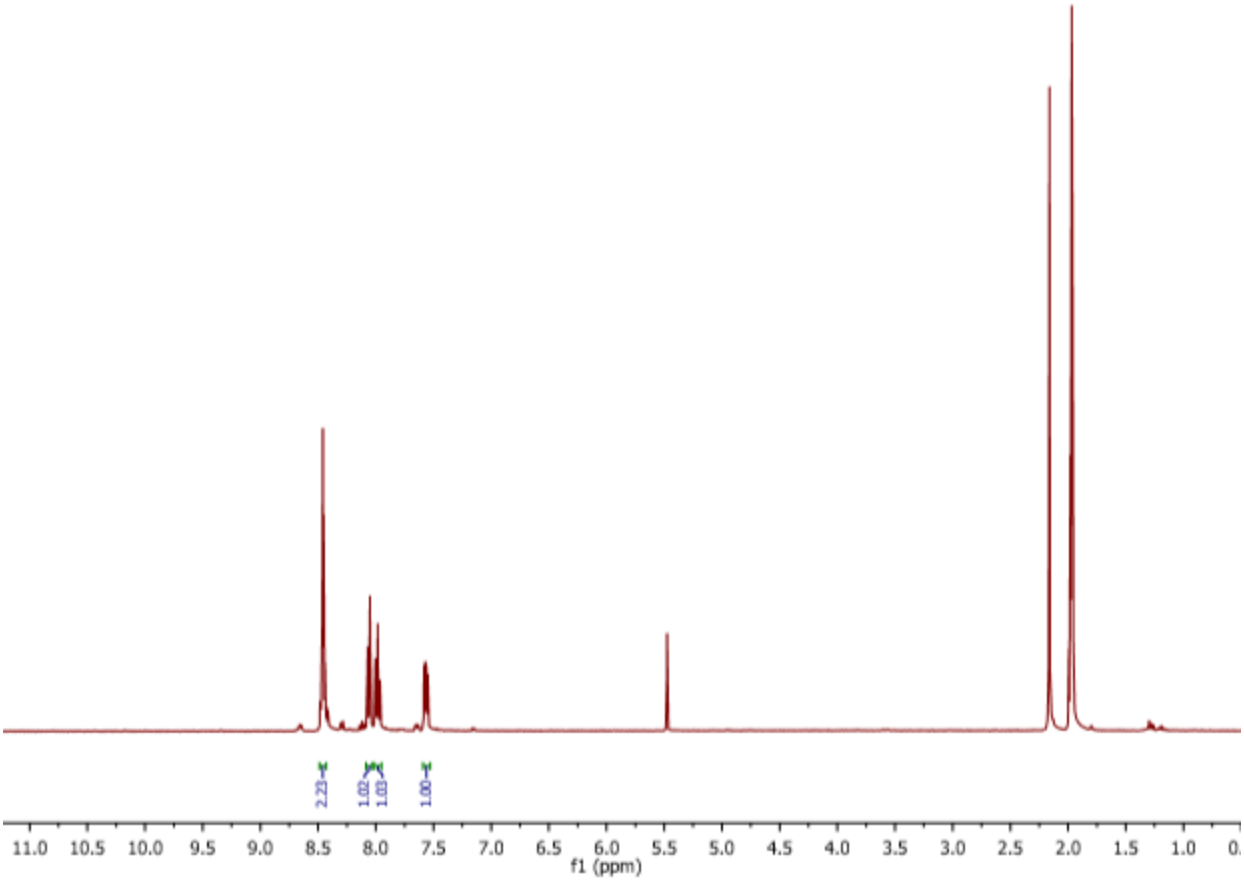

Figure S4. ^{1}H NMR spectrum of Sulfone-TPS (400 MHz, MeCN-*d*$_3$) (21)

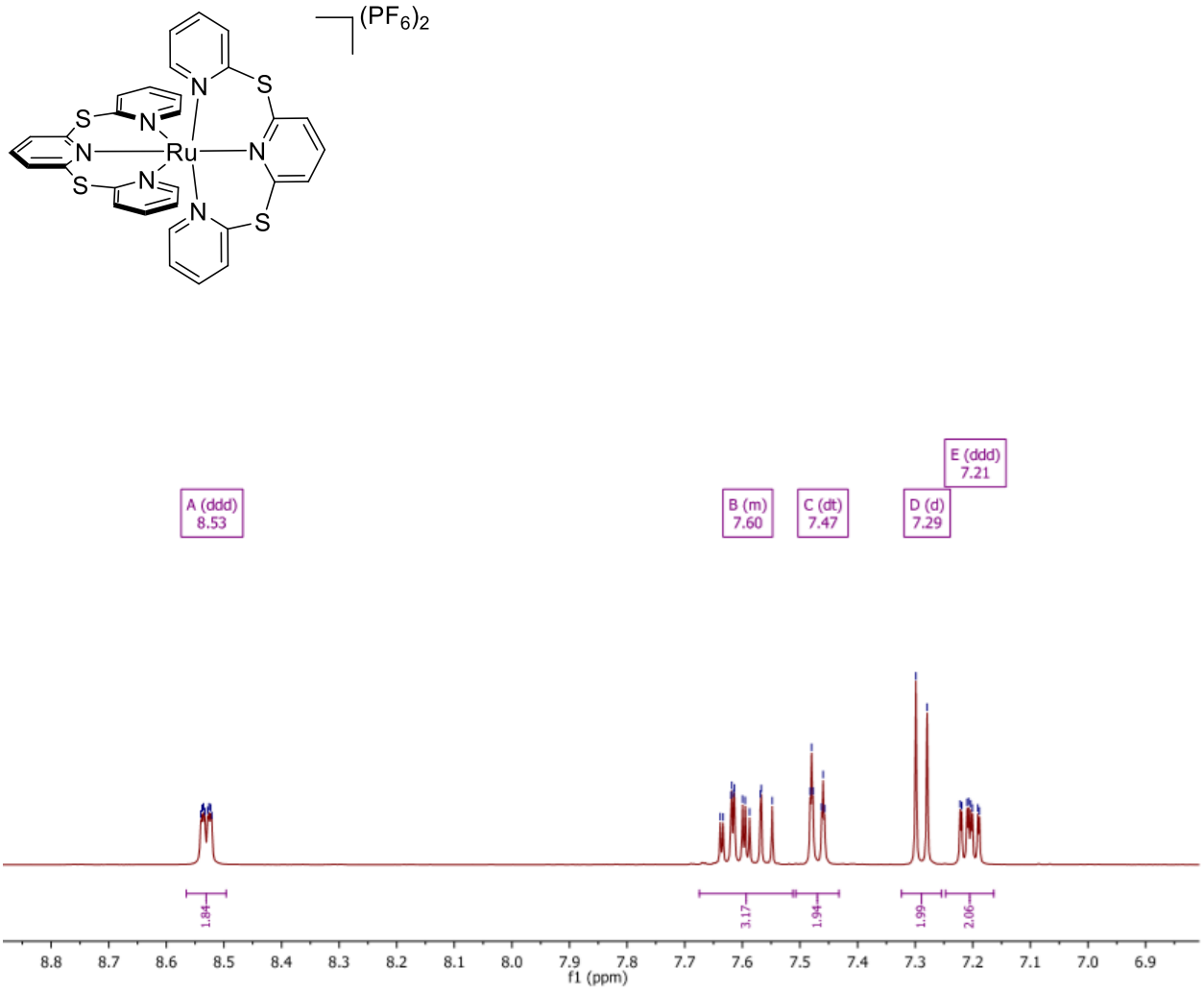

Figure S5. ^{1}H NMR spectrum of Ru(TPS)$_2$ (400 MHz, DCM-d_2) (22)

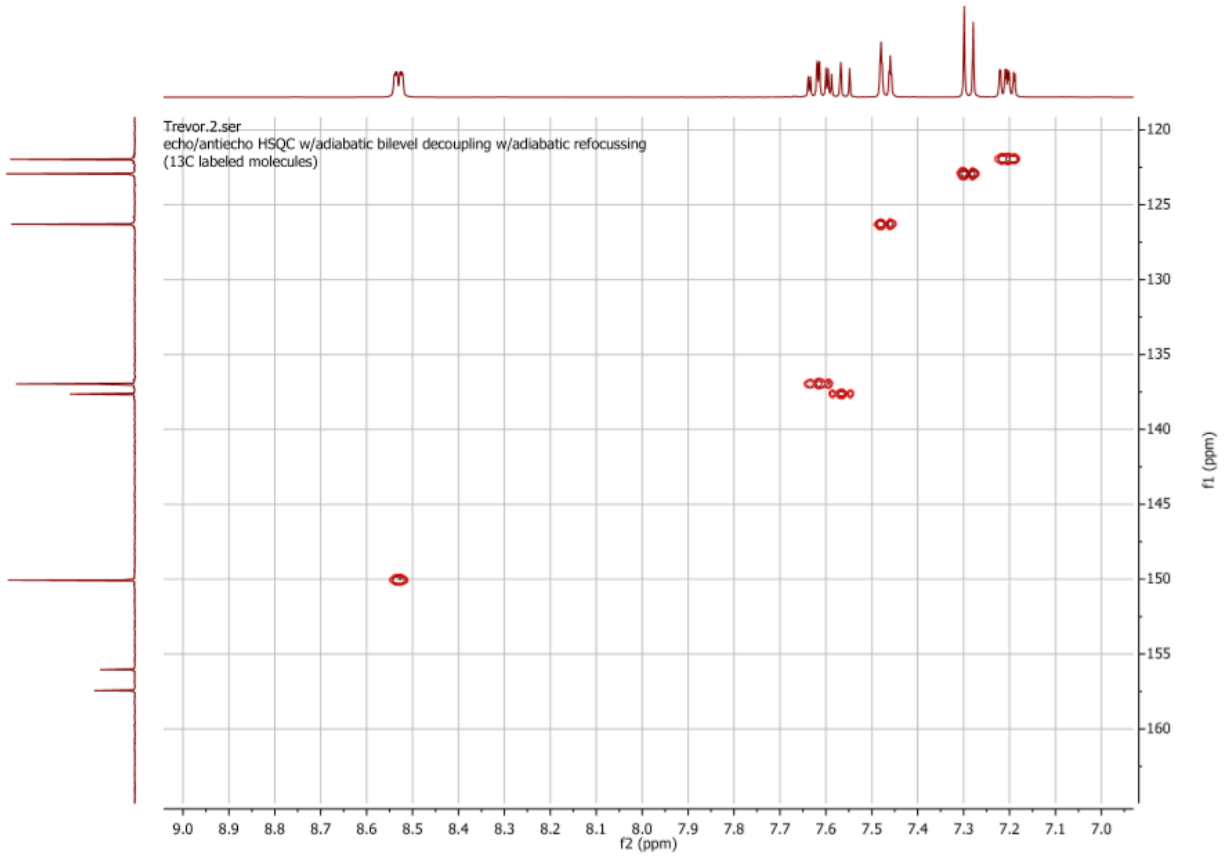

Figure S6. HSQC spectrum of Ru(TPS)$_2$ (400 MHz, DCM-d_2) (22)

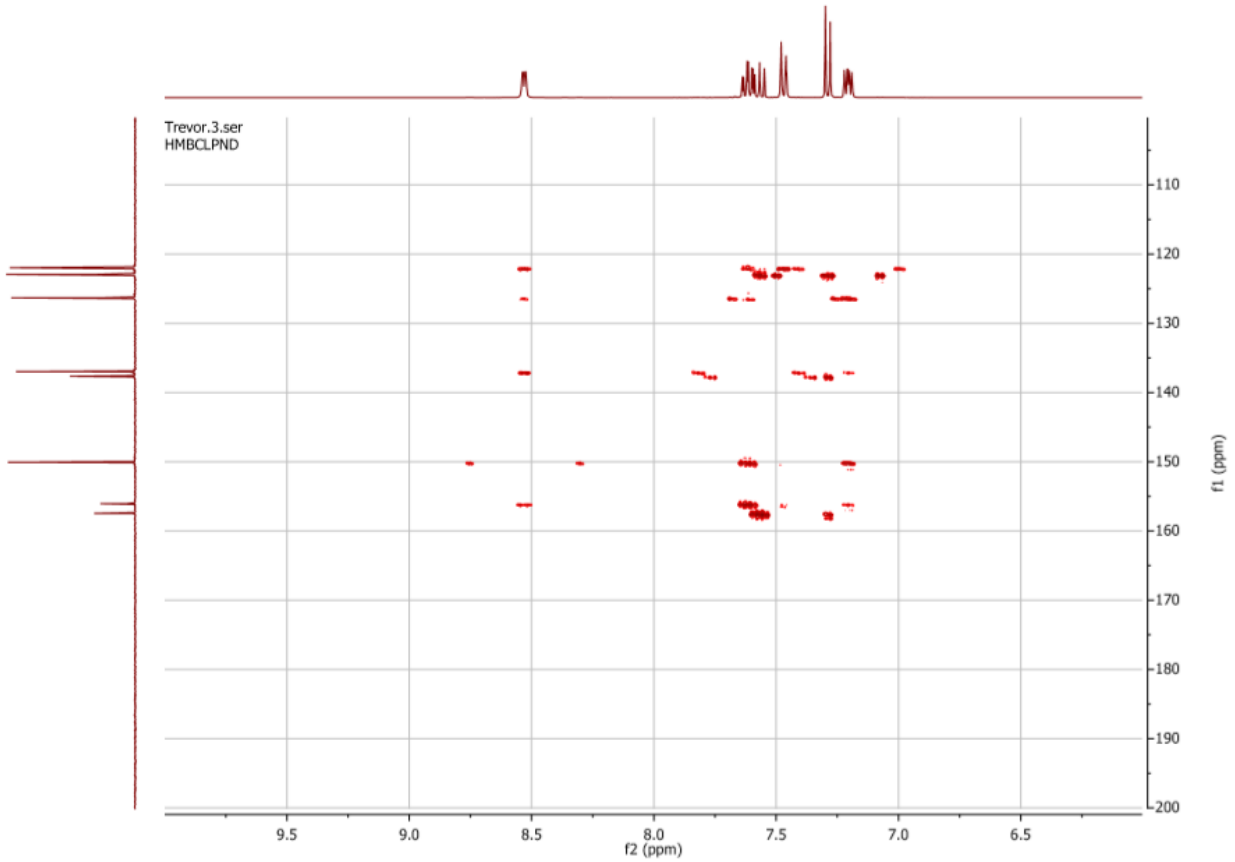

Figure S7. HMBC spectrum of Ru(TPS)$_2$ (400 MHz, DCM-d_2) (22)

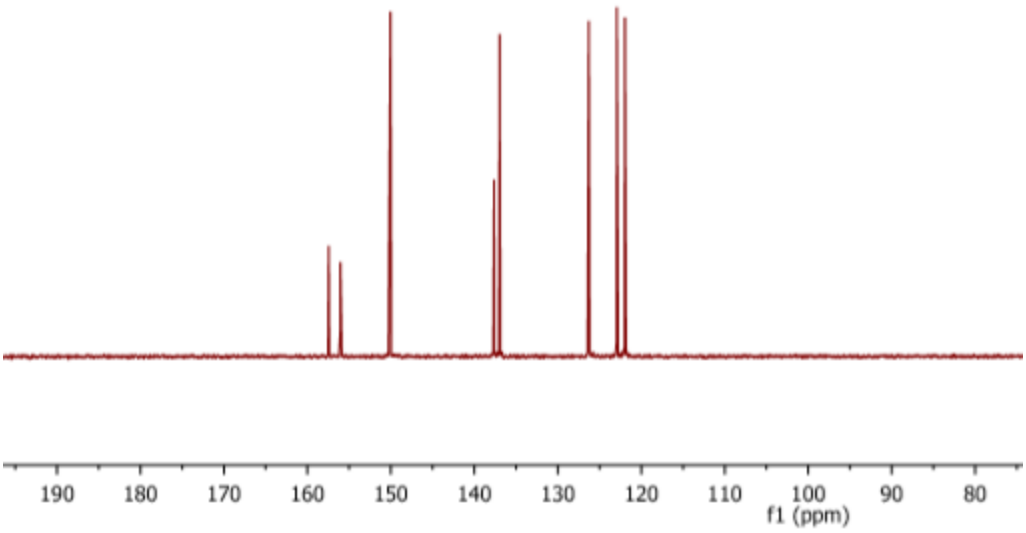

Figure S8. ^{13}C NMR spectrum of Ru(TPS)$_2$ (400 MHz, DCM-d_2) (22**)**

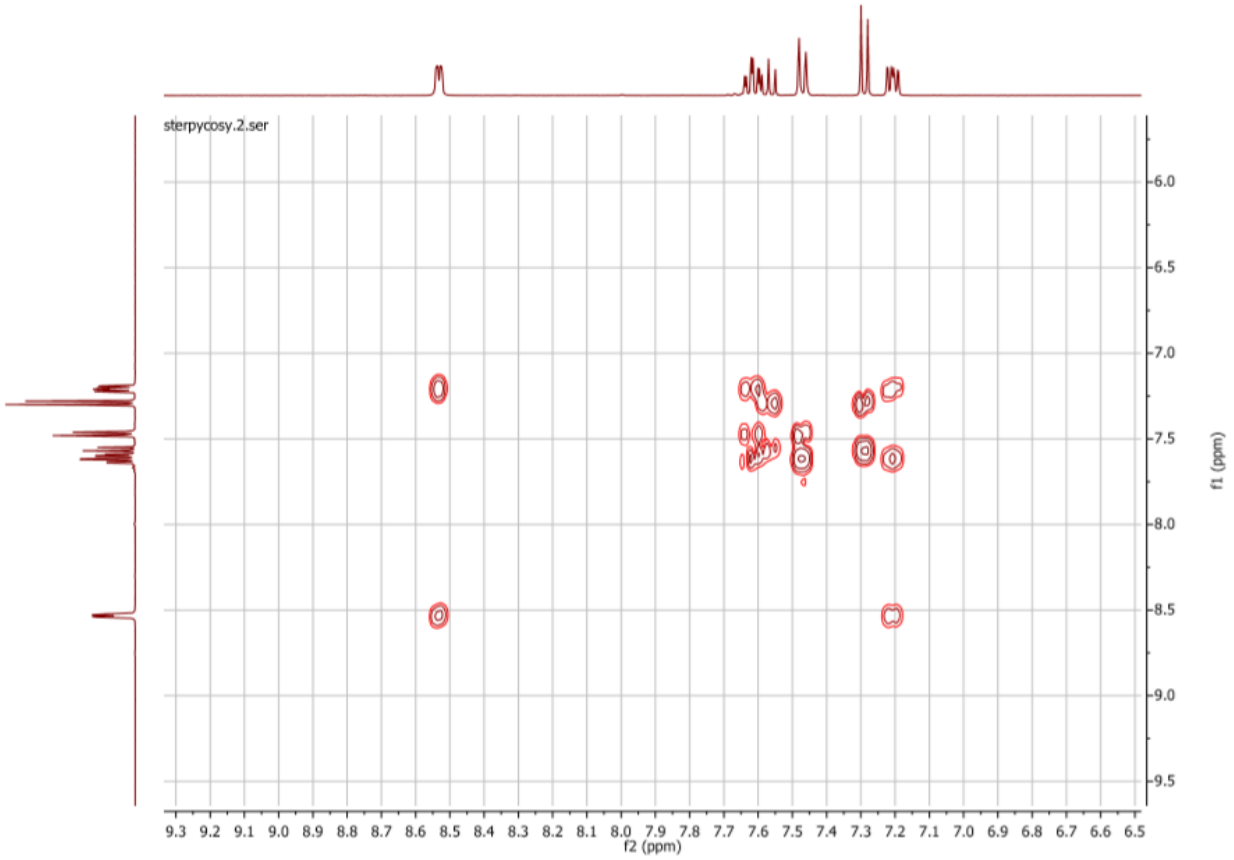

Figure S9. COSY spectrum of Ru(TPS)$_2$ (400 MHz, DCM-d_2) (22)

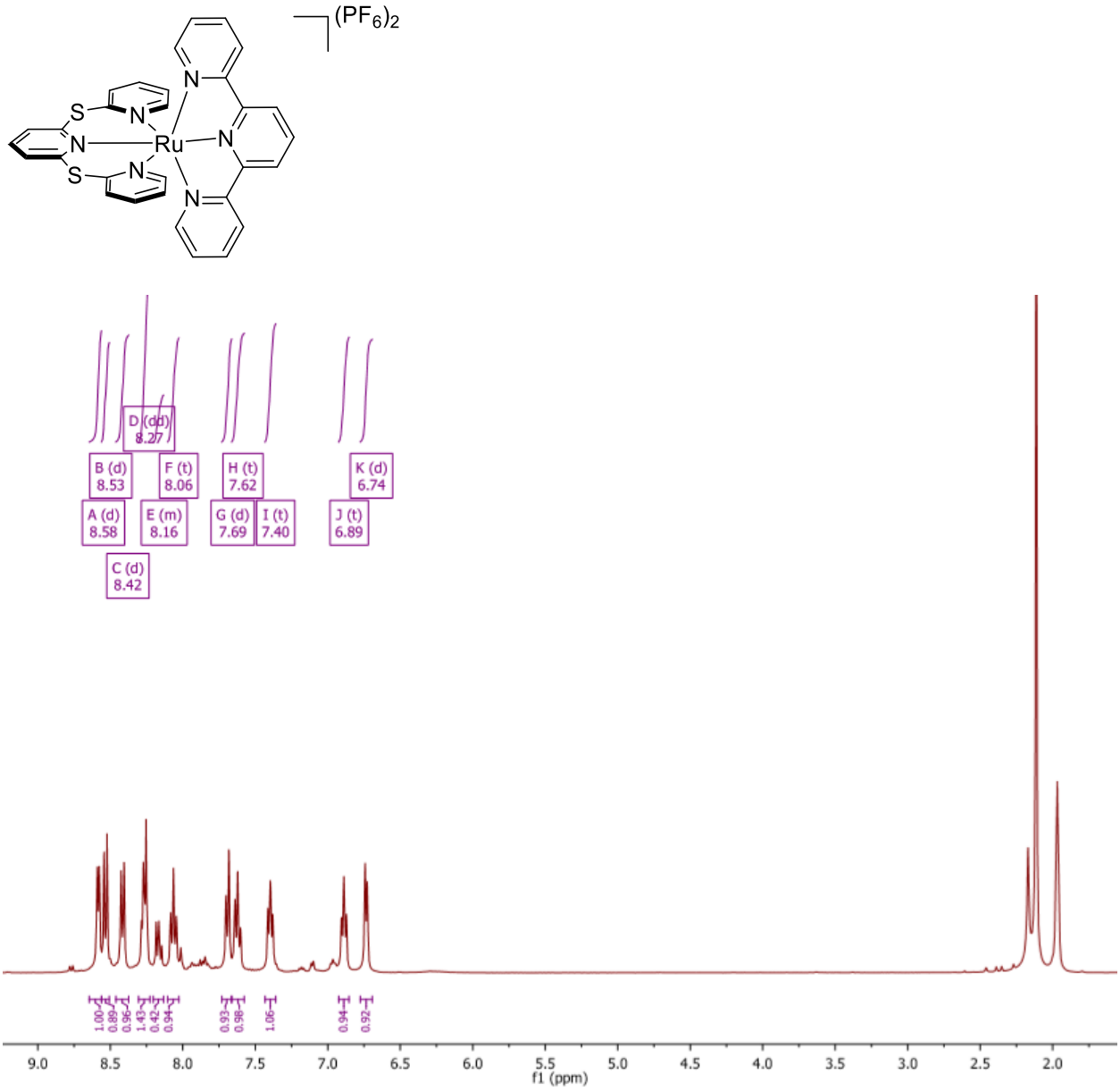

Figure S10. ^{1}H NMR spectrum of *Ru(TPS)(tpy)(PF$_6$)$_2$* (400 MHz, MeCN-*d*$_3$) (25)

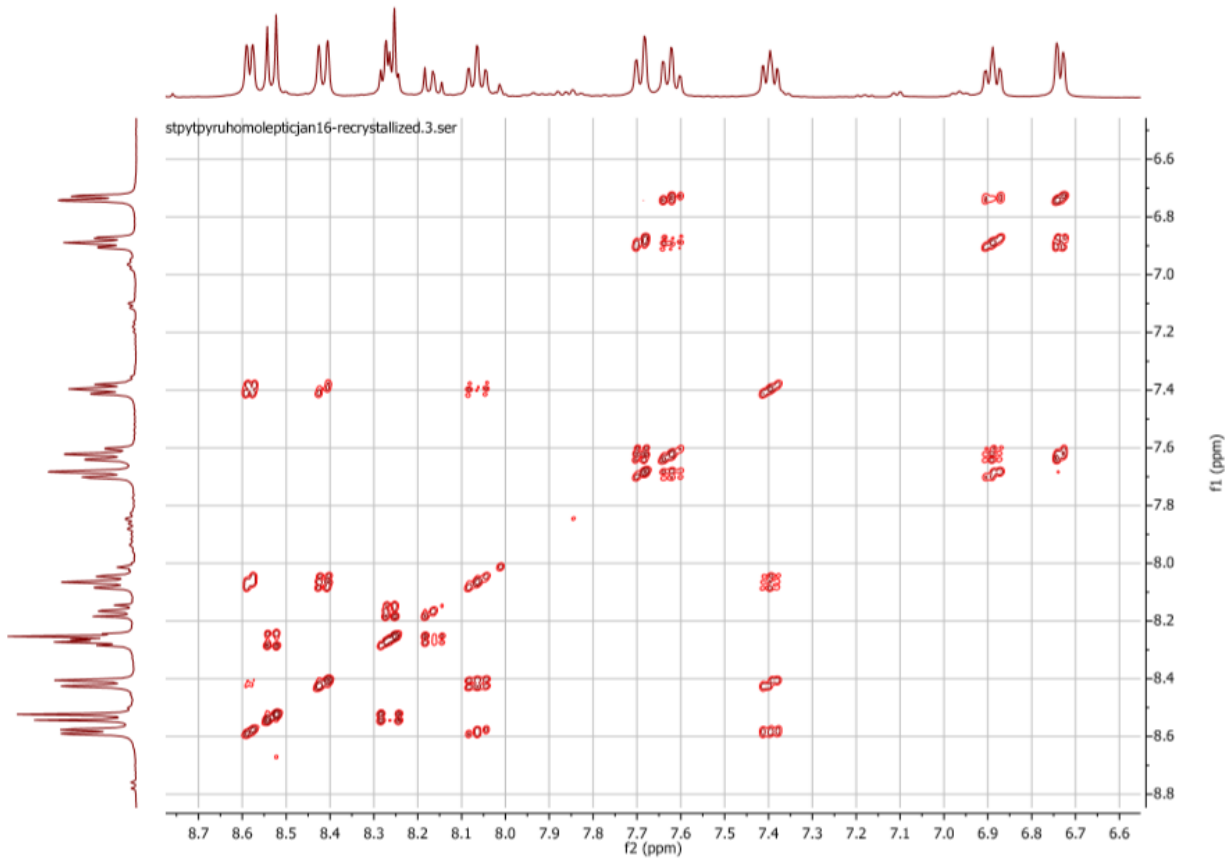

Figure S11. COSY spectrum of *Ru(TPS)(tpy)(PF$_6$)$_2$* (400 MHz, MeCN-*d*$_3$) (25)

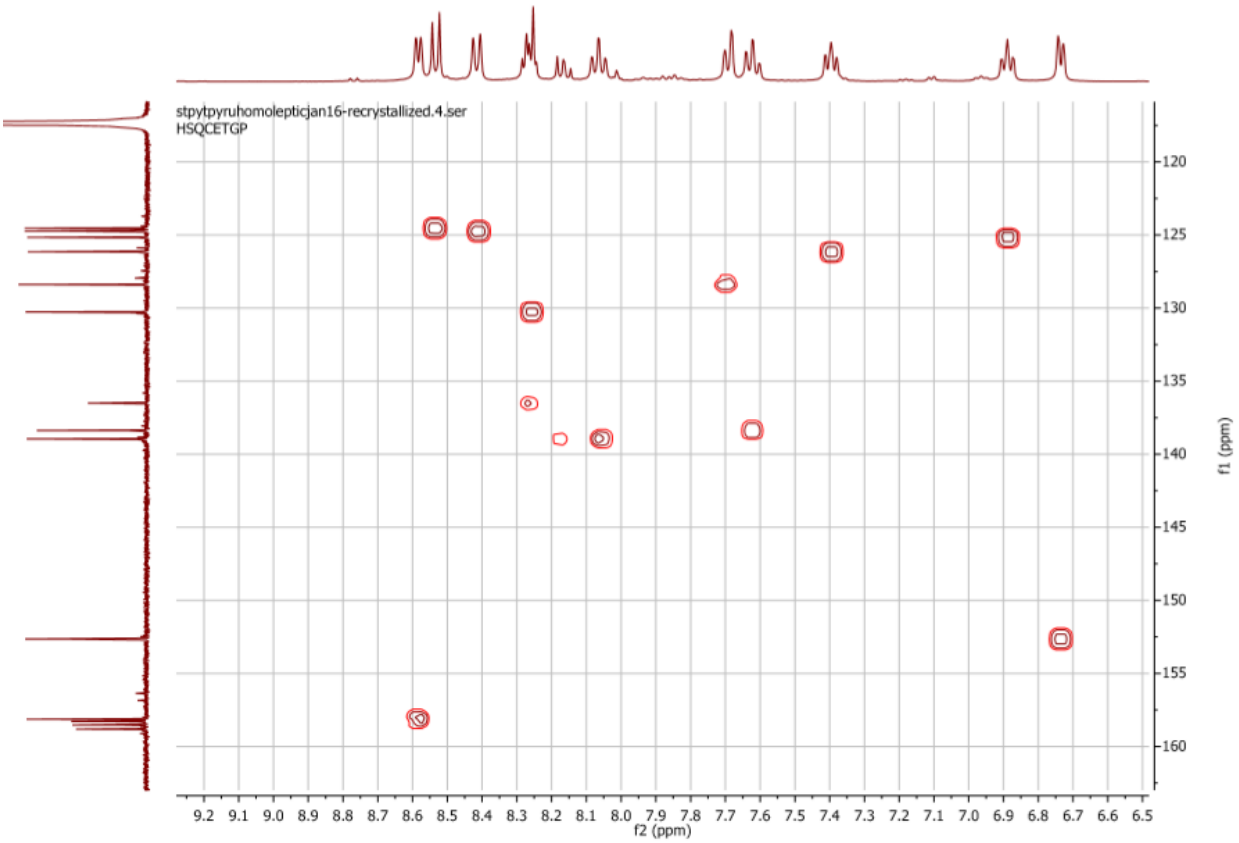

Figure S12. HSQC spectrum of *Ru(TPS)(tpy)(PF$_6$)$_2$* (400 MHz, MeCN-*d*$_3$) (25)

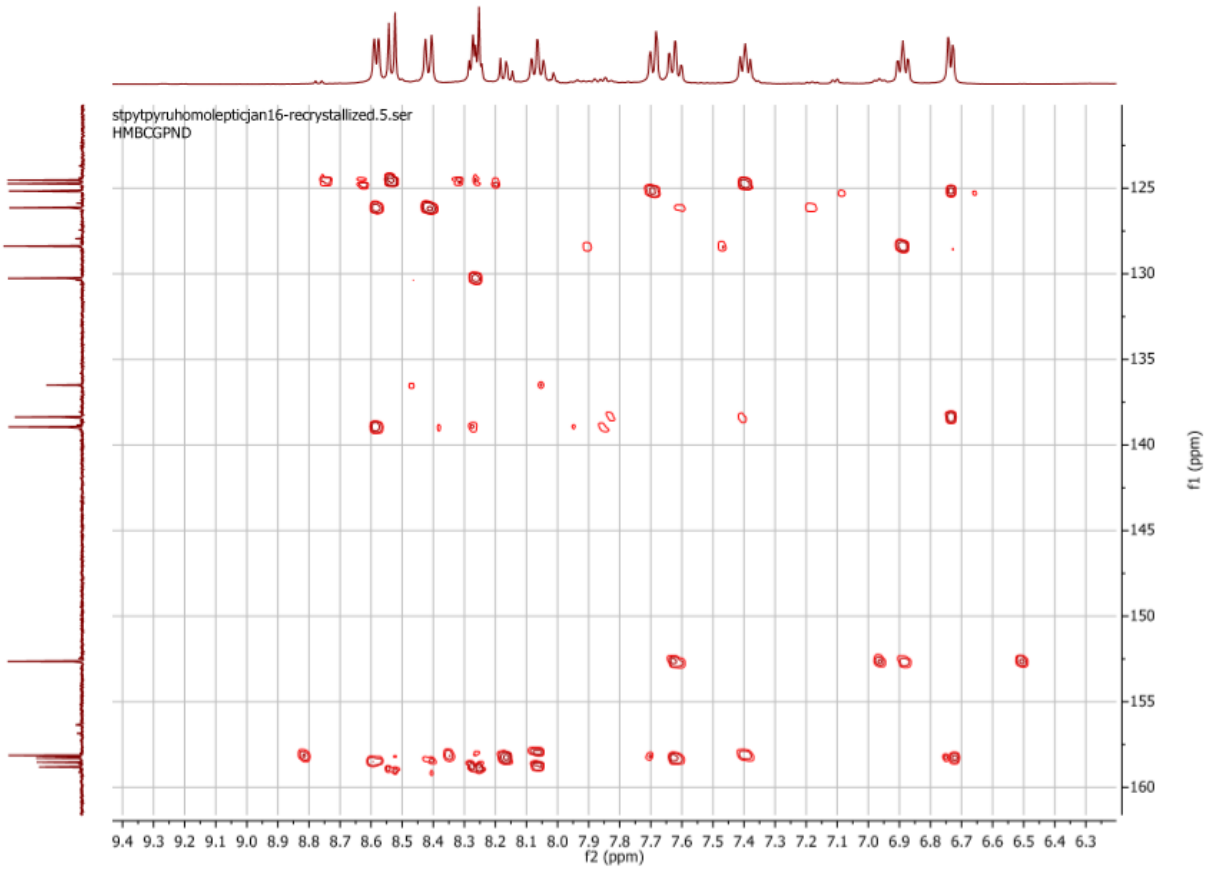

Figure S13. HMBC spectrum of *Ru(TPS)(tpy)(PF$_6$)$_2$* (400 MHz, MeCN-*d*$_3$) (25)

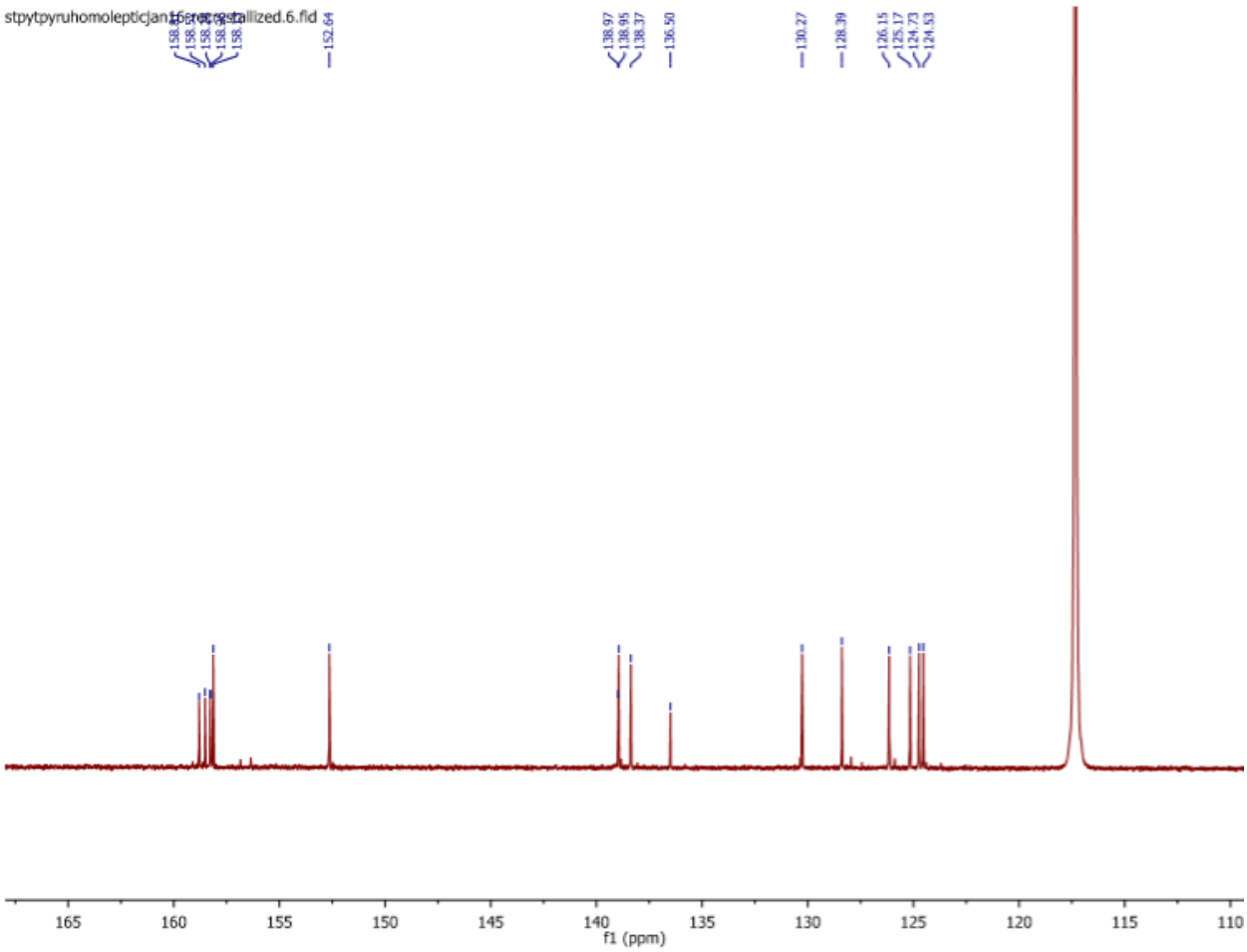

Figure S14. ^{13}C NMR spectrum of *Ru(TPS)(tpy)(PF$_6$)$_2$* (400 MHz, MeCN-*d*$_3$) (25)

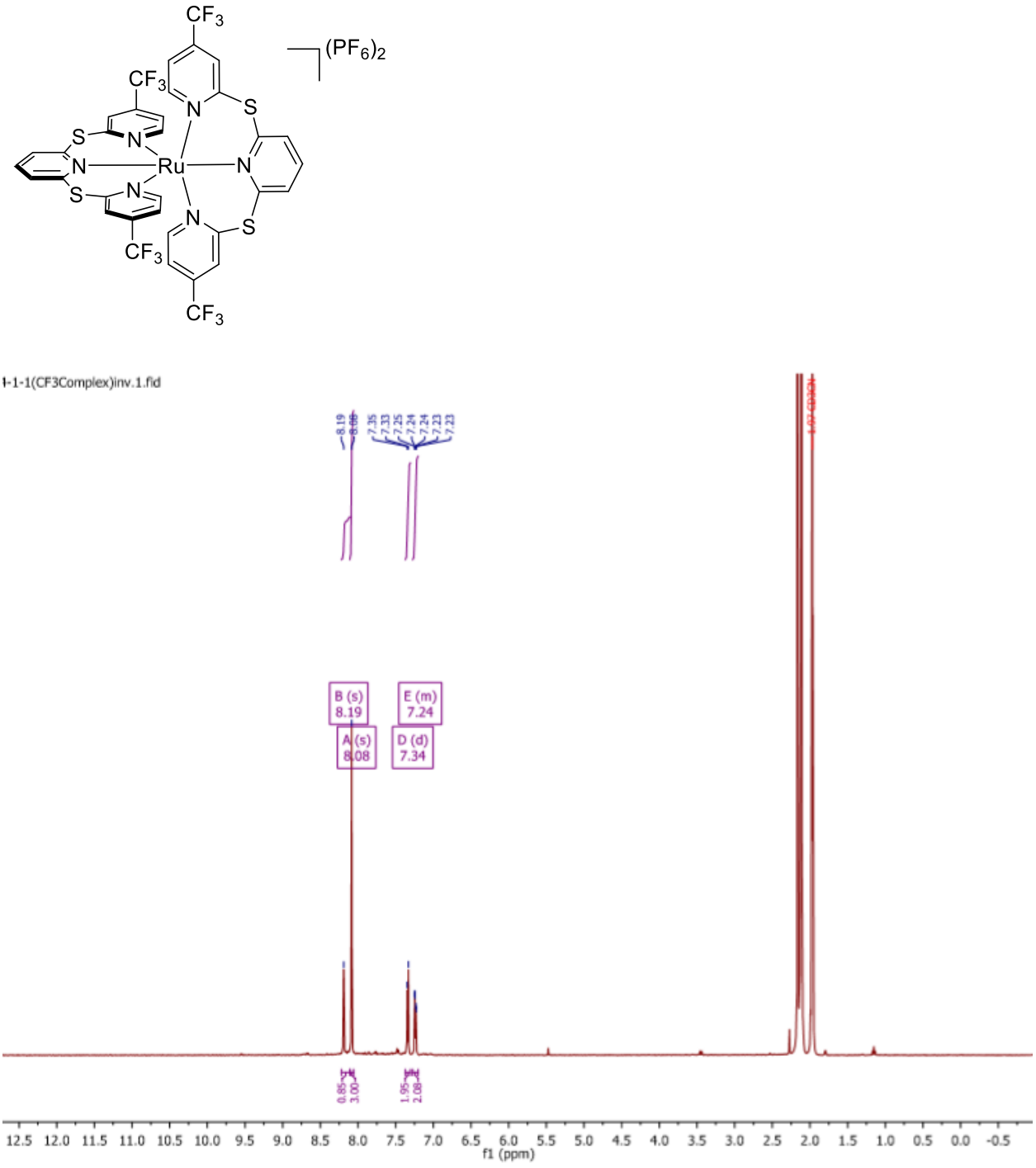

Figure S15. ^{1}H NMR spectrum of *Ru(TFM-TPS)$_2$(PF$_6$)$_2$*(400 MHz, DCM-*d*$_2$) (24)

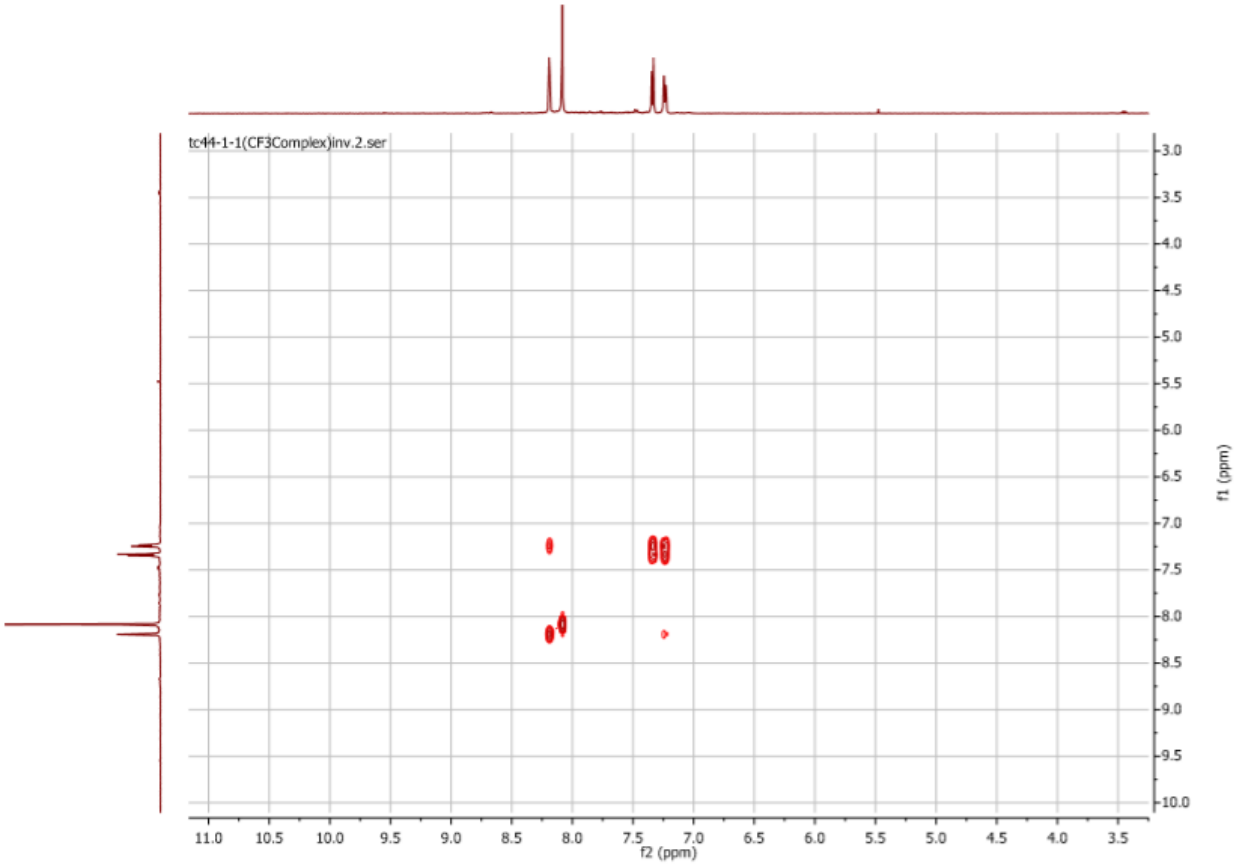

Figure S16. COSY spectrum of *Ru(TFM-TPS)$_2$(PF$_6$)$_2$* (400 MHz, DCM-*d$_2$*) (24)

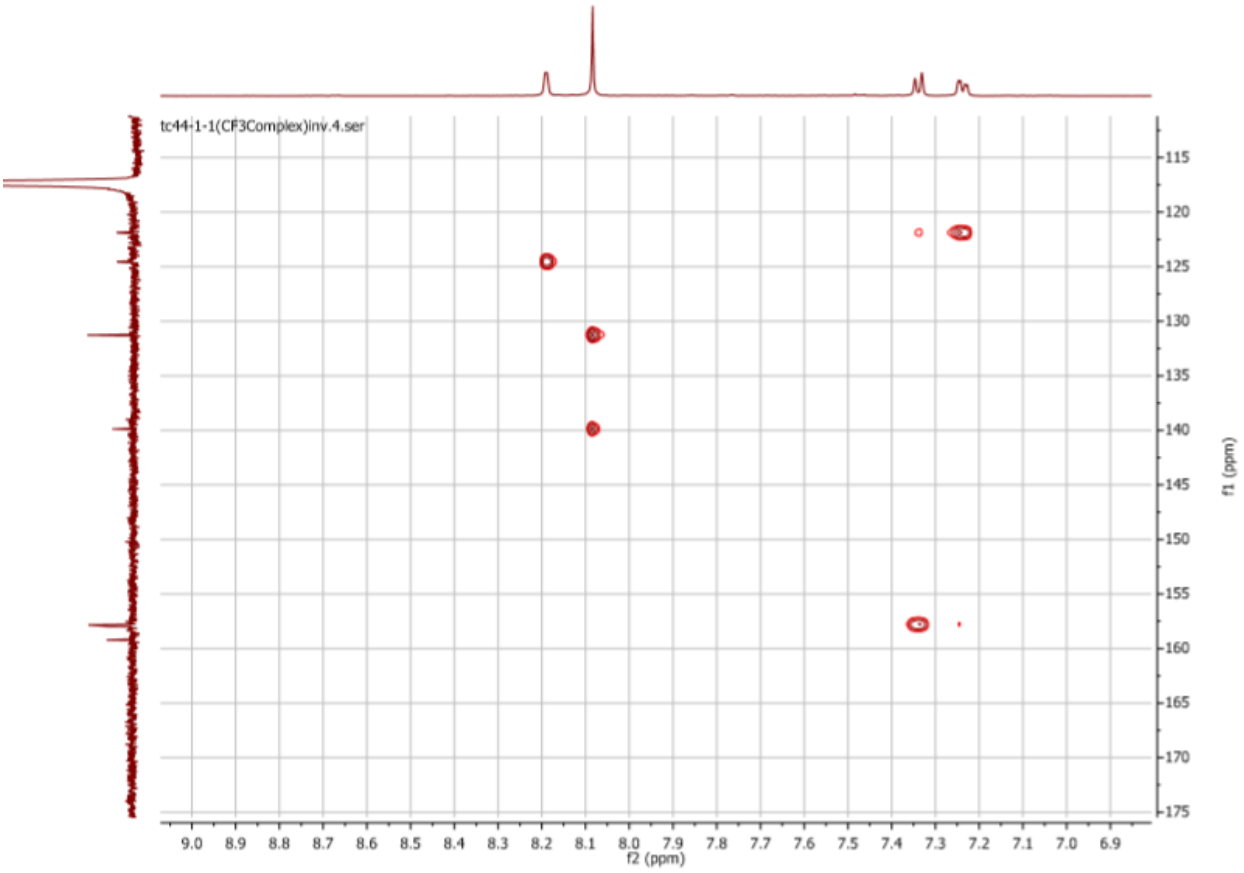

Figure S17. HSQC spectrum of *Ru(TFM-TPS)$_2$(PF$_6$)$_2$* (400 MHz, DCM-*d$_2$*) (24)

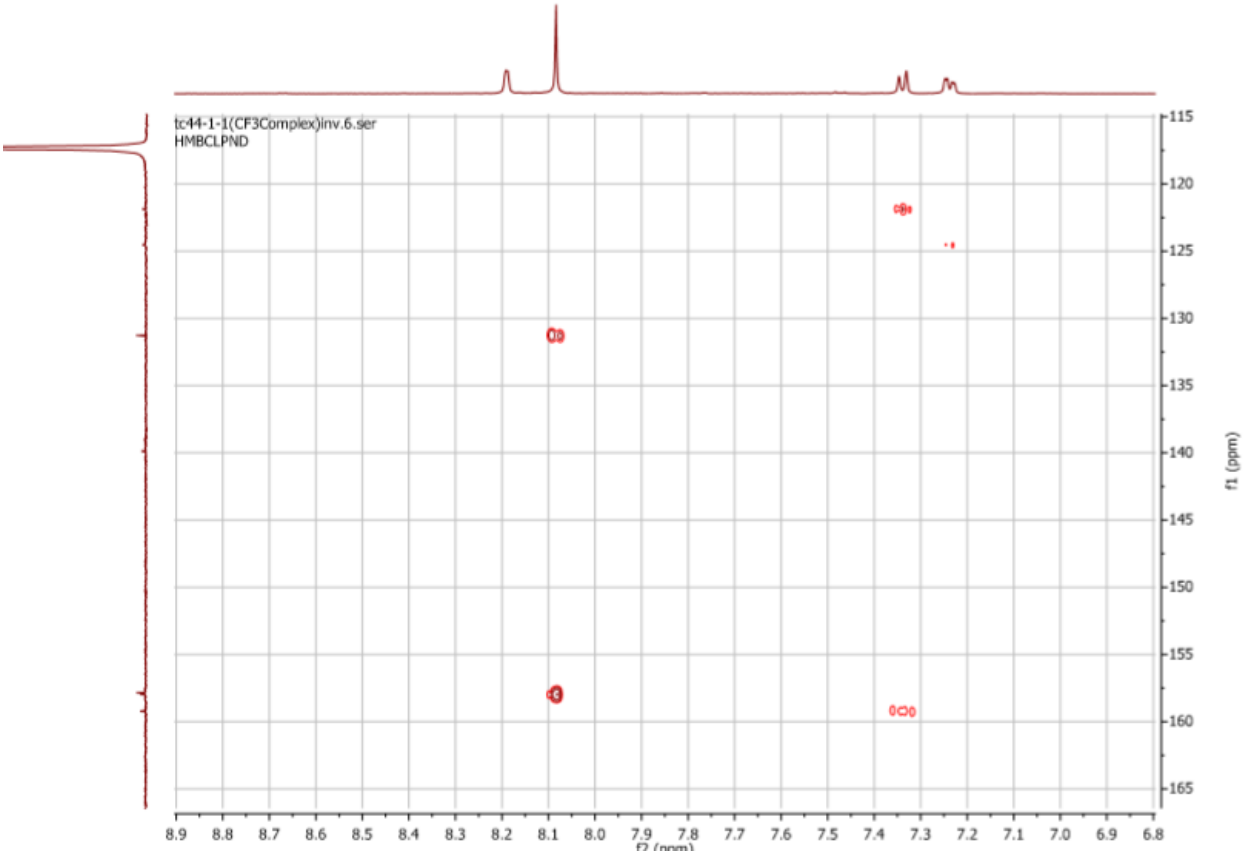

Figure S18. HMBC spectrum of *Ru(TFM-TPS)$_2$(PF$_6$)$_2$* (400 MHz, DCM-*d$_2$*) (24)

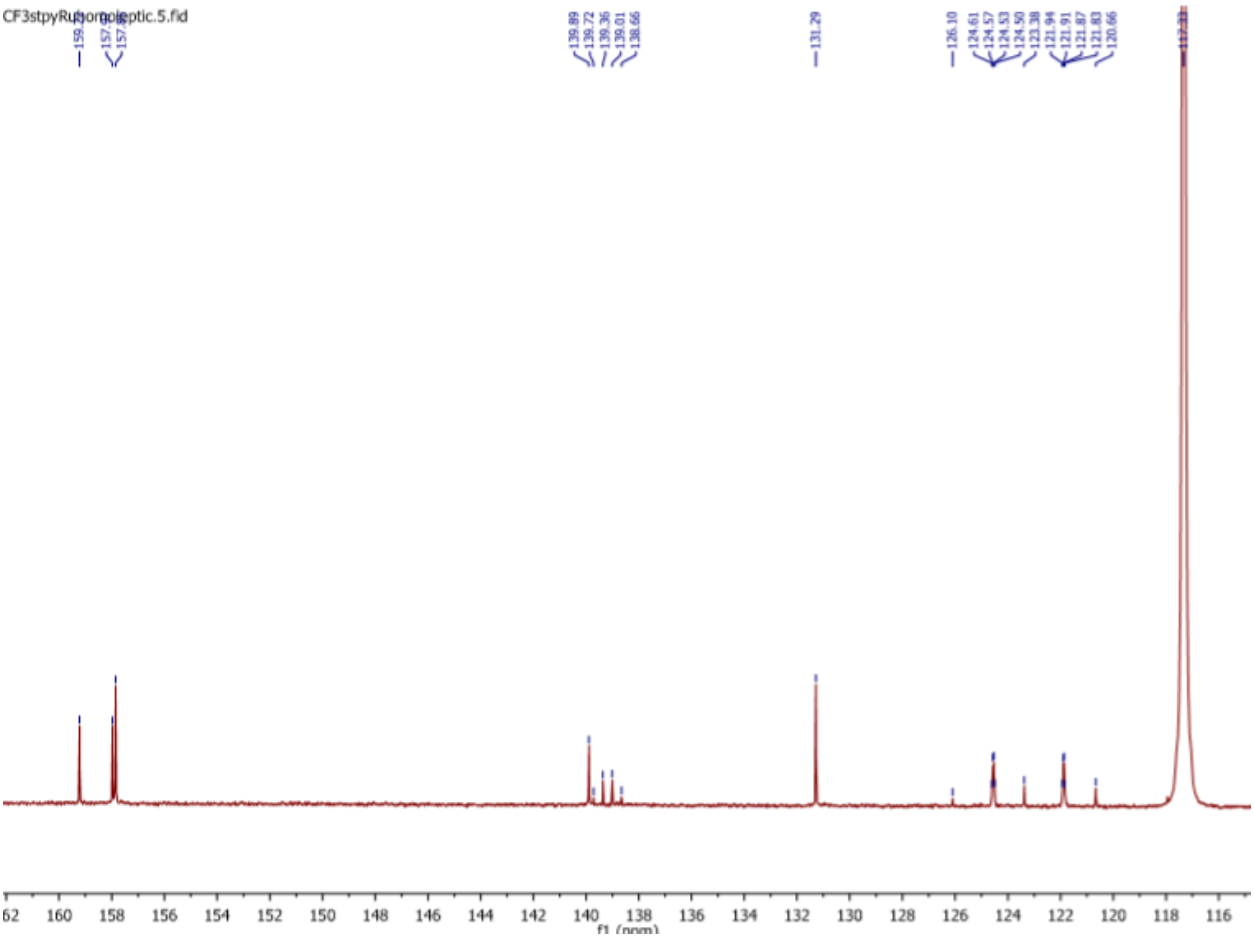

Figure S19. ^{13}C NMR spectrum of *Ru(TFM-TPS)$_2$(PF$_6$)$_2$*(400 MHz, DCM-*d$_2$*) (24)

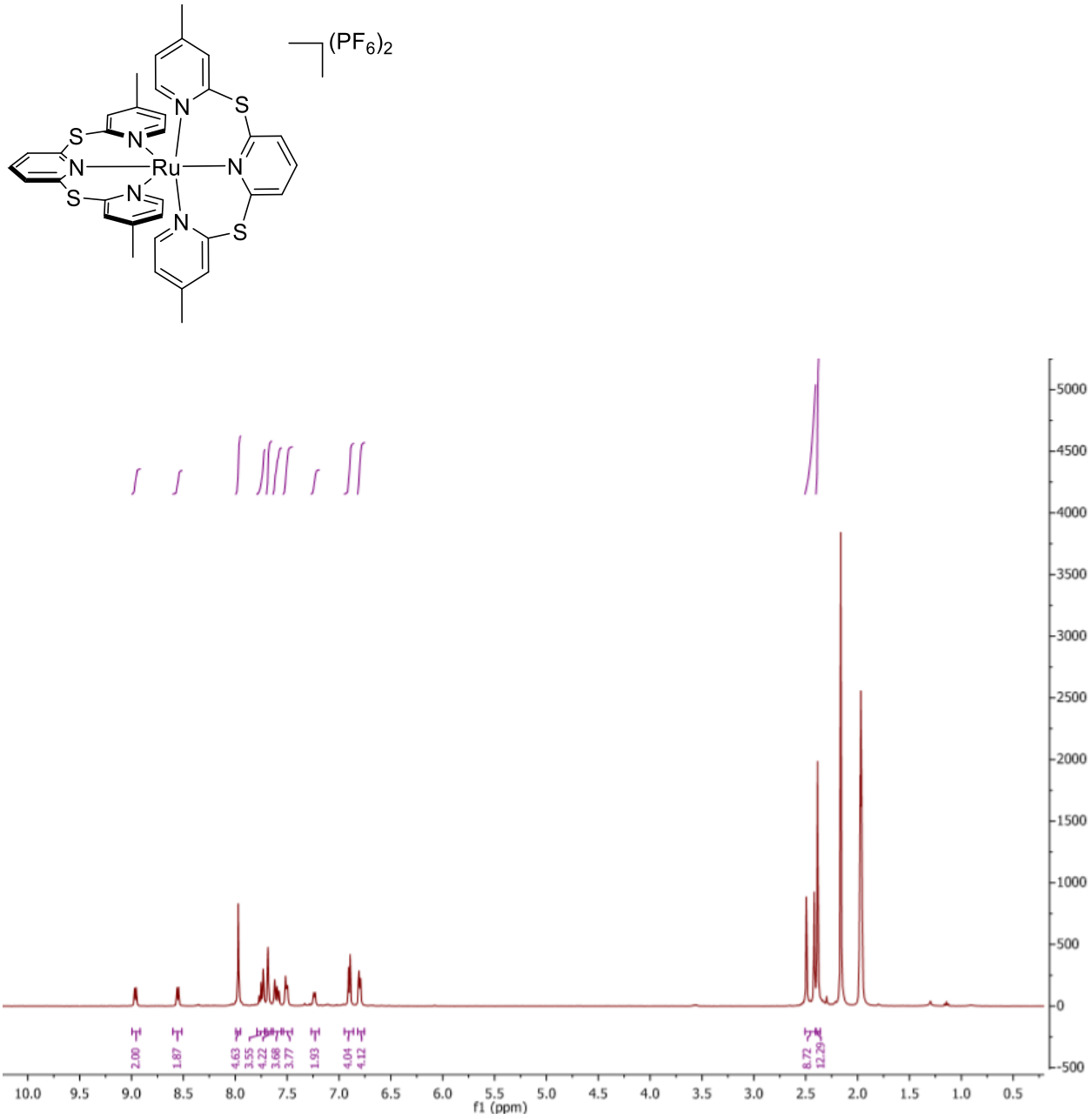

Figure S20. ^{1}H NMR spectrum of *Ru(Me-TPS)$_2$(PF$_6$)$_2$* (400 MHz, MeCN-*d*$_3$) (23)

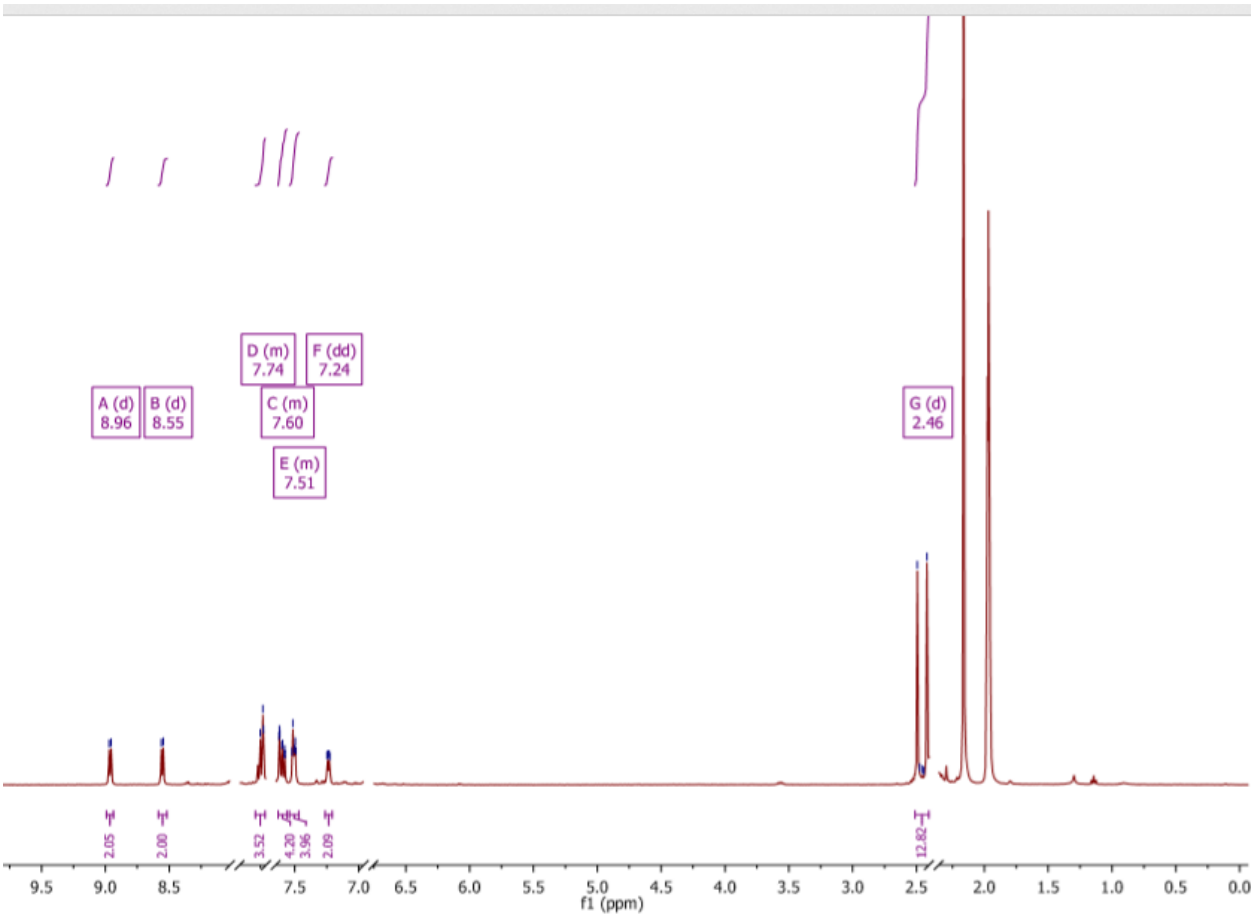

Figure S21. ^{1}H NMR spectrum of *Ru(Me-TPS)$_2$(PF$_6$)$_2$* with *mer*- peaks cut out (400 MHz, DCM-*d$_2$*) (23)

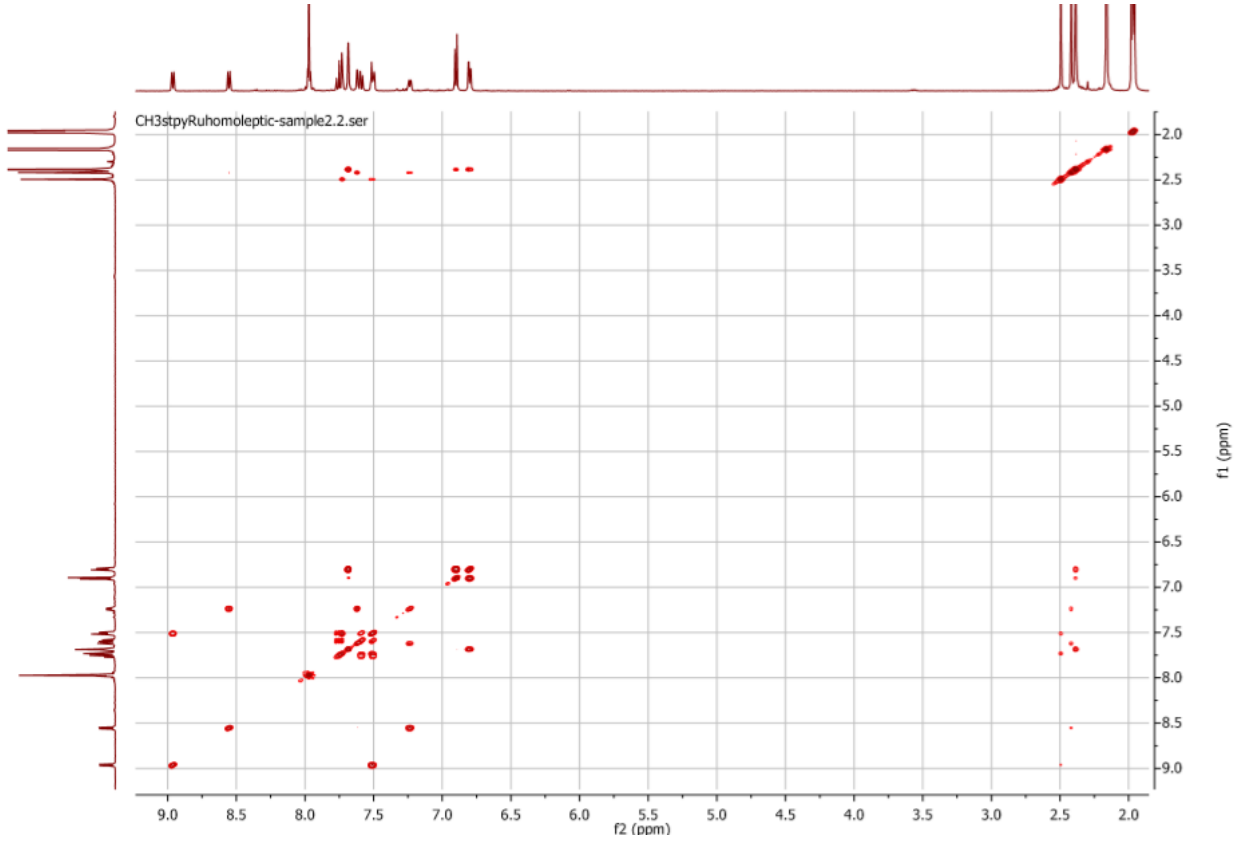

Figure S22. COSY spectrum of *Ru(Me-TPS)$_2$(PF$_6$)$_2$* (400 MHz, DCM-*d$_2$*) (23)

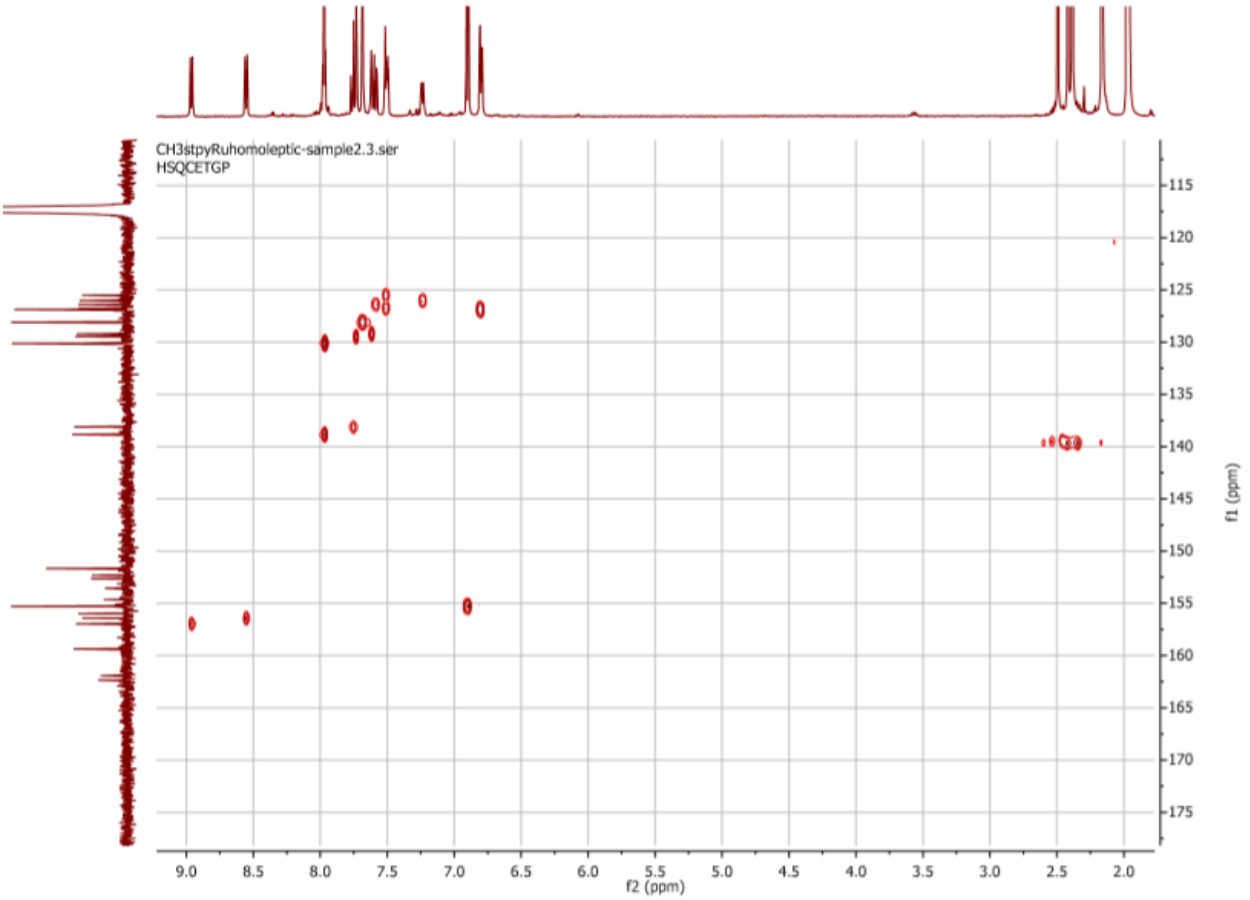

Figure S23. HSQC spectrum of *Ru(Me-TPS)$_2$(PF$_6$)$_2$* (400 MHz, DCM-*d$_2$*) (23)

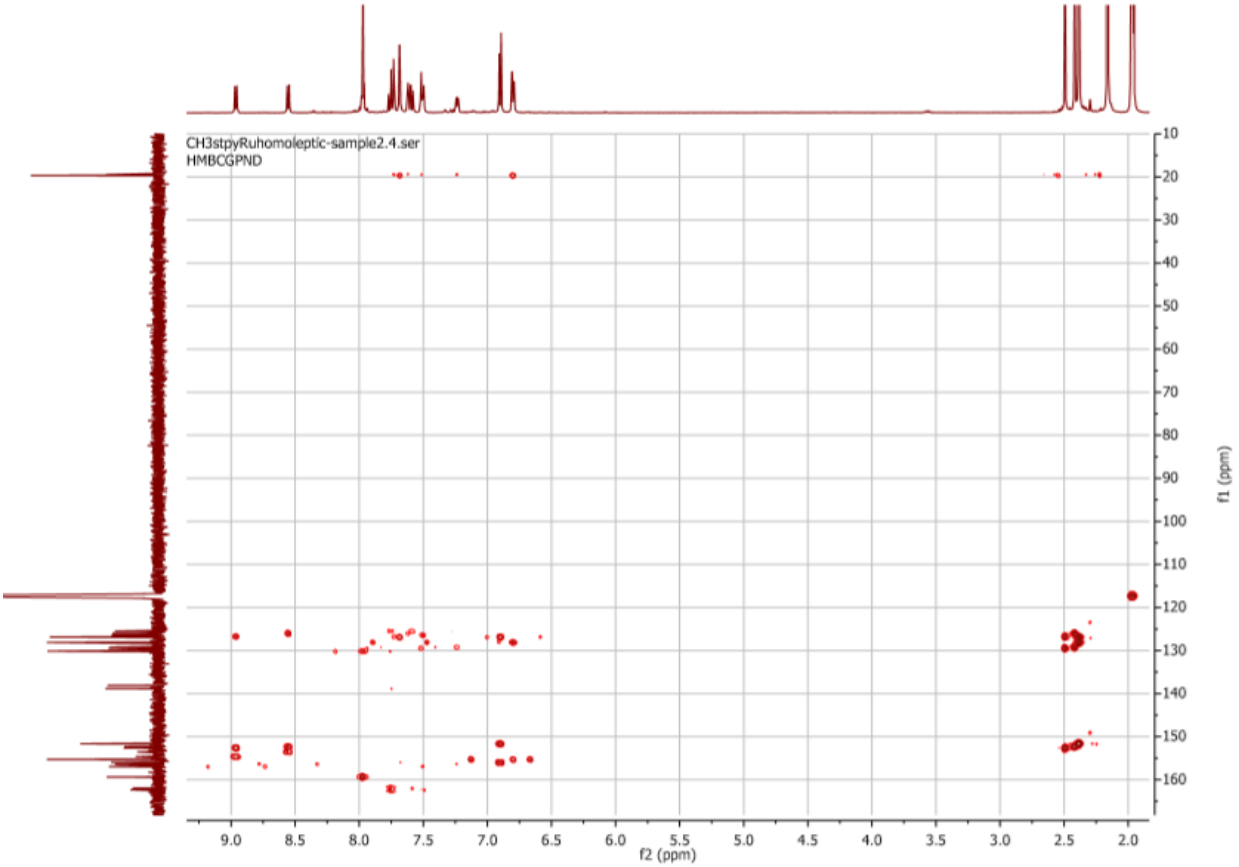

Figure S24. HMBC spectrum of *Ru(Me-TPS)$_2$(PF$_6$)$_2$*(400 MHz, DCM-*d$_2$*) (23)

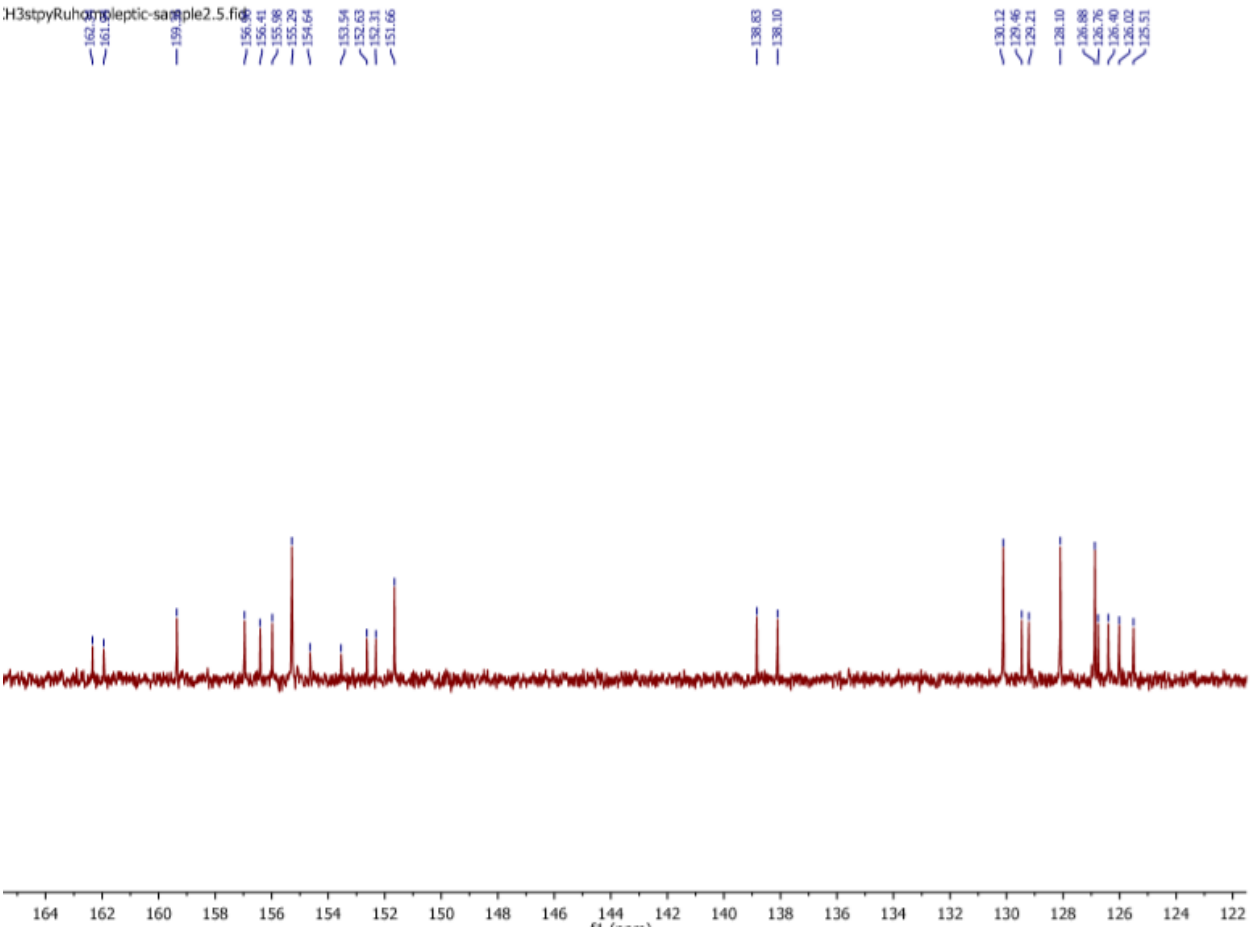

Figure S25. ^{13}C NMR spectrum of *Ru(Me-TPS)$_2$(PF$_6$)$_2$* (400 MHz, DCM-*d$_2$*) (23)

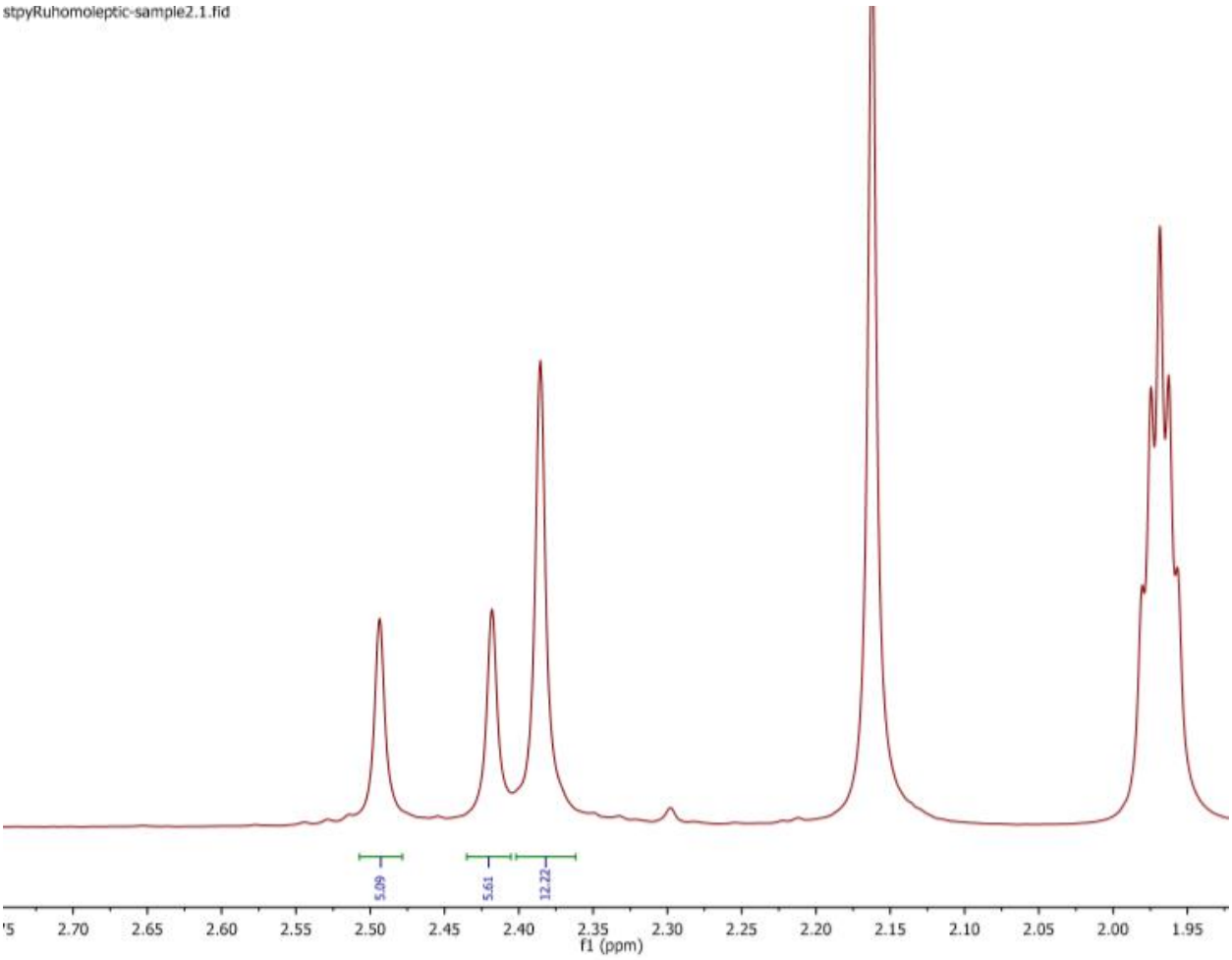

Figure S26. Zoom in of methyl peaks in ^{1}H NMR spectrum of *Ru(Me-TPS)$_2$(PF$_6$)$_2$* (400 MHz, DCM-*d*$_2$) (23)

A.2 NMR data for Chapter 3

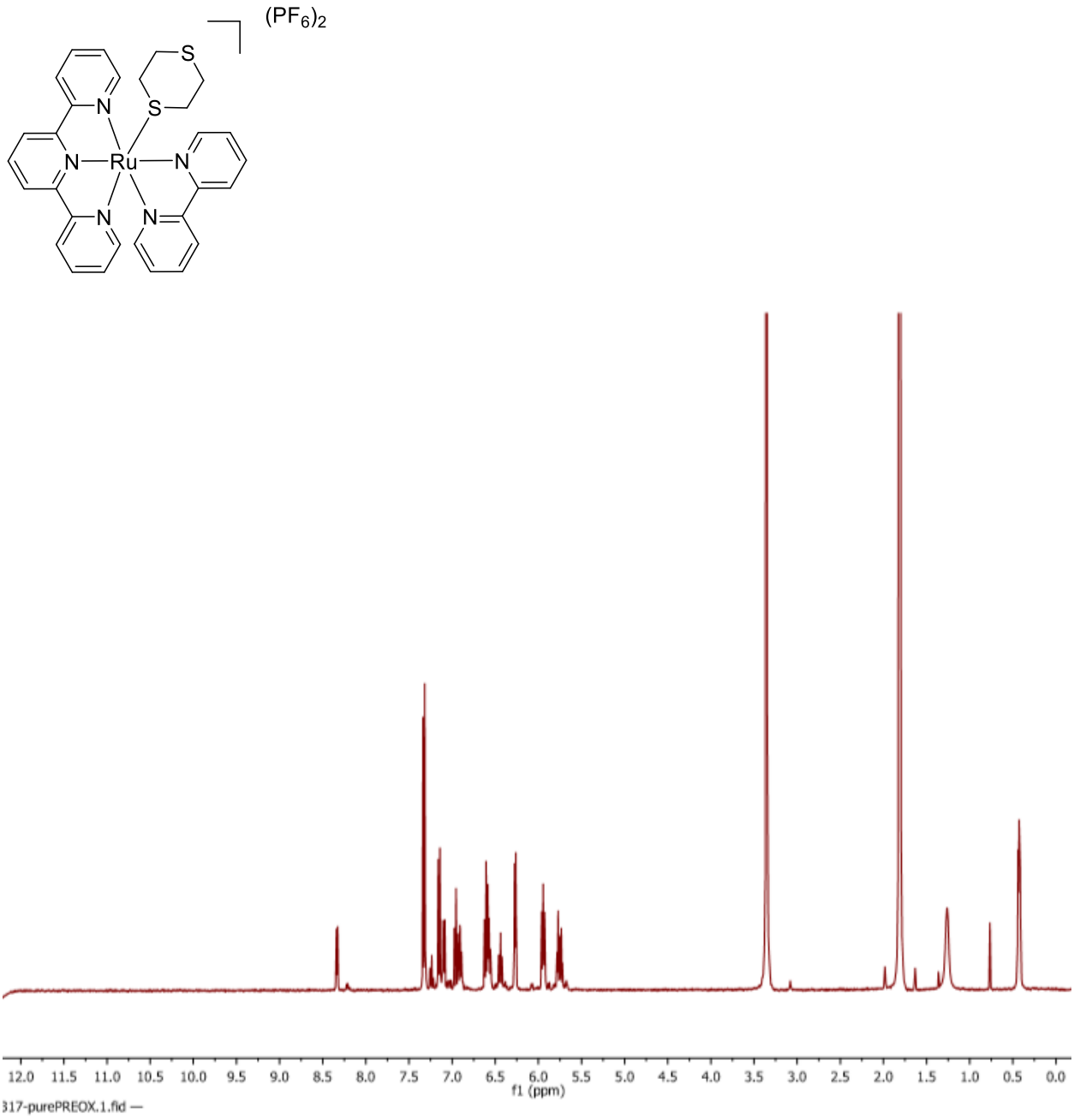

Figure S27. ^{1}H NMR spectrum of *[Ru(II)(tpy)(bpy)(1,4-dithiane)](PF$_6$)$_2$* (400 MHz, MeOD-*d*$_4$) (39)

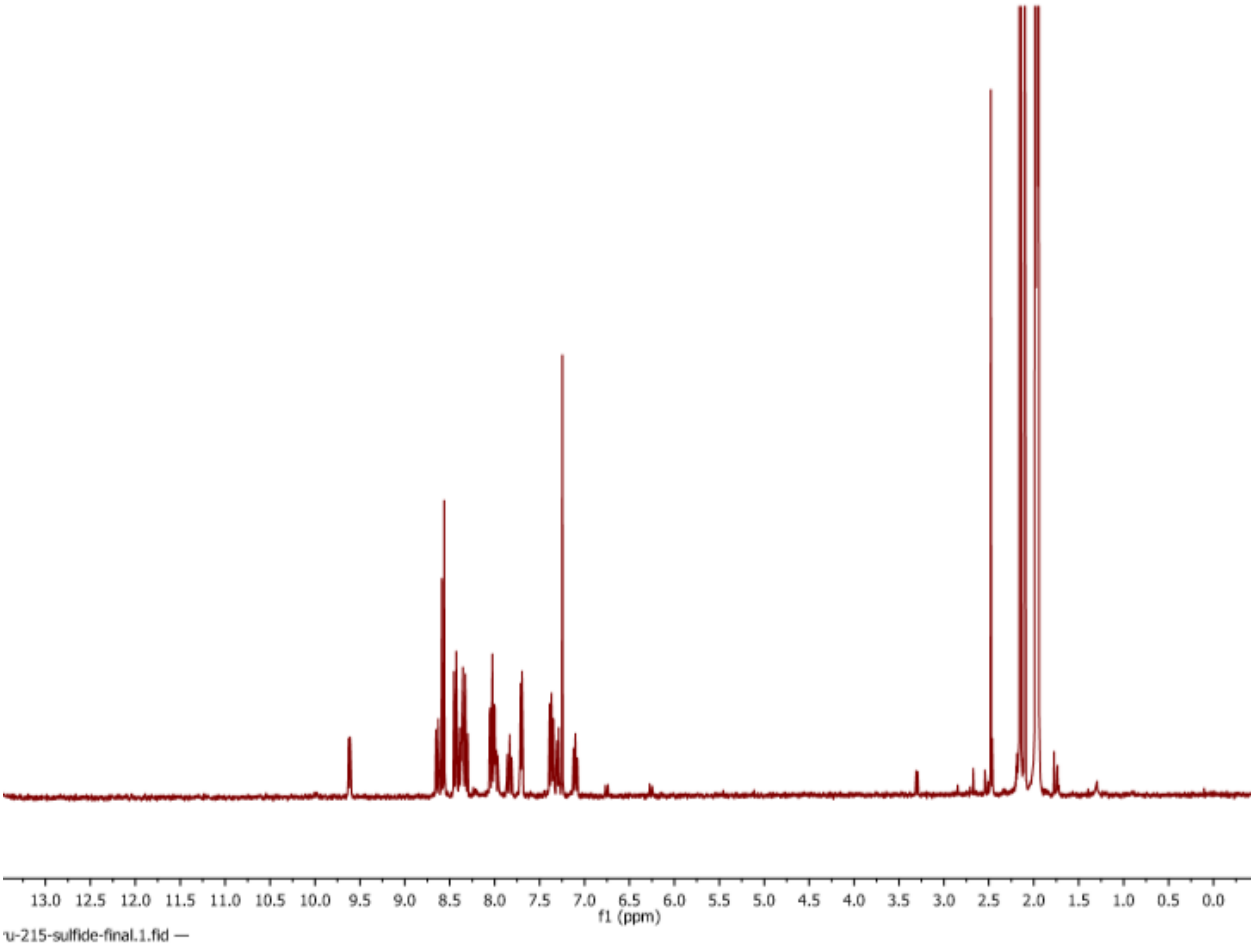

Figure S28. ^{1}H NMR spectrum of *[Ru(II)(tpy)(bpy)(1,4-bismethylthiobenzene)]* (400 MHz, MeOD-*d*$_4$) *(PF*$_6$*)*$_2$ (40)

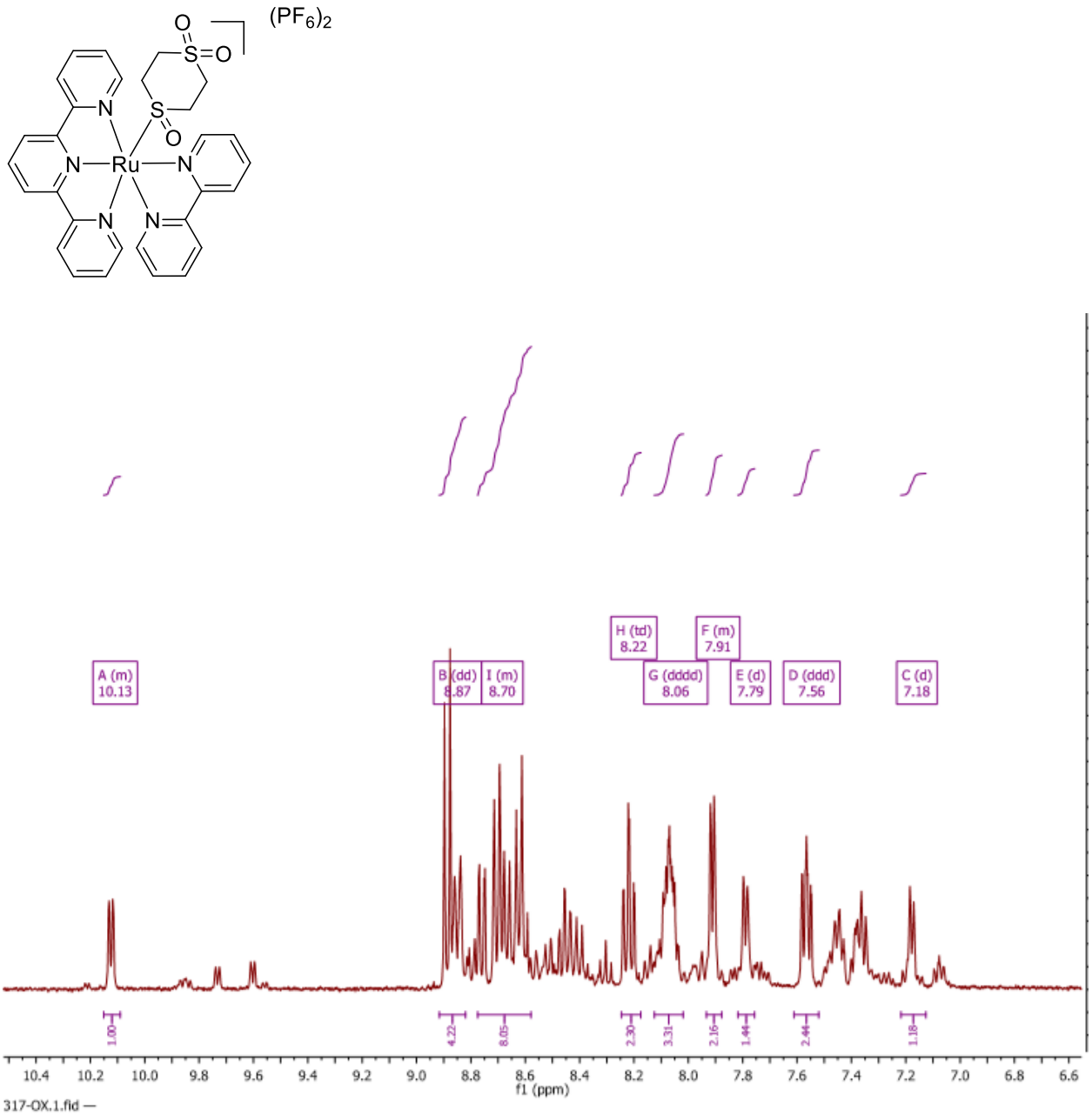

Figure S29. ^{1}H NMR spectrum of *Ru(bpy)(tpy)(1,4-dithiane, 1-dioxide,4-sulfone)* $(PF_6)_2$ (400 MHz, MeCN-d_3) (34)

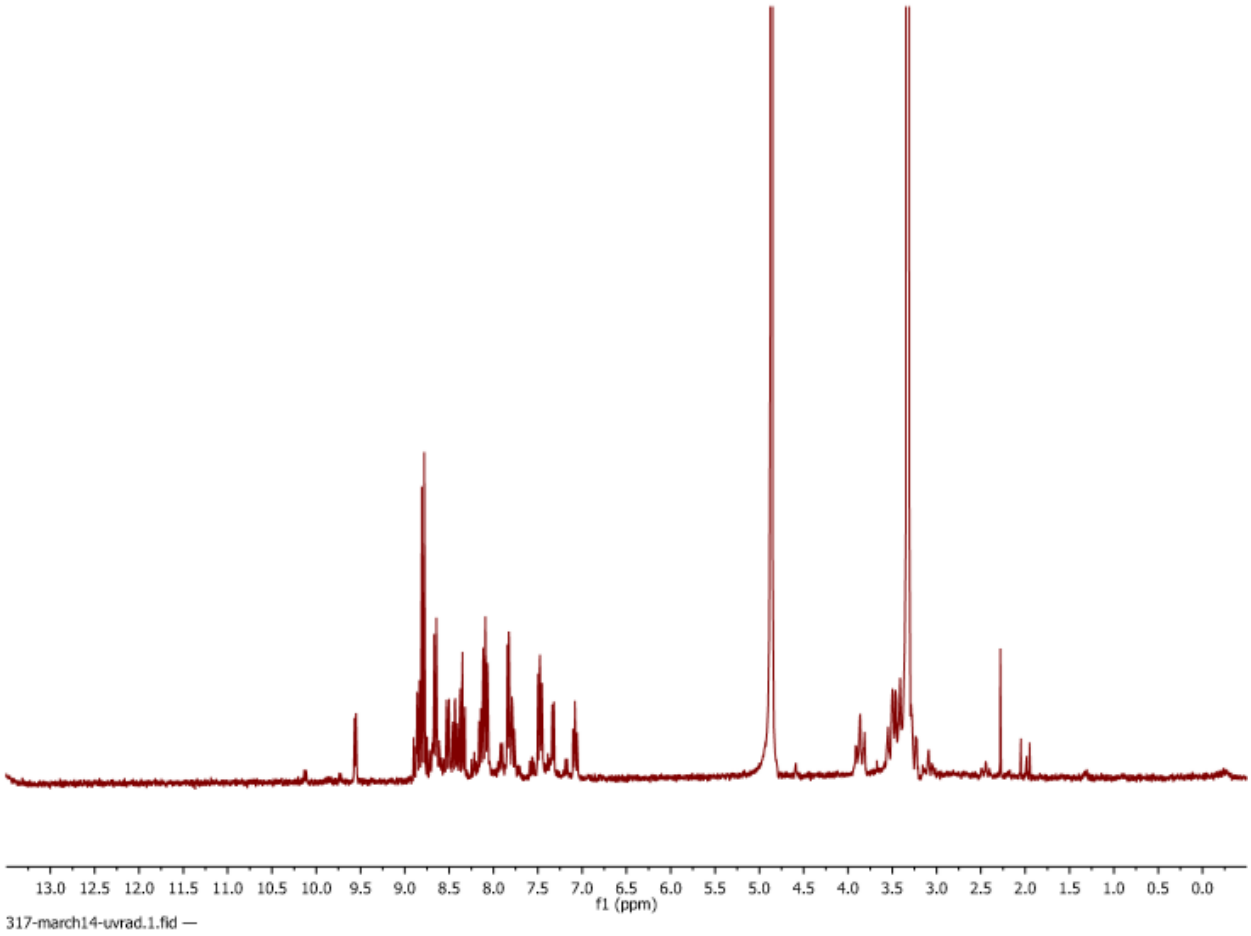

Figure S29. ^{1}H NMR spectrum of *Ru(bpy)(tpy)(1,4-dithiane, 1-dioxide,4-sulfone)* $(PF_6)_2$ (34) after UV irradiation(400 MHz, MeOD-d_4)

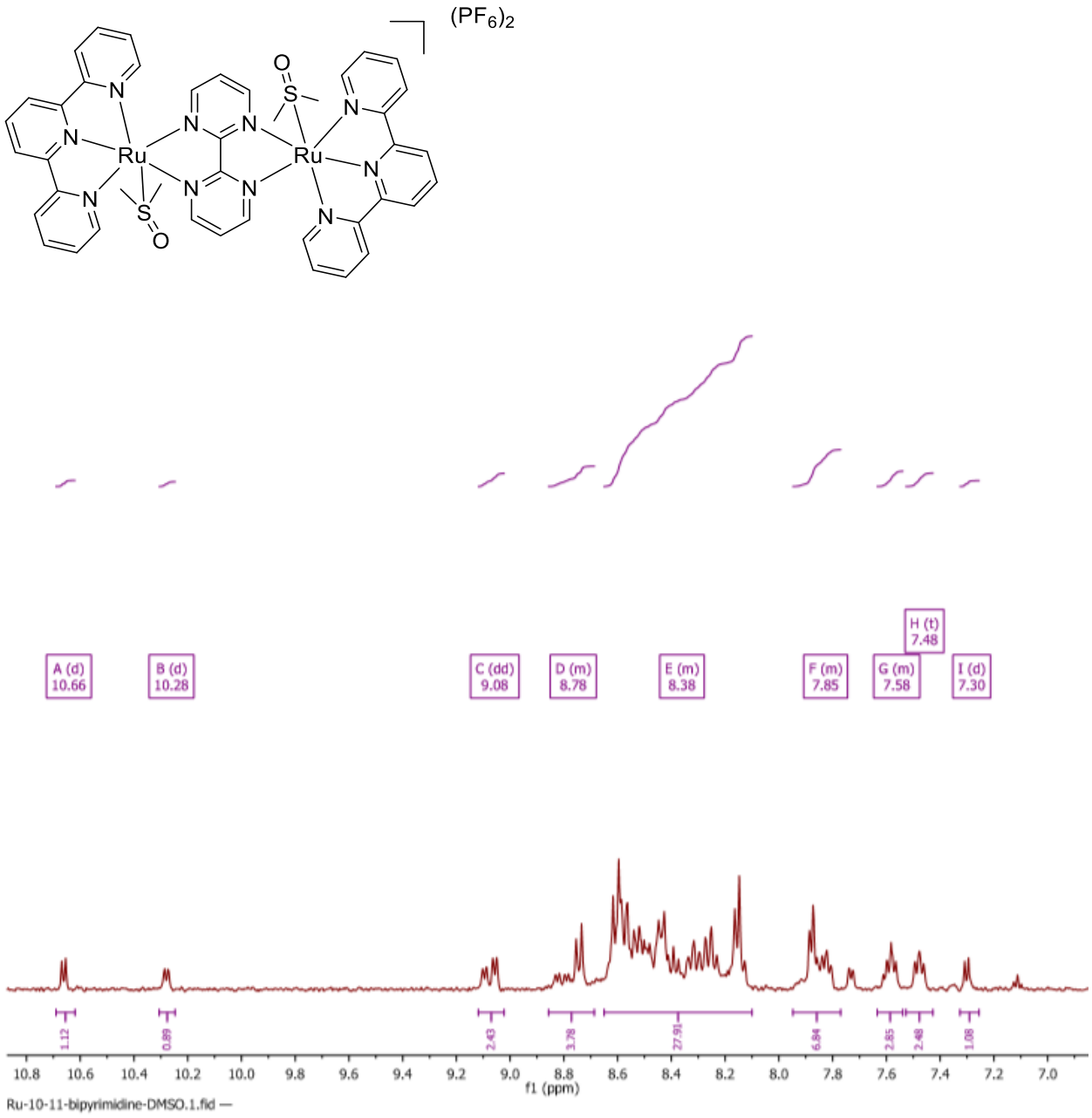

Figure S30. ^{1}H NMR spectrum of *[Ru(II)(tpy)(dmso)(bpym)(dmso)(tpy)Ru(II)](PF$_6$)$_2$* (400 MHz, MeCN-*d*$_4$) (36)

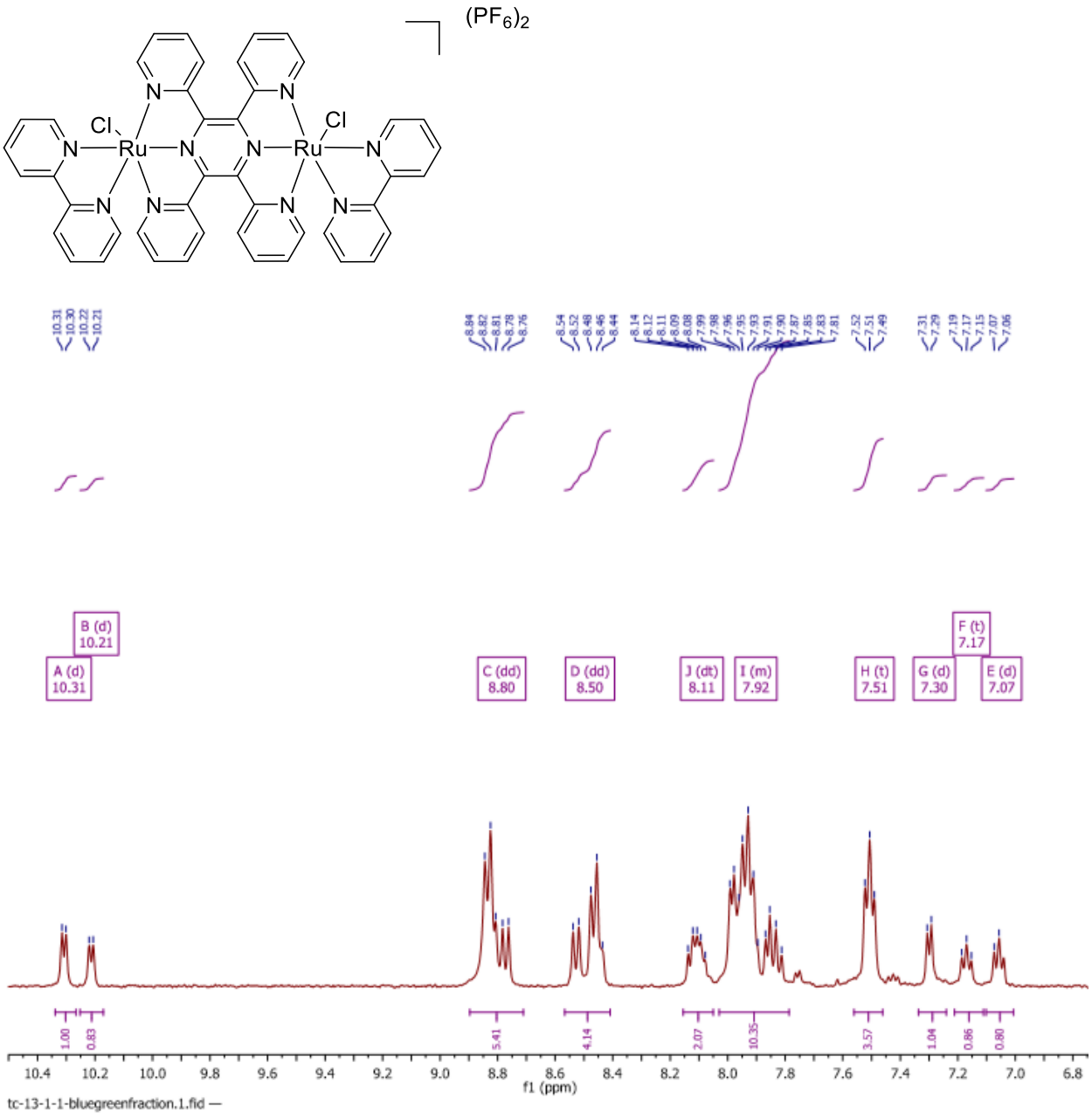

Figure S31. ^{1}H NMR spectrum of *[(bpy)ClRu(tppz)RuCl(bpy)](PF$_6$)$_2$* (400 MHz, MeOD-*d*$_4$) (43)

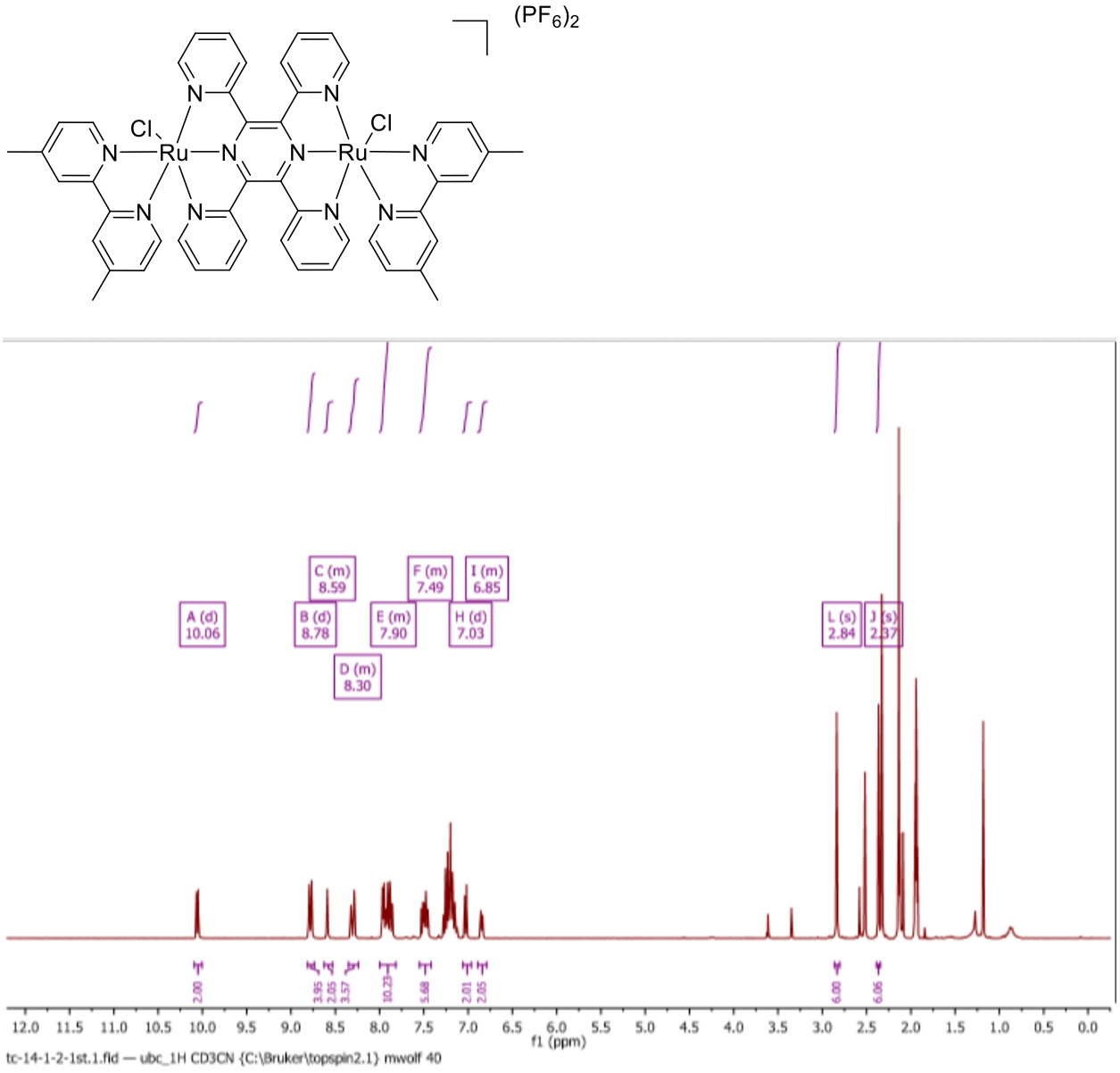

Figure S32. ^{1}H NMR spectrum of *[(dmbpy)ClRu(tppz)RuCl(dmbpy)](PF$_6$)$_2$* (400 MHz, MeCN-*d*$_4$) *(44)* first fraction of column

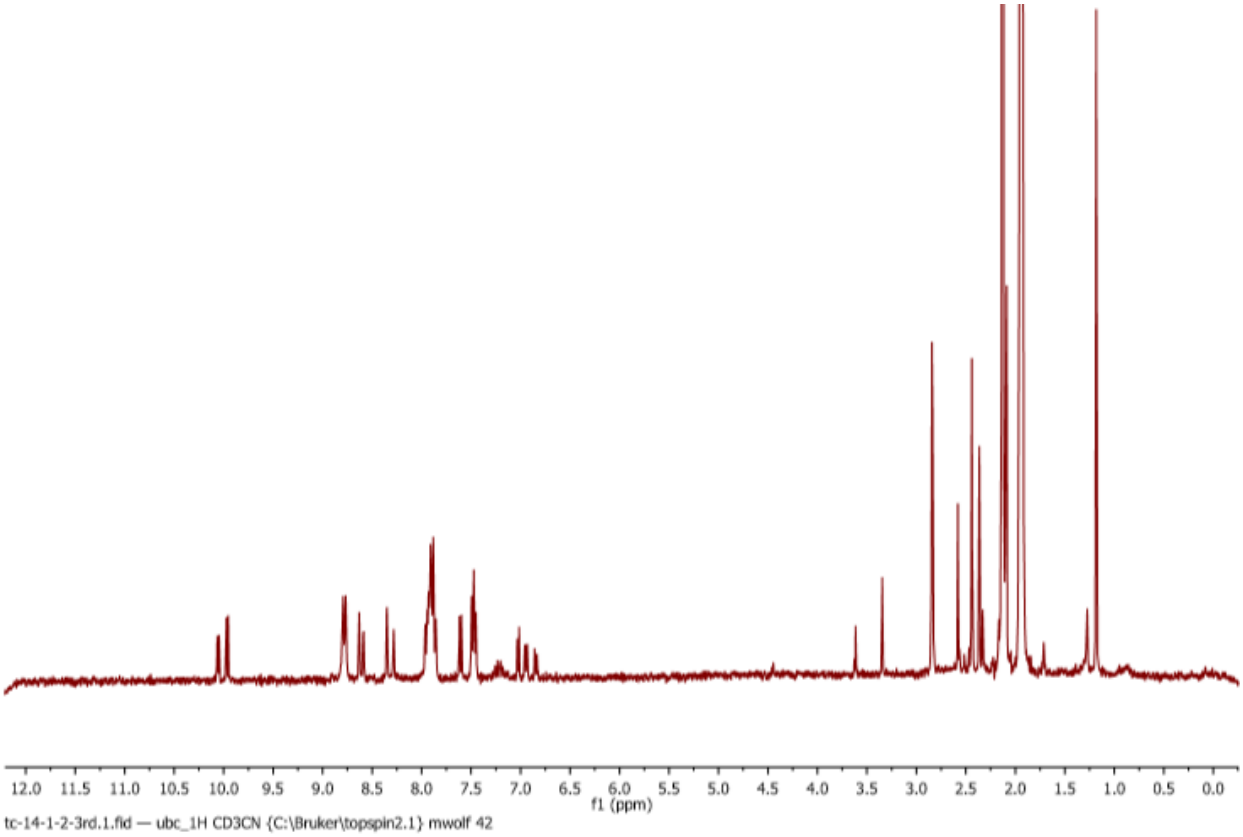

Figure S33. ^{1}H NMR spectrum of *[(dmbpy)ClRu(tppz)RuCl(dmbpy)](PF$_6$)$_2$* (400 MHz, MeCN-*d*$_4$) *(44)* third fraction of column

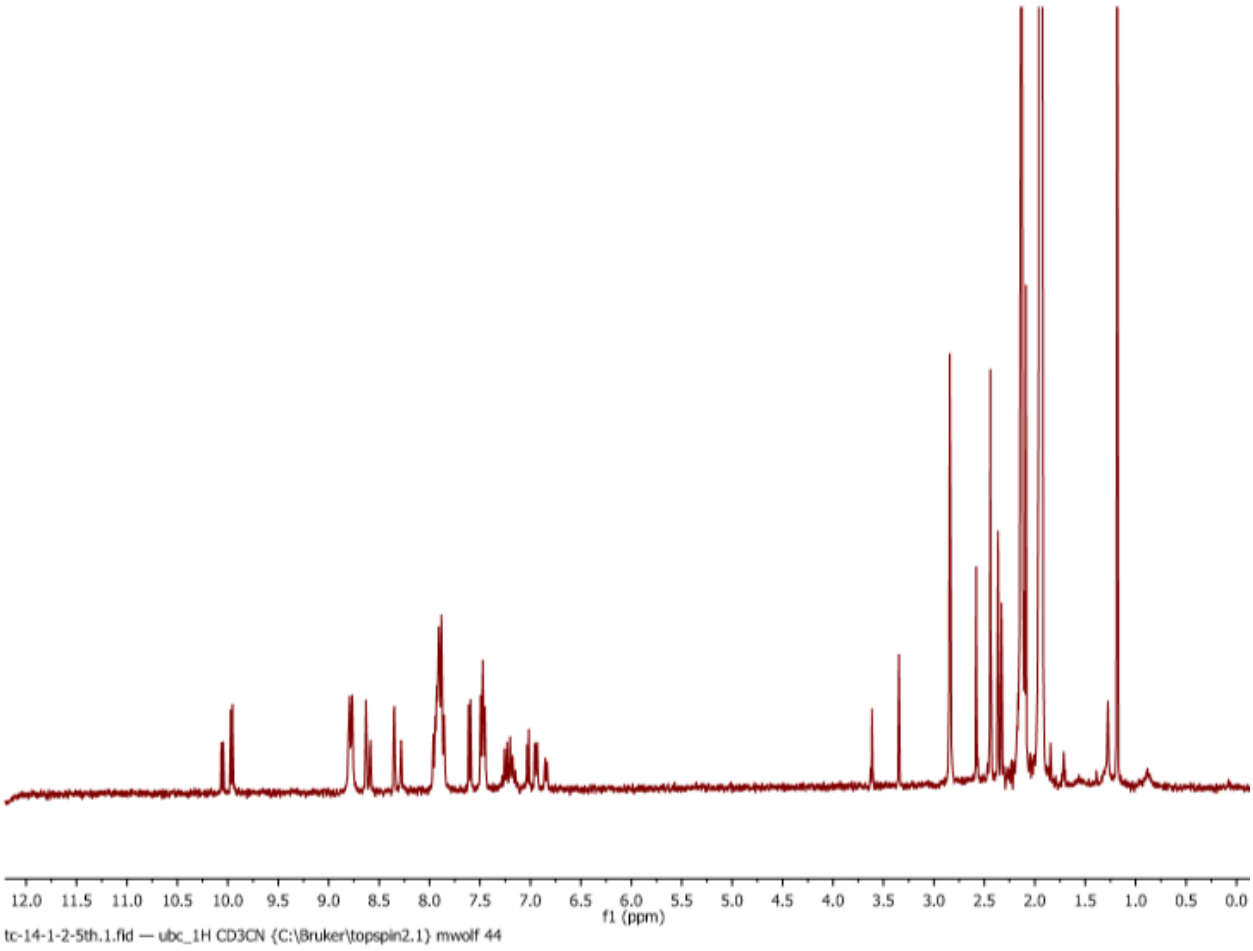

Figure S34. ^{1}H NMR spectrum of *[(dmbpy)ClRu(tppz)RuCl(dmbpy)](PF$_6$)$_2$* (400 MHz, MeCN-*d*$_4$) *(44)* fifth fraction of column

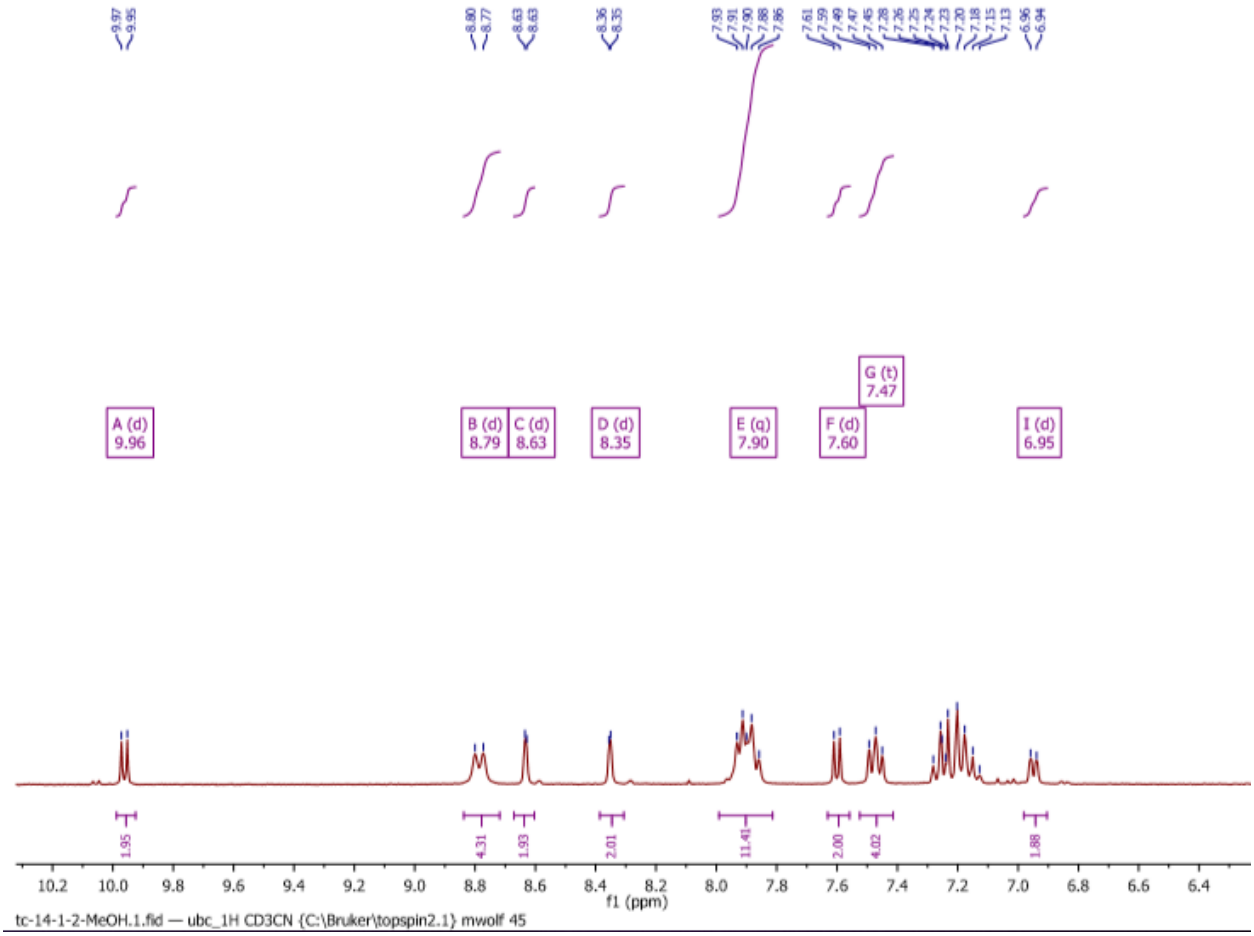

Figure S35. ^{1}H NMR spectrum of *[(dmbpy)ClRu(tppz)RuCl(dmbpy)](PF$_6$)$_2$* (400 MHz, MeCN-*d*$_4$) *(44)* MeOH rinse of column

Appendix B Crystallographic Data

Ru(TPS)2 (22)

Table A-1 Crystal data and structure refinement for Ru(TPS)2.

Identification code	Ru(TPS)2
Empirical formula	$C_{36.04}H_{32.45}F_{12}N_{8.32}O_{0.35}P_2RuS_4$
Formula weight	1106.93
Temperature/K	90(2)
Crystal system	monoclinic
Space group	$P2_1/n$
a/Å	11.5073(16)
b/Å	13.617(2)
c/Å	28.041(4)
α/°	90
β/°	93.835(3)
γ/°	90
Volume/Å^3	4384.0(11)
Z	4
ρ_{calc}g/cm^3	1.677
μ/mm^{-1}	0.713
F(000)	2223.0
Crystal size/mm^3	0.23 × 0.2 × 0.15
Radiation	MoKα (λ = 0.71073)
2Θ range for data collection/°	2.912 to 60.094
Index ranges	$-16 \le h \le 15$, $-19 \le k \le 19$, $-39 \le l \le 39$
Reflections collected	56991
Independent reflections	12809 [R_{int} = 0.0598, R_{sigma} = 0.0504]
Data/restraints/parameters	12809/206/648
Goodness-of-fit on F^2	1.019
Final R indexes [I>=2σ (I)]	R_1 = 0.0352, wR_2 = 0.0710
Final R indexes [all data]	R_1 = 0.0545, wR_2 = 0.0786
Largest diff. peak/hole / e Å^{-3}	0.74/-0.88

Ru(Me-TPS)2 (23)

Table S-2 Crystal data and structure refinement for Ru(Me-TPS)2.

Identification code	Ru(Me-TPS)2
Empirical formula	$C_{37.91}H_{36.54}F_{12}N_{7.95}O_{0.34}P_2RuS_4$
Formula weight	1128.15
Temperature/K	100.15
Crystal system	triclinic
Space group	P-1
a/Å	13.4994(9)
b/Å	13.7178(9)
c/Å	21.4293(14)
α/°	105.009(3)
β/°	93.222(3)
γ/°	116.426(3)
Volume/Å^3	3364.3(4)
Z	3
ρ_{calc}g/cm^3	1.670
μ/mm^{-1}	0.698
F(000)	1705.0
Crystal size/mm^3	0.455 × 0.1 × 0.05
Radiation	MoKα (λ = 0.71073)
2Θ range for data collection/°	2.008 to 53.492
Index ranges	$-15 \leq h \leq 16$, $-17 \leq k \leq 17$, $-26 \leq l \leq 27$
Reflections collected	50853
Independent reflections	13842 [R_{int} = 0.0598, R_{sigma} = 0.0842]
Data/restraints/parameters	13842/2014/1034
Goodness-of-fit on F^2	1.182
Final R indexes [I>=2σ (I)]	R_1 = 0.1011, wR_2 = 0.2026
Final R indexes [all data]	R_1 = 0.1400, wR_2 = 0.2159
Largest diff. peak/hole / e Å^{-3}	0.84/-0.68

Ru(TPS)(tpy) (25)

Table S-3 Crystal data and structure refinement for Ru(TPS)(tpy).

Identification code	Ru(TPS)(tpy)
Empirical formula	$C_{34}H_{25}F_{12}N_8O_{0.5}P_2RuS_2$
Formula weight	1008.75
Temperature/K	100.15
Crystal system	triclinic
Space group	P-1
a/Å	10.560(9)
b/Å	11.093(10)
c/Å	17.565(15)
α/°	86.58(2)
β/°	73.703(16)
γ/°	77.28(3)
Volume/Å^3	1927(3)
Z	2
ρ_{calc}g/cm^3	1.739
μ/mm^{-1}	0.698
F(000)	1006.0
Crystal size/mm^3	0.3 × 0.09 × 0.05
Radiation	MoKα (λ = 0.71073)
2Θ range for data collection/°	2.416 to 61.232
Index ranges	$-15 \leq h \leq 15$, $-15 \leq k \leq 15$, $-24 \leq l \leq 25$
Reflections collected	40622
Independent reflections	11508 [R_{int} = 0.0267, R_{sigma} = 0.0392]
Data/restraints/parameters	11508/0/608
Goodness-of-fit on F^2	1.004
Final R indexes [I>=2σ (I)]	R_1 = 0.0415, wR_2 = 0.1007
Final R indexes [all data]	R_1 = 0.0523, wR_2 = 0.1062
Largest diff. peak/hole / e Å^{-3}	1.50/-0.59